METSÄNTUTKIMUSLAITOKSEN TIEDONANTOJA 770, 2000
FINNISH FOREST RESEARCH INSTITUTE, RESEARCH PAPERS 770, 2000

Effect of snow cover on the mobility of a towed wheel

Jari Ala-Ilomäki

VANTAAN TUTKIMUSKESKUS – VANTAA RESEARCH CENTRE
METLA

METSÄNTUTKIMUSLAITOKSEN TIEDONANTOJA 770, 2000
FINNISH FOREST RESEARCH INSTITUTE, RESEARCH PAPERS 770, 2000

Effect of snow cover on the mobility of a towed wheel

Jari Ala-Ilomäki

Finnish Forest Research Institute
Vantaa Research Centre

Academic dissertation

To be presented, with the permission of the Faculty of Agriculture and Forestry of the University of Helsinki, for public critisism in Auditorium M III, Metsätalo, Unioninkatu 40 B, Helsinki, on 9 June 2000, at 12 o'clock noon.

Supervisor:

Professor Rihko Haarlaa
University of Helsinki, Finland
Faculty of Agriculture and Forestry

Reviewers:

Dr. Jukka Ahokas
Agricultural Research Centre of Finland
Agricultural Engineering Research VAKOLA

Dr. Dvoralai Wulfsohn
Aalborg University, Denmark
Institute of Mechanical Engineering

Opponent:

Professor Iwan Wästerlund
Swedish University of Agricultural Sciences
Faculty of Forestry

Publisher: Finnish Forest Research Institute, Vantaa Research Centre
P.O. Box 18, FIN-01301 Vantaa, Finland.
Accepted by Matti Kärkkäinen, Research Director, 12.4.2000.

ISBN 951-40-1730-7
ISSN 0358-4283

CONTENTS

ABSTRACT

A model describing the interaction between a towed pneumatic vehicle wheel and snow covering the ground surface is presented. The model is based on the cycloidal compression of snow. The starting angle and the width of the compressing surface of the tyre with elliptical cross section are determined by the pressure components normal and perpendicular to the tyre surface as well as the rubber-snow interface friction coefficient. The snow outside the compressive range is assumed to induce flow resistance. Compression displacement is determined as the elapsed length of the cycloid, and the length of the snow layer to be compressed as the distance from the tyre surface to the ground in the direction of the cycloid tangent. The resulting forces in vertical and horizontal direction in addition to the torque on the wheel axle resulting from snow compression and shearing, flow resistance and internal motion resistance are calculated. Wheel slip and wheel-snow contact entry angle are varied in an iterative manner until a state of equilibrium, where resultant torque on wheel axle equals zero and resultant vertical force is equal to wheel load, is reached for six consecutive passes.

In order to test the model mobility data was collected using an instrumented axle with 0.425 m diameter wheels, towed in snow bins. The bins were filled with snow extracted from one uniform layer of natural snow cover at a time. Temperature, density, moisture content, grain size, pressure-sinkage relationship and shear stress-strain relationship were determined for a total of six different snow types. Empirical relationships for rubber-snow interface friction and flow resistance of snow were developed on the basis of separate sets of data.

In the field tests with constant 0.15 m snow depth, the effect of snow properties on motion resistance on the first pass was small, but the behaviour of other mobility parameters and the resistance on the following passes differed between the snow types. In constant snow type the effect of snow depth variation from 0.05 to 0.15 m on mobility parameters was clear.

The mobility model yielded realistic values for mobility parameters. The role of the starting angle of compression, determined by the coefficient of rubber-snow interface friction, and the magnitude of flow resistance proved to be decisive. The compression mechanism and the cyclic loading of snow, as well as the role of tyre tread pattern should be addressed in future work.

Key words: off-road transportation, modelling, scale model testing, tyres.

Author's address: Finnish Forest Research Institute, Vantaa Research Centre, P.O. Box 18, FIN-01301 Vantaa, Finland. Fax: +358 9 8570 5361, e-mail: jari.ala-ilomaki@metla.fi

ACKNOWLEDGEMENTS

The study was carried out at the Vantaa Research Centre of the Finnish Forest Research Institute (FFRI) as a part of research project 3149 Predicting the level and cost of soil and tree damage in logging, which belonged to Environmental impacts of forestry -research programme. I am grateful to FFRI and my superiors, both present and past, for the opportunity and support in the course of the work. The field work in Sodankylä was carried out in collaboration with the Finnish Defence Forces, the community of Sodankylä, Sodankylä Vocational Institute and machine contractor Mauri Rissanen. At the Suonenjoki Research Station of FFRI Martti Kuikka and Aimo Nurminen were both willing and able to fulfil my wishes regarding the necessary hardware and field study preparations.

At the Vantaa Research Centre of FFRI, Dr. Risto Sievänen and Erkki Pesonen provided invaluable help in the field of mathematics and physics. In the field I was assisted by Tapio Järvinen, Hannu Kalaja, Jukka Lehtimäki, Tapio Nevalainen, who additionally was in charge of woodwork and snow grain measurements, and Jari Sirviö. In the diverse world of computer-related problems I have always been able to count on the help of Hannu Aaltio. Several colleagues have shared their thoughts on the subject with me, especially Dr. Martti Saarilahti, Dr. Matti Sirén, Arto Rummukainen and Pentti Sairanen deserve to be mentioned here. The artistic capabilities of Pentti Sairanen's Sairart Graphic Studios were behind the wire-frame figures and the snow grain montage. The English language was revised by Matthew Barnette. The Vantaa staff as a whole contributed to the fruitful atmosphere necessary for the work.

Constructive criticism on the manuscript was given by the official reviewers Dr. Jukka Ahokas and Dr. Dworalai Wulfsohn, my supervisor Professor Rihko Haarlaa and Professor Pentti Hakkila from FFRI. I also wish to thank my old friends Timo Karppinen and Vesa-Pekka Peräkylä for their assistance in the development of the model, as well as Jaana and Tapio Pouta for offering me protection against the elements up north in Sodankylä.

I guess one's family is to suffer most during a process of this kind. I therefore wish to thank my mother Tellervo and father Sauli, who additionally assisted me in data collection and equipment design, for their support and encouragement. My dear wife Päivi, our lovely kids Konsta, Valtteri and Lea, and wee little westie Otto deserve the warmest of thanks for keeping the spirit high.

Vantaa, 28 April 2000 Jari Ala-Ilomäki

LIST OF MAIN SYMBOLS

a, b = Ellipse axes, m
$a_{dR}(\theta)$ = Deformed a-axis, m
A_f = Cross sectional area, m^2
B = Bandwidth in snow, MHz
B_{air} = Bandwidth in air, MHz
b_{avg} = Average perpendicular distance between ellipse circumference and a-axis at $\theta=\theta_{max}$, m
b_{coc} = Constant compression width of tyre, m
$b_{co\mu}(\theta)$ = Maximum tyre-snow friction defined compressive width of tyre, m
$b_{co}(\theta)$ = Tyre compressive width, m
$b_{dR}(\theta)$ = Deformed b-axis, m
$b_{max}(\theta)$ = Maximum tyre-snow contact width for given snow depth and wheel rotation angle, m
$b_{\mu}(\theta)$ = Tyre-snow friction defined compressive width of tyre, m
$b_{2\pi}(\theta)$ = Tyre width at $2 \cdot \pi$ region, m
$b_{2\pi lim}(\theta)$ = Minimum tyre width at $2 \cdot \pi$ region, m
d = Plate diameter, m
d_t = Tyre deflection, m
$d_R(\theta)$ = Deformation of wheel, m
$diff_b$ = Snow depth and compression length adjustment for the following pass, m
f = Resonant frequency in snow, MHz
f_{air} = Resonant frequency in air, MHz
F_f = Flow resistance force, N
F_{r0} = Internal motion resistance of tyre, N
F_y = Force acting on tyre in y-direction, N
F_z = Force acting on tyre in z-direction, N
$F\tau_y$ = y-component of shear force in the flow region, N
$F\tau_z$ = z-component of shear force in the flow region, N
i = Wheel slip
l_{rR} = Distance between the wheel centre and the contact surface circle centre, m
j = Shear displacement, m
k = Number of estimated parameters
K_w = Shear displacement at τ_{max}, m
K_r = Ratio of residual shear strength to maximum shear strength
n = Number of observations
N = Normal load, N
p = Pressure, Pa
$p(\theta)$ = Compression pressure, Pa

p_{da} = Proportion of tyre deformation taking place in the direction of a-axis

p_{db} = Proportion of tyre deformation taking place in the direction of b-axis

p_f = Flow resistance pressure, Pa

$p_{fn}(\theta)$ = Component of flow resistance pressure normal to tyre surface, Pa

$p_{ftg}(\theta)$ = Component of flow resistance pressure tangential to tyre surface, Pa

p_n = Normal pressure, Pa

p_v = Velocity dependent part of flow resistance pressure, Pa

$p_y(\theta)$ = y-component of compression pressure along the tyre-snow contact path, Pa

$p_z(\theta)$ = z-component of compression pressure along the tyre-snow contact path, Pa

p_0 = Starting value of flow resistance pressure, Pa

$p_n(\theta)$ = Component of compression pressure normal to wheel, Pa

$p_{tg}(\theta)$ = Component of compression pressure tangential to wheel, Pa

$p_y(\theta)$ = y-component of compression pressure, Pa

$p_z(\theta)$ = z-component of compression pressure, Pa

$\underline{p} \parallel T_2$ = Component of pressure $\underline{p}$ parallel to axis T_2

$\underline{p} \perp T_2$ = Component of pressure $\underline{p}$ perpendicular to axis T_2

$\underline{p} \perp T_2 \in \tau$ = Component of $\underline{p} \perp T_2$ in plane τ

$\underline{p} \parallel \tau$ = Component of pressure $\underline{p}$ parallel to plane τ

$p \perp \tau$ = Component of pressure p perpendicular to plane τ

R = Radius of the wheel-soil contact circle, m

r = Undeformed radius of circle or wheel, m

r_0 = Zero condition rolling radius of wheel, m

r_d = Deflected radius of wheel, m

r_f = Average radius of the tyre in the flow region, m

rel_{rn} = Relation of maximum sinkage to snow depth in plate loading test with plate radius r_n (n=1,2)

r_n = Compression plate radius (n=1,2), m

r_p = Compression plate radius, m

r_{pc} = Largest allowable compression plate radius in pressure calculations, m

$r_R(\theta)$ = Deformed radius of wheel, m

Δr_p = An infinitely small fraction of compression plate radius, m

s = Standard deviation

s_c = Share of tyre carcass of total tread area

$s_{co}(\theta)$ = Length of compression accomplished at rotation angle θ, m

s_{cop} = Length of compression on the previous passes, m

$s_M(\theta)$ = Perpendicular distance from straight of action of pressure to centre of wheel, m

$s_{coi}(\theta)$ = Initial length of snowpack in compression at rotation angle θ, m

s_{sn} = Snow depth on the following pass, m

s_{si} = Initial snow cover depth, m

s_{sf} = Final length of compressed snow cover, m

$s_{tg}(\theta)$ = Snowpack length from wheel surface to ground along the tangent of the cycloid at rotation angle θ, m

T = Torque acting on tyre axle, N m

T_f = Torque induced by the flow resistance of snow, N m

T_{r0} = Torque induced by the internal motion resistance of tyre, N m

T_τ = Torque induced by snow shearing in the flow region, N m

T_1, T_2 = Axes of plane

v = Linear velocity, m s^{-1}

w = Free water content of snow, %wgt

w_{vol} = Free water content of snow, %vol

$\bar{x}$ = Mean

y_i = Observed value of i^{th} observation

$\hat{y}_i$ = Predicted value of i^{th} observation

$y(\theta)$ = y co-ordinate of cycloid

$y_{el}(x,\theta)$ = y co-ordinate of ellipse, m

$y_i(\theta)$ = y co-ordinate of cycloid of a slipping wheel

$y_{iR}(\theta)$ = y co-ordinate of cycloid of a deforming slipping wheel

z = Sinkage, m

$z(\theta)$ = z co-ordinate of cycloid

$z_i(\theta)$ = z co-ordinate of cycloid of a slipping wheel

$z_{iR}(\theta)$ = z co-ordinate of cycloid of a deforming slipping wheel

$z_t(\theta)$ = The height of tyre circumference from the ground at rotation angle θ, m

$\alpha(\theta)$ = Angle between cycloidal pressure and z-axis, rad

α_{Rz} = Angle between z-axis and the imaginary wheel radius R having a common point on wheel circumference with radius $r_R(\theta)$ at rotation angle θ, rad

α_1 = Leading contact angle, rad

α_2 = Trailing contact angle, rad

$\beta(\theta)$ = Sharp angle between wheel tangent and y-axis, rad

$\gamma(\theta,\sigma)$ = Angle between ellipse a-axis and T_1 at eccentric angle σ and rotation angle θ, rad

$\gamma_{lim}(\theta)$ = Limit angle between ellipse a-axis and T_1 meeting the friction condition at rotation angle θ, rad

$\delta(\theta)$ = Angle between cycloidal pressure and wheel tangent, rad

ε' = real part of relative dielectric constant of snow

ε'' = imaginary part of relative dielectric constant of snow

$\Delta_\theta(\theta)$ = Angle between the bisector of $(\alpha_1+\alpha_2)$ and the radius corresponding to rotation angle θ, rad

θ = Rotation angle, rad

θ_e = Rotation angle at wheel-snow contact entry, rad

θ_{max} = Maximum rotation angle at wheel-snow contact, rad

θ_p = Rotation angle in r_{pc} calculations, rad

θ_{cs} = Rotation angle where snow compression starts, rad

θ_{ss} = Rotation angle meeting the friction condition at $\sigma = 3 \cdot \pi/2$, rad

θ_τ = Rotation angle where tangential pressure exceeds the shear strength of snow, rad

μ = Friction coefficient

$\mu(\theta)$ = Friction coefficient at rotation angle θ

μ_r = Motion resistance coefficient

μ_{p0} = Friction coefficient at zero normal pressure

ρ = Snow density, kg m^{-3}

ρ_f = Snow density assessed by snow fork, kg m^{-3}

ρ_s = Snow density assessed by snow scale, kg m^{-3}

σ = Eccentric angle of the ellipse, rad

$\sigma_{lim}(\theta)$ = Limit eccentric angle of the ellipse meeting the friction condition at rotation angle θ, rad

τ = Shear strength, Pa

$\tau_f(\theta)$ = Shear strength of snow under the normal pressure of $p_{fn}(\theta)$, Pa

τ_{max} = Maximum shear strength, Pa

$\tau_{max}(\theta_\tau)$ = Maximum shear strength at θ_τ, Pa

ϕ = Angle of internal friction, rad

ω = Angular velocity, rad s^{-1}

1 INTRODUCTION

In Finland, winter has a remarkable effect on forest harvesting operations. In the past, most of harvesting was done in the winter with manual methods. Snow cover formed a hindrance to manual labour, yet it also facilitated primary transportation by sledges and made the work easier by reflecting the little light available in the forest during the winter period.

In 1998, roughly 95% of timber harvesting by the forest industries and the Finnish Forest and Park Service was fully mechanised (Finnish... 1999). Today harvesting equipment is almost exclusively based on wheeled machinery. In the times of modern harvesting, snow seldom is a hindrance to harvesting, nor a necessity. In fact winter is still the busiest season for harvesting. On average, the ground can be estimated to be covered by snow for five months, during which roughly 50 % of the annual commercial roundwood production is accomplished (Kolkki 1969, Finnish... 1999). A strong tendency towards lower seasonal variation in harvesting volume can thus be seen. Generally, the conditions for harvesting are more favourable in the winter, since the ground is usually frozen, which improves terrain trafficability and reduces damage to the soil and the trees remaining. The higher up in the north the site is located, the longer the frozen period and the thicker the frost layer is. During some winters, the frost is non-existing in the south. Snow cover reduces terrain roughness and offers protection for remaining trees. At its best, the result is improved productivity and a decreased level of environmental damage.

From a vehicle mobility point of view, the snow mainly forms a hindrance, the severity of which depends on the properties of snow cover and the vehicle, as well as the terrain and the task of the vehicle. Due to snow cover, the traction of the running gear is reduced and the motion resistance increased on all but the roughest of terrain given the equal state of the underlying ground. A considerable amount of energy is being expended in snow compression.

Increasing environmental concern on the adverse effects of harvesting is promoting stricter requirements on the level of environmental damage after mechanised harvesting. Lower levels of damage to the soil and the remaining stand may be achieved through improved planning and operation methods, the use of smaller and lighter harvesting machinery, and new machine concepts. Besides improved methods, light harvesting machinery has been used to achieve these goals with varying success. Presently, the trend seems to be towards the universal use of machinery with net vehicle weights of 100 to 150 kN. In addition to the need for environmental certifications in timber production, the demand for lighter machinery may increase in the future, and new machinery under the presently dominating size class has already been introduced during the recent years.

In conjunction with vehicle mobility, snow is subject to at least compressive and shear loading by the vehicle. Hence, mobility is defined by the physical and mechanical properties of snow and the characteristics of the vehicle. Snow originates in the clouds in the form of crystals but the structure varies greatly passing through many phases before settling on the ground (Mellor 1964, Mellor 1977, Langham 1981, LaChapelle 1992). Once on the ground, the structure of the crystals changes further through metamorphism, the resulting snow grains may be interconnected to varying degrees and ways (Colbeck 1982, Colbeck 1997). Langham (1981) and LaChapelle (1992) describe several classification systems that exist for the identification and characterisation of precipitating and metamorphosed snow. Requirements for a snow classification system for vehicle mobility purposes have also been presented (ISTVS, 1978). In the review by Shoop and Alger (1991), the various snow characterisation techniques used in conjunction with vehicle mobility testing are presented. The mechanical properties of snow depend on physical properties and the bonding between the grains (Bader 1962, Mellor 1964, Mellor 1975, Mellor 1977, Salm 1982, Edens and Brown 1993, Shapiro et al. 1997). The physical properties and structure of snow vary greatly and only for a few cases have its mechanical properties been determined (Brown 1989, Shapiro et al. 1997).

The snow cover encountered normally in the course of a Finnish winter does not form an obstacle to the mobility of harvesting machinery of the dominating size class, yet during the worst snow conditions machinery may be slowed down considerably for periods of time. Unusually severe snow conditions, as encountered during the winter of 1999-2000, may occasionally even prevent mobility in the northern and north-eastern parts of the country. While conventional forest machinery can normally cope with the snow cover, farm tractor based machinery and lighter machinery, depending on size class and terrain type, can be severely effected by difficult snow conditions (Sirén et al. 1987).

Most people working in the field of timber harvesting in Finland have a practical knowledge on the effect of snow and different snow types on vehicle mobility, but quantitative knowledge is lacking. A number of reports on vehicle mobility in snow have been published, however the number of papers dealing with wheeled vehicles is relatively small. The most relevant for the purpose of this study are Blaisdell (1981), Harrison (1981), Blaisdell (1987), Osborne and Alger (1989), Blaisdell et al. (1990), Richmond et al. (1990) and Richmond (1995).

Very few reports have dealt directly with the effect of snow properties on wheel mobility. Since the studies are usually conducted in natural snow covers in ambient conditions, the possibilities to influence the properties of snow cover are limited and it is not simple to differentiate between the effect of snow properties and snow depth (Haarlaa 1971, Silvennoinen and Haarlaa 1971,

Silvennoinen 1980, Högnäs and Silvennoinen 1981, Sirén et al. 1987). The free water content of snow in particular has gained very little attention in mobility studies, the study of Osborne and Alger (1989) being one of the few exceptions. The measurement of free water content has been very tedious with traditional methods. Blaisdell et al. (1990) and Richmond (1995) address the need for a reliable motion resistance model for wheel in snow. Richmond et al. (1990) also state the need for a model for motion resistance of multiple wheel passes in snow. In particular, there is a need for a field operable model that is based on the theory of wheel mobility.

The purpose of this investigation was:

1. To find out the effect of selected properties of ground laying snow cover on the mobility parameters of a towed pneumatic vehicle wheel. Pneumatic vehicle wheel is later referred to as wheel.
2. To construct a mathematical model describing the interaction of towed wheel and snow. The model should be general enough to be expandable to describe the interaction of driven wheel and snow.
3. To study the feasibility of a microwave sensor for determining the free water content and density of snow for vehicle mobility analysis.

The hypothesis was that the motion resistance of a towed wheel would increase with increasing snow depth and through the metamorphosis of snow from newly fallen to old, coarse-grained snow. The hypothesis seemed logical on the basis of snow strength studies by Yong and Metaxas (1985), where energy expended in snow compression and shearing increased as snow density and age increased. The data by Blaisdell (1987) and Richmond et al. (1990) support the assumption of increasing motion resistance with increasing snow depth and density. In addition according to further analysis of the data of Ala-Ilomäki (1986), the energy expended in compacting snow by a wheeled vehicle increases with increasing density and snow depth.

In this paper mobility of towed wheel in snow, covering the ground surface, is investigated. Firstly, a mobility model, based on cycloidal compression and variable compression width of snow, for a towed wheel and the data for testing the model are presented. Secondly, the modelled and observed mobility results are reported. Finally, implications of the findings concerning the mobility of towed wheel in snow are discussed.

2 MOBILITY MODEL FOR A TOWED WHEEL IN SNOW

2.1 Introduction

The model for motion resistance of a towed wheel in snow presented here, was accomplished with Mathcad 6.0 mathematical software (Mathcad... 1995). Besides its computational capabilities, the software used is capable of producing mathematical notation of good readability. The notation system of Mathcad 6.0 therefore is used in the following.

There are a few peculiarities in the notation, deserving further clarification. Firstly, in assigning a variable or constant, a colon-equal-to sign (:=) is used instead of the equal-to sign, whereas the normal equal-to sign is used in the meaning of boolean equal-to and to announce the computed value of a variable. Secondly, if boolean operators are used in defining a variable or constant, the definitions are preceded by a vertical bar. Thirdly, three dots at the end of a line of mathematical expression means, that the expression is continuing on the next line.

Due to the three dimensional nature of the problem, a Cartesian co-ordinate system is used throughout the model (Figure 3, p. 21). The sign of pressure divided into components follows the sign of the y- and z-axes. The positive direction of torque is the direction rotation producing forward motion. Resulting y- and z-forces are treated as positive values.

2.2 Model development

2.2.1 Snow compression geometry

In order to model the motion resistance of a towed wheel in snow, the motion of a non-deforming circle is first examined. A point on the circumference of a circle follows a cycloidal path as the wheel rolls on a straight line. The parametric representation of the cycloid equation at zero slip is the following (Bajpai et al., 1989):

$$y(\theta) := r \cdot (\theta - \sin(\theta)) \tag{1}$$

$$z(\theta) := r \cdot (1 - \cos(\theta)) \tag{2}$$

where r = Undeformed radius of circle or wheel, m
$y(\theta)$ = y co-ordinate of cycloid
$z(\theta)$ = z co-ordinate of cycloid
θ = Rotation angle of circle, rad.

Cycloidal compression of snow has earlier been proposed by Blaisdell (1981). In the present model, the snow in contact with the wheel is assumed to follow the cycloidal compaction path up to the point, where the shear strength of snow is exceeded. Thereafter the compaction is assumed to take place in the direction of the wheel normal.

Wheel slip is 'a measure of relative movement at the mutual contact surface of the traction or transport device and the surface which supports it...' (ASAE... , 1995) or , according to ISTVS standards, 'an indication of how the speed of the traction elements differs from the forward speed of the vehicle' (International... ,1977). If the speed of the traction elements is less than the forward speed of the vehicle, ISTVS standards use the term skid instead of slip. The absence of relative movement or speed difference is denoted by zero slip according to both ASAE and ISTVS definitions. The ISTVS slip/skid definition is used in this work. In the present work, both ISTVS-defined skid and slip are covered by the term slip, so that negative values denote wheel skid and positive values wheel slip (Equation 3). To sum up, the present definition of slip covers values from +1 for an immobilized rotating wheel to –1 for a locked-up wheel with forward velocity. Instead of velocities, slip can defined in terms of distances travelled, as well.

In wheel operation, some amount of slip is usually present. Due to motion resistance, a towed wheel is usually unable to maintain zero slip in relation to the ground, but is operating in negative slip (Equation 3, upper expression). The cycloid equation must be reformulated correspondingly, so that slip has an effect on the first term of the y co-ordinate equation, defining the linear motion (Equations 4 and 5). For the sake of simplicity, the wheel is first assumed cylindrical, and an infinitely narrow cross section is examined.

$$i = \begin{cases} \dfrac{r_0 \cdot \omega - v}{v} & \text{if } v > r_0 \cdot \omega \\ \dfrac{r_0 \cdot \omega - v}{r_0 \cdot \omega} & \text{if } v \le r_0 \cdot \omega \end{cases} \qquad (3)$$

$$y_i(\theta) = \begin{cases} \dfrac{r_0 \cdot \theta}{i + 1} - r_0 \cdot \sin(\theta) & \text{if } -1 < i < 0 \\ r_0 \cdot (1 - i) \cdot \theta - r_0 \cdot \sin(\theta) & \text{if } 0 \le i \le 1 \end{cases} \qquad (4)$$

$$z_i(\theta) = r_0 \cdot (1 - \cos(\theta)) \qquad (5)$$

where i = Wheel slip
r_0 = Zero condition rolling radius of wheel, m (See p. 18)
v = Linear velocity, m s^{-1}
$y_i(\theta)$ = y co-ordinate of cycloid of a slipping wheel
$z_i(\theta)$ = z co-ordinate of cycloid of a slipping wheel
ω = Angular velocity, rad s^{-1}.

In reality, vehicle tyres are subject to deformation. The wheel-soil interaction model proposed by Baladi and Rohani (1984) was chosen to describe wheel deformation. In the model, the difference between the z co-ordinates of the trailing edge of the contact path and the undeformed wheel at $\theta=2\cdot\pi$ is equal to tyre deflection d_t (Figure 1). Being based on circles, the model is well-suited for the purpose in hand, although it is not ideally realistic in describing the deformation. Baladi and Rohani describe the contact surface between the wheel and the soil as an arc of an imaginary circle with a radius R equal to or larger than the undeformed radius r of the actual wheel (Figure 1). The centre of the circle is located at the intersection of the vertical line through trailing edge of the soil contact, point A, and the bisector of the angle AOB.

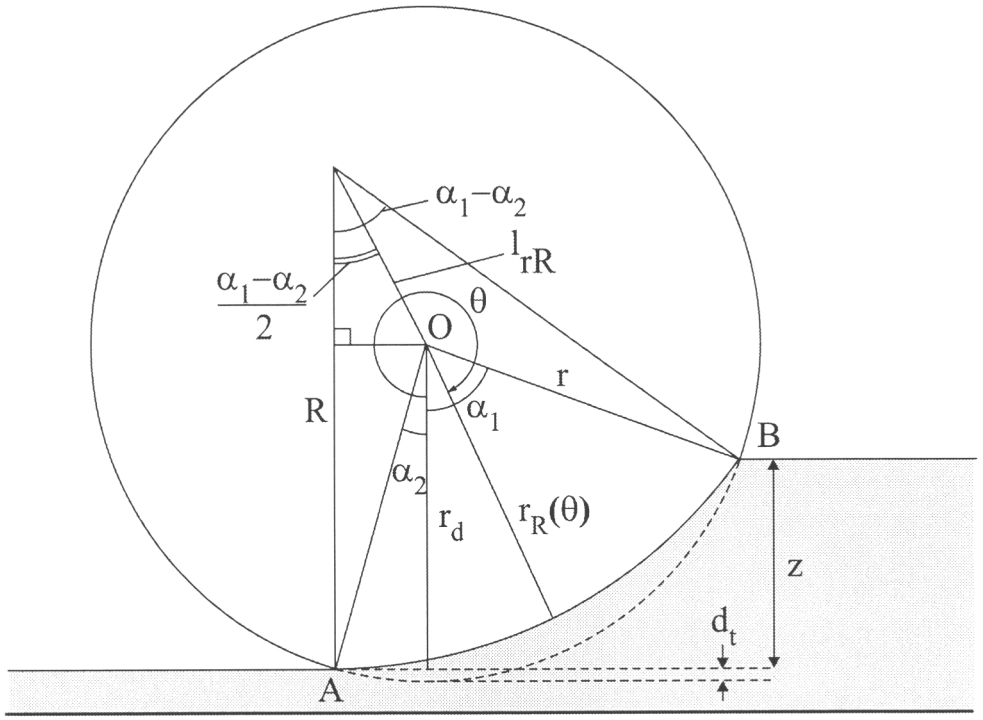

Figure 1. Soil-wheel interaction model presented by Baladi and Rohani (1984).

From the geometry of Figure 1, the following equations can be written:

$$\alpha_1 := \operatorname{acos}\left(\frac{r_d - z}{r}\right) \tag{6}$$

$$\alpha_2 := \operatorname{acos}\left(\frac{r_d}{r}\right) \tag{7}$$

$$R := \frac{z}{1 - \cos(\alpha_1 - \alpha_2)} \tag{8}$$

where r_d = Deflected radius of wheel, m
R = Radius of the wheel-soil contact circle, m
z = Wheel sinkage, m
α_1 = Leading contact angle, rad
α_2 = Trailing contact angle, rad.

Consequently, radius and deformation of the deformed wheel can be expressed as a function of rotation angle θ (Equations 9 and 10). In Equation 9, the distance between the wheel centre and the contact surface circle centre l_{rR} is solved from the right angled triangle in Figure 1. In the model, leading contact angle α_1 must be greater or equal to trailing contact angle α_2, and the minimum entry angle of wheel-snow contact θ_e is assumed to be greater or equal to $3\cdot\pi/2$.

$$r_R(\theta) = l_{rR}\cdot\cos\left(\pi - \Delta_\theta(\theta)\right) + \frac{1}{2}\cdot\sqrt{4\cdot l_{rR}^2\cdot\cos\left(\pi - \Delta_\theta(\theta)\right)^2 + 4\cdot R^2 - 4\cdot l_{rR}^2} \tag{9}$$

$$d_R(\theta) = r - r_R(\theta) \tag{10}$$

where $d_R(\theta)$ = Deformation of wheel, m
l_{rR} = Distance between the wheel centre and the contact surface circle centre, m
$r_R(\theta)$ = Deformed radius of wheel, m
$\Delta_\theta(\theta)$ = Angle between the bisector of $(\alpha_1+\alpha_2)$ and the radius corresponding to rotation angle θ, rad.

Next, the equation of cycloid for a deformed wheel with slip must be formed. The model by Rohani and Baladi is assumed to define wheel geometry in the present model. However, determination of true rolling radius for a deformable

wheel is difficult, resulting in difficulties in defining slip. The concept of zero condition rolling radius (r_0) (Upadhyaya et. al 1988, ASAE..., 1995) has been proposed to overcome these difficulties. Zero torque condition rolling radius, defined as the distance travelled by wheel, rolling with zero input torque, during one rotation divided by $2 \cdot \pi$, is applied in the model for a towed wheel. Zero condition rolling radius is always specified with respect to a surface condition. ISTVS standards (International... ,1977) define zero condition rolling radius on a rigid surface. The equation of cycloid for a deformed wheel with slip is given by Equations 11 and 12. The first term of the y co-ordinate equation, defining the linear motion, is affected by the rolling radius r_0 and slip of the wheel, whereas the second term for the rotary motion is defined solely by the deformed radius and the rotation angle. In the case of the z co-ordinate equation, the first term, giving location of the wheel axle, is defined by the deflected radius, whereas the rotary motion term is formed in a manner similar to that in the y co-ordinate equation.

If snow compaction is assumed to take place along the cycloid (Figure 2), the angle between the pressure due to compaction and z-axis can be determined by taking the derivatives of the cycloid y and z co-ordinates (Equation 13). If the derivative of $z_{iR}(\theta)$ is equal to zero, the trajectory is horizontal. To avoid problems arising from division by zero in this case, the angle is given the value $\pi/2$. Further, the sharp angle between the cycloidal pressure and the tangent of the wheel is given by Equation 14.

$$y_{iR}(\theta) := \begin{cases} \dfrac{r_0 \cdot \theta}{i+1} - r_R(\theta) \cdot \sin(\theta) & \text{if } -1 < i < 0 \\ r_0 \cdot (1-i) \cdot \theta - r_R(\theta) \cdot \sin(\theta) & \text{if } 0 \le i \le 1 \end{cases} \tag{11}$$

$$z_{iR}(\theta) := r_d - r_R(\theta) \cdot \cos(\theta) \tag{12}$$

$$\alpha(\theta) := \begin{cases} \dfrac{\pi}{2} & \text{if } \dfrac{d}{d\theta} z_{iR}(\theta) = 0 \\ \operatorname{atan}\left[\dfrac{\frac{d}{d\theta} y(\theta)}{\frac{d}{d\theta} z(\theta)} \right] & \text{otherwise} \end{cases} \tag{13}$$

$$\delta(\theta) = \frac{\pi}{2} - \alpha(\theta) - \beta(\theta) \tag{14}$$

where $y_{iR}(\theta)$ = y co-ordinate of cycloid of a deforming slipping wheel
$z_{iR}(\theta)$ = z co-ordinate of cycloid of a deforming slipping wheel
$\alpha(\theta)$ = Angle between cycloidal pressure and z-axis, rad
$\beta(\theta)$ = Sharp angle between wheel tangent and y-axis, rad
$\delta(\theta)$ = Sharp angle between cycloidal pressure and wheel tangent, rad.

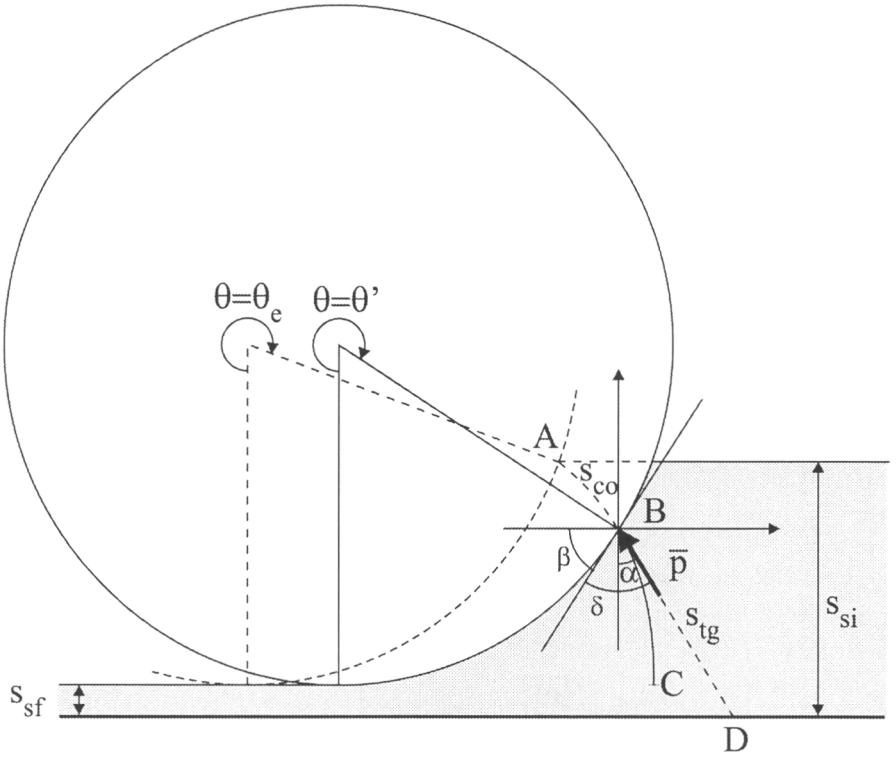

Figure 2. Cycloidal compression of snowpack with initial snow depth s_{si} by an undeformed wheel with i=0. Measures in conjunction with cycloidal compression: A to C= cycloidal trajectory, A to B= compression accomplished at $\theta=\theta'$ (s_{co}), B to D= snowpack length in the direction of cycloid tangent (s_{tg}), A to D= initial length of snowpack in compression at $\theta=\theta'$ (s_{coi}), s_{sf}= final length of compressed snow cover.

2.2.2 Tyre model

A lot of computing capacity is needed in handling a three dimensional tyre model. Therefore, although the model proposed here is basically three dimensional, several simplifying assumptions are made in the following. Tractor drive tyre, with its typical chevron lugged tread, was simplified by

excluding lugs from the geometry of the model. This was accomplished by defining the unloaded radius r as an average of the radius over carcass and radius over lugs, weighted by their respective proportions of area on tyre surface. The cross section of the tyre tread in contact with snow was assumed to be elliptical, with axes a and b (Figure 3). Deflection is assumed to take place mainly in the elliptical part, with proportions p_{da} and p_{db} of the deflection d_R changing the axes. Hence, the deformed axes of the ellipse are defined as follows:

$$a_{dR}(\theta) = a + p_{da} \cdot d_R(\theta) \tag{15}$$

$$b_{dR}(\theta) = b - p_{db} \cdot d_R(\theta) \tag{16}$$

where a, b = Ellipse axes, m
$a_{dR}(\theta)$ = Deformed a-axis, m
$b_{dR}(\theta)$ = Deformed b-axis, m
p_{da} = Proportion of tyre deformation taking place in the direction of a-axis
p_{db} = Proportion of tyre deformation taking place in the direction of b-axis.

Due to the elliptical cross section and cycloidal motion, the angle between compression pressure and the tyre surface is bound to vary according to the angle of rotation θ and the eccentric angle of the ellipse σ. Therefore, the width of the tyre surface able to hold the snow for compression at a specific rotation angle is determined by the friction coefficient between tyre and snow. In the latter, this is called the friction condition.

Let us first imagine plane τ, touching the tyre surface at the intersection of wheel radius $\bar{R}$ and plane axes T_1 and T_2 (Figure 3). Axes T_1 and T_2 touch the ellipse of tyre cross section at point $(a \cdot \cos(\sigma), b \cdot \sin(\sigma))$. The slope of axis T_2 in respect to ellipse a-axis, equal to $\tan(\gamma(\theta,\sigma))$, is determined by the derivatives of the ellipse coordinates. Also the angle between the ellipse normal, i.e. the component of pressure perpendicular to plane τ, and the component of $\underline{p}$ressure perpendicular to T_2 equals to $\gamma(\theta,\sigma)$, given by Equation 17. Pressure $\underline{p}$ can be divided into components parallel (Equation 18) and perpendicular (Equation 19) to T_2, the former belonging and the latter not belonging to the plane τ. Further, the component perpendicular to T_2 has a component in plane τ (Equation 20).

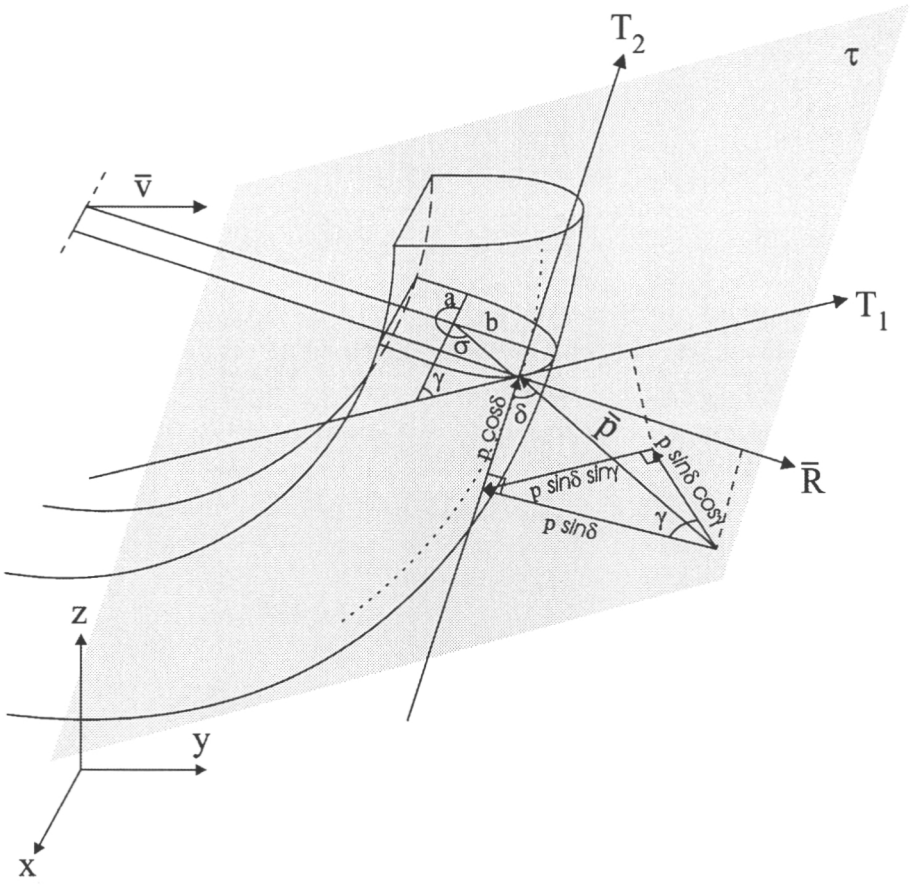

Figure 3. Division of compression pressure $\bar{p}$ into components on the surface of a tyre tread with elliptical cross-section

$$\gamma(\theta,\sigma) = \operatorname{atan}\left(\frac{b\, dR(\theta)}{a\, dR(\theta)\cdot\tan(\sigma)}\right) \tag{17}$$

$$\left| \bar{p} \parallel T_2 \right| = p\cdot\cos(\delta(\theta)) \tag{18}$$

$$\left| \bar{p} \perp T_2 \right| = p\cdot\sin(\delta(\theta)) \tag{19}$$

$$\left| \bar{p} \perp T_2 \in \tau \right| = p\cdot\sin(\delta(\theta))\cdot\sin(\gamma(\theta,\sigma)) \tag{20}$$

where $\bar{p} \parallel T_2$ = Component of pressure $\bar{p}$ parallel to axis T_2
$\bar{p} \perp T_2$ = Component of pressure $\bar{p}$ perpendicular to axis T_2
$\bar{p} \perp T_2 \in \tau$ = Component of $\bar{p} \perp T2$ in plane τ
$\gamma(\theta,\sigma)$ = Angle between ellipse a-axis and T_1 at eccentric angle σ and rotation angle θ, rad
σ = Eccentric angle of the ellipse, rad.

Pressure $\bar{p}$ can now be divided into components parallel (Equation 21) and normal (Equation 22) to plane τ, and friction condition formed (Equation 23).

$$| \bar{p} \parallel \tau | = \sqrt{[p \cdot \cos(\delta(\theta))]^2 + [p \cdot \sin(\delta(\theta)) \cdot \sin(\gamma(\theta,\sigma))]^2} \quad (21)$$

$$| \bar{p} \perp \tau | = p \cdot \sin(\delta(\theta)) \cdot \cos(\gamma(\theta,\sigma)) \quad (22)$$

$$\mu \cdot | \bar{p} \perp \tau | = | \bar{p} \parallel \tau | \quad (23)$$

where $\bar{p} \parallel \tau$ = Component of pressure $\bar{p}$ parallel to plane τ
$p \perp \tau$ = Component of pressure p perpendicular to plane τ
μ = Friction coefficient.

If friction coefficient is assumed to be a function of rotation angle, a limit angle $\gamma_{lim}(\theta)$ exists, giving the angle per rotation angle, after which the friction is no longer able to hold the snow for compression, but instead snow begins to slide along the tyre surface, i.e. the friction condition is no longer met. The limit angle is obtained by first replacing $\gamma(\theta,\sigma)$ by $\gamma_{lim}(\theta)$ in Equations 21 and 22, then substituting Equations 21 and 22 into Equation 23, and finally solving for $\gamma_{lim}(\theta)$ (Equation 24). The corresponding eccentric angle $\sigma_{lim}(\theta)$ is solved from Equation 17 by substituting $\gamma_{lim}(\theta)$ for $\gamma(\theta,\sigma)$ (Equation 25).

At the angle of rotation where compression starts (θ_{ss}), i.e. the snow stops sliding along the tyre surface in the middle of the tread ($\sigma=3 \cdot \pi/2$), $\gamma_{lim}(\theta)$ is equal to zero, and hence $\sin(\delta(\theta) \cdot [1+\mu(\theta)^2]^{0.5}$ must be equal to 1. θ_{ss} can thus be solved from Equation 26. The real compression start angle θ_{cs} is equal to θ_{ss}, except if θ_{ss} is smaller than entry angle θ_e, when θ_{cs} naturally is assigned the value of θ_e. The effect of lugs in determining the start of compression is not taken into consideration due to the complexity of the phenomena. With the deep sinkage of wheel with lugs angled at $\pi/4$ rad, the angle between a lug and the direction of snow sliding on the tyre surface is small near θ_{cs}, therefore the

ability of the lugs to hold snow to a great extent in this region of rotation is assumed to be rather limited, and is thus overlooked.

$$\gamma_{lim}(\theta) := \begin{cases} 0 & \text{if } \sin(\delta(\theta)) \cdot \sqrt{1 + \mu(\theta)^2} \le 1 \\ \left(\operatorname{acos}\left(\dfrac{1}{\sin(\delta(\theta)) \cdot \sqrt{1 + \mu(\theta)^2}} \right) \right) & \text{otherwise} \end{cases} \tag{24}$$

$$\sigma_{lim}(\theta) := \begin{cases} \dfrac{3 \cdot \pi}{2} & \text{if } \sin(\delta(\theta)) \cdot \sqrt{1 + \mu(\theta)^2} \le 1 \\ \left(\operatorname{atan}\left(\dfrac{b_{dR}(\theta)}{a_{dR}(\theta) \cdot \tan\left(\gamma_{lim}(\theta)\right)} \right) + \pi \right) & \text{otherwise} \end{cases} \tag{25}$$

$$\sin\left(\delta\left(\theta_{ss}\right)\right) \cdot \sqrt{1 + \mu_{p0}^2} - 1 := 0 \tag{26}$$

where $\gamma_{lim}(\theta)$ = Limit angle between ellipse a-axis and T_1 meeting the friction condition at rotation angle θ, rad

θ_{ss} = Rotation angle meeting the friction condition at $\sigma = 3 \cdot \pi/2$, rad

$\mu(\theta)$ = Friction coefficient at rotation angle θ

μ_{p0} = Friction coefficient at zero normal pressure

$\sigma_{lim}(\theta)$ = Limit eccentric angle of the ellipse meeting the friction condition at rotation angle θ, rad.

2.2.3 Calculation of compression pressure

Plate load tests are generally used in describing the pressure-sinkage relationship of snow (Wong 1989). The pressure-sinkage model proposed by Wong (1989) was selected for the application due to its ability to realistically predict the maximum sinkage, i.e. predicted maximum sinkage does not generally exceed initial snow cover depth. In an in-situ plate load test situation, the snow is compressed vertically against the ground. In this model, compression is assumed to follow the cycloidal path, until snow shear strength is exceeded, and thereafter in the direction of wheel normal. The compression immediately after the entry angle θ_{cs} often does not fulfil the conditions for cycloidal compression, since normal pressure is low, and shear strength may be exceeded. The area of discrepancy is small, and it is omitted in the following. In addition to reduce the execution time of the model, pressure due to compression is calculated assuming it was initiated at θ_{cs} across the tread.

Let us again return to the cylindrical wheel, and examine an indefinitely narrow cross section of it. In the region of cycloidal compression, the snow is being compressed in the direction of the tangent of the cycloid (Figure 2, page 17). Hence, the direction of compression deviates from z-axis throughout the contact region almost exclusively. The magnitude of deviation changes constantly, and the tangential length of the snowpack in compression, as opposed to snowpack depth in vertical compression, is given by Equation 27. The length of the arc of a plane curve can be calculate with an application of definite integration (Bajpai et al., 1989). This yields to Equation 28 for calculating the length of cycloidal compression already accomplished at a specific angle of rotation. The initial length of the snowpack in compression at a specific angle of rotation, i.e. the compressed length plus the tangential length, is given by Equation 29.

$$s_{tg}(\theta) := \frac{z_t(\theta)}{\cos(\alpha(\theta))} \tag{27}$$

$$s_{co}(\theta) := \int_{\theta_{cs}}^{\theta} \sqrt{\left(\frac{d}{d\theta} y_{iR}(\theta)\right)^2 + \left(\frac{d}{d\theta} z_{iR}(\theta)\right)^2}\, d\theta + s_{cop} \tag{28}$$

$$s_{coi}(\theta) := s_{co}(\theta) + s_{tg}(\theta) \tag{29}$$

where $s_{co}(\theta)$ = Length of compression accomplished at rotation angle θ, m
s_{cop} = Length of compression on the previous passes, m
$s_{coi}(\theta)$ = Initial length of snowpack in compression at rotation angle θ, m
$s_{tg}(\theta)$ = Snowpack length from wheel surface to ground along the tangent of the cycloid at rotation angle θ, m
$z_t(\theta)$ = The height of tyre circumference from the ground at rotation angle θ, m
θ_{cs} = Rotation angle where snow compression starts, rad.

In Wong (1989), the pressure-sinkage relationship is determined by performing the plate load test with plates of two radii, r_1 and r_2, in the snow type of interest. The radii of the plates should be in the order magnitude of the vehicle running gear loading surface radius. The pressure-sinkage relationship has the form of Equation 30 (Wong 1989), where the parameters p_w and z_w, the latter defining

the sinkage asymptote of the curve (See Figure 5, page 44), are derived from the data (Equations 31 and 32).

$$p := p_w \cdot -\ln\left(1 - \frac{z}{z_w}\right) \tag{30}$$

$$p_w := k_{p1} + r_p \cdot k_{p2} \tag{31}$$

$$z_w := k_{z1} + \frac{k_{z2}}{r_p} \tag{32}$$

where $k_{p1}, k_{p2}, k_{z1}, k_{z2}, p_w, z_w$ = Parameters
p = Pressure, Pa
r_p = Compression plate radius, m
z = Compression plate sinkage, m.

Since the maximum length in cycloidal compression is greater than the vertical snowpack depth, the asymptote of the curve z_w from the plate load data can not be used directly for defining the pressure in cycloidal compression. To calculate the asymptote in cycloidal compression $z_{wrn}(\theta)$ (Equation 33), the relationship of z_w to initial snowpack depth in plate load test was determined for both plate radii and this relationship was also assumed to be applicable to cycloidal compression since the maximum snowpack length $s_{coi}(\theta)$ did not differ from the vertical snowpack depth to a great extent. With two sets of values of p_w and z_w, the values for k_{p1}, k_{p2}, $k_{z1}(\theta)$ and $k_{z2}(\theta)$ can now be determined (Equations 34 to 37).

$$z_{wrn}(\theta) := s_{coi}(\theta) \cdot rel_{rn} \tag{33}$$

$$k_{p1} := -\left(\frac{p_{wr1} \cdot r_2 - p_{wr2} \cdot r_1}{r_1 - r_2}\right) \tag{34}$$

$$k_{p2} := \frac{-p_{wr2} + p_{wr1}}{r_1 - r_2} \tag{35}$$

$$k_{z1}(\theta) := -\left(\frac{-z_{wr1}(\theta) \cdot r_1 + z_{wr2}(\theta) \cdot r_2}{r_1 - r_2}\right) \tag{36}$$

$$k_{z2}(\theta) = \frac{r_1 \cdot r_2 \cdot \left(z_{wr2}(\theta) - z_{wr1}(\theta)\right)}{r_1 - r_2} \tag{37}$$

where $k_{z1}(\theta)$ = Parameter k_{z1} at rotation angle θ
$k_{z2}(\theta)$ = Parameter k_{z2} at rotation angle θ
p_{wrn} = Parameter p_w with compression plate radius r_n
r_1 = Radius of smaller compression plate, m
r_2 = Radius of larger compression plate, m
rel_{rn} = Relation of maximum sinkage to snow depth in plate loading test with plate radius r_n (n=1,2)
$z_{wrn}(\theta)$ = Parameter z_w with plate compression radius r_n at rotation angle θ.

Due to the increased final length of accomplished compression, the original plate radii can not be used, and the applicable plate radius for calculating the pressure in cycloidal compaction has to be determined with Equation 38. In Equation 38, Δr_p denotes an infinitely small term, subtracted in order to keep the operand of logarithmic function in Equation 39 greater than zero. Any rotation angle in the range of wheel-snow contact may be used in Equation 38. Finally, the pressure in cycloidal compression with plate of radius r_{pc}, when snow shear strength is not exceeded, is calculated with Equation 39. Equation 39 is obtained by substituting Equations 34 to 38 into Equation 30. The pressure can further be divided into components according to Equations 40 to 43.

$$r_{pc} = \frac{k_{z2}(\theta_p)}{s_{max}(\theta_p) - k_{z1}(\theta_p)} - \Delta r_p \tag{38}$$

$$p(\theta) = \left(k_{p1} + r_p \cdot k_{p2}\right) \cdot -\ln\left[1 - \frac{s_{co}(\theta)}{k_{z1}(\theta) + \frac{k_{z2}(\theta)}{r_{pc}}}\right] \tag{39}$$

$$p_y(\theta) = p(\theta) \cdot \sin(\alpha(\theta)) \tag{40}$$

$$p_z(\theta) = p(\theta) \cdot \cos(\alpha(\theta)) \tag{41}$$

$$p_n(\theta) = p(\theta) \cdot \sin(\delta(\theta)) \tag{42}$$

$$p_{tg}(\theta) = p(\theta) \cdot \cos(\delta(\theta)) \tag{43}$$

where $p(\theta)$ = Compression pressure, Pa
$p_n(\theta)$ = Component of compression pressure normal to wheel, Pa
$p_{tg}(\theta)$ = Component of compression pressure tangential to wheel, Pa
$p_y(\theta)$ = y-component of compression pressure, Pa
$p_z(\theta)$ = z-component of compression pressure, Pa
Δr_p = An infinitely small fraction of compression plate radius, m
r_{pc} = Largest allowable compression plate radius in pressure calculations, m
θ_p = Rotation angle in r_{pc} calculations, rad.

As mentioned previously, the snow in contact with the tyre at angles greater than θ_{cs} is assumed to follow the cycloidal path until tangential pressure exceeds the shear strength of snow. Omitting shear displacement for the sake of simplicity, the angle of rotation, where the shear strength of snow is exceeded, may be calculated by solving Equation 44 for $\theta\tau$. At rotation angles from $\theta\tau$ to θ_{max}, pressure $p(\theta\tau)$ is used, since the pressure calculation model possibly can not deal with the increasing values of accomplished compression $s_{co}(\theta)$ for following passes.

$$\tau_{max}(\theta_\tau) - \left| p_{tg}(\theta_\tau) \right| = 0 \qquad (44)$$

where $\tau_{max}(\theta\tau)$= Maximum shear strength at $\theta\tau$, Pa
$\theta\tau$ = Rotation angle where tangential pressure exceeds the shear strength of snow, rad.

2.2.4 Form and width of tyre compressive surface

Due to the elliptical cross section of the tyre tread, the varying angle of the pressure, and the varying friction coefficient, the true starting angle of compression and pressure are bound to change across the tread and with the angle of rotation. Taking this into consideration in the calculation of pressure would make the model unsuitable for operative use with current portable computers. The solution of dealing with the varying starting angle of compression was presented earlier (p. 23). Hence, the form of the compressive surface of the tyre is assumed to be cylindrical, with width determined by the tyre-snow friction on the elliptical cross section of the tread (Equation 45). Snow pack depth and tyre rotation angle may also limit the width (Equation 46).

$$b_{\mu}(\theta) := -2 \cdot a_{dR}(\theta) \cdot \cos\left(\sigma_{lim}(\theta)\right) \qquad (45)$$

$$b_{co\mu}(\theta) := \begin{cases} b_{max}(\theta) & \text{if } b_{\mu}(\theta) > b_{max}(\theta) \\ b_{\mu}(\theta) & \text{otherwise} \end{cases} \qquad (46)$$

where $b\mu(\theta)$ = Tyre-snow friction defined compressive width of tyre, m
$b_{co}\mu(\theta)$ = Maximum tyre-snow friction defined compressive width of tyre, m
$b_{max}(\theta)$ = Maximum tyre-snow contact width for given snow depth and wheel rotation angle, m

If the tyre-snow friction coefficient is assumed to decrease with increasing pressure and increasing temperature (Mellor 1975), the friction condition for compressive width (Equation 45) would result in narrow, and in some conditions even non-existing compressive surface near $\theta=2 \cdot \pi$, this is later referred to as the $2 \cdot \pi$ region of the tyre. This is firstly due to the fact, that the tyre tread cross section is assumed to maintain its curved form even when deflected. Secondly, the model does not take into account the internal bonding of snow and its bonding against the ground. Therefore, a minimum of compressive width, subject to the limitations set by snow depth and tyre width, is assumed for the $2 \cdot \pi$ region (Equation 47). The $2 \cdot \pi$ region consists of rotation angles greater than $2 \cdot \pi$ and rotation angles with $\delta(\phi)$ greater than $\pi/2$. The latter means, that the pressure forces snow into the v formed by the angled lugs, and the lugs are thus assumed to be capable of retaining the snow. The combined compressive width through the rotation angles of snow contact is finally given by Equation 48.

$$b_{2\pi}(\theta) := \begin{cases} b_{2\pi lim}(\theta) & \text{if } \theta > 2 \cdot \pi \\ b_{2\pi lim}(\theta) & \text{if } \delta(\theta) > \frac{\pi}{2} \end{cases} \qquad (47)$$

$$b_{co}(\theta) := \begin{cases} b_{2\pi}(\theta) & \text{if } b_{2\pi}(\theta) > b_{co\mu}(\theta) \\ b_{co\mu}(\theta) & \text{otherwise} \end{cases} \qquad (48)$$

where $b_{co}(\theta)$ = Tyre compressive width, m
$b_2\pi(\theta)$ = Tyre width at $2 \cdot \pi$ region, m
$b_2\pi_{lim}(\theta)$ = Minimum tyre width at $2 \cdot \pi$ region, m.

2.2.5 Snow not subject to compression

Following on from the definitions set previously, part of the snow is not subject to compression by the tyre, since the friction condition is not met, hence some snow is assumed to flow past along the tyre surface. This occurs through the width of the tyre at angles of snow contact smaller than θ_{cs}, and with varying width on the shoulders of the tread on the area of compression.

The flow of snow forms flow resistance pressure p_f. For determining the total flow resistance force, laminar approximation is used (Leyton 1975). The section of the tyre, along which snow flows between rotation angles θ_e and θ_{cs}, is modelled as a flat inclined surface. The cross sectional area A_f of the inclined surface in the direction of y-axis is used in calculating the resisting force (Equation 49).

$$F_f = -p_f A_f \tag{49}$$

where A_f = Cross sectional area, m^2
F_f = Flow resistance force, N
p_f = Flow resistance pressure, Pa.

The fact, that snow initially flows in the direction of the y-axis and that the wheel is rotating, is assumed to result in snow shearing along the surface of the tyre in the region of snow flow. The snow is sheared under the normal pressure component $p_{fn}(\theta)$ of flow resistance pressure p_f, resulting in shear stress $p_{ftg}(\theta)$ (Equations 50 and 51). Shearing occurs between the lugs, which is taken into account by multiplying the maximum shear strength by the share of carcass area of total tread area. The effect of shear displacement is omitted for the sake of simplicity. Friction on the faces of the lugs is also neglected. The fact, that the direction of snow flow is likely to deviate when it meets the tyre surface, and the above mentioned simplifications are represented by the empirical parameter $c_{f\tau}$. The shearing of snow in the flow region results in force components in y- and z-directions, as well as a braking torque (Equations 52 to 54).

$$p_{fn}(\theta) = p_f \sin(\beta(\theta)) \tag{50}$$

$$p_{ftg}(\theta) = p_f \cos(\beta(\theta)) \tag{51}$$

$$F_{\tau y} = 2 \cdot s_c \cdot c_{f\tau} \cdot r_f \cdot a \cdot \int_{\theta_e}^{\theta_{cs}} \tau_f(\theta) \cdot \cos(\beta(\theta))\, d\theta \qquad (52)$$

$$F_{\tau z} = 2 \cdot s_c \cdot c_{f\tau} \cdot r_f \cdot a \cdot \int_{\theta_e}^{\theta_{cs}} \tau_f(\theta) \cdot \sin(\beta(\theta))\, d\theta \qquad (53)$$

$$T_\tau = -2 \cdot s_c \cdot c_{f\tau} \cdot r_f^2 \cdot a \cdot \int_{\theta_e}^{\theta_{cs}} \tau_f(\theta)\, d\theta \qquad (54)$$

where $c_{f\tau}$ = Parameter
$F_{\tau y}$ = y-component of shear force in the flow region, N
$F_{\tau z}$ = z-component of shear force in the flow region, N
$p_{ftg}(\theta)$ = Component of flow resistance pressure tangential to tyre surface, Pa
$p_{fn}(\theta)$ = Component of flow resistance pressure normal to tyre surface, Pa
r_f = Average radius of the tyre in the flow region, m
s_c = Share of tyre carcass of total tread area
T_τ = Torque induced by snow shearing in the flow region, N m
θ_e = Rotation angle at wheel-snow contact entry, rad
$\tau_f(\theta)$ = Shear strength of snow under the normal pressure $p_{fn}(\theta)$, Pa.

2.2.6 Calculation of resultant forces in z- and y-directions

The forces on the tyre-snow contact surface in the model are due to snow compaction, shearing and flow, as well as the internal motion resistance due to tyre deformation. Several force components, such as flow resistance on the area of partial compression, are omitted. Ideally, the determination of the area of the tyre surface would call for the double integration of the radius in a spherical polar co-ordinate system over the rotation angle and the ellipse eccentric angle. Since the form of the compressive surface of the tyre is assumed to be cylindrical, cylindrical co-ordinate system is used instead (Arfken 1970), and the radius is integrated over the rotation angle and the compressive width. Hence, the resulting forces in z- and y-directions are obtained with Equations 55 and 56.

$$F_z := \int_{\theta_{cs}}^{\theta_{max}} \int_0^{b_{co}(\theta)} r_R(\theta) \cdot p_z(\theta)\, dx\, d\theta + F_{\tau z} \quad (55)$$

$$F_y := \int_{\theta_{cs}}^{\theta_{max}} \int_0^{b_{co}(\theta)} r_R(\theta) \cdot p_y(\theta)\, dx\, d\theta + F_{\tau y} + F_f + F_{r0} \quad (56)$$

where F_{r0} = Internal motion resistance of tyre, N
F_y = Force acting on tyre in y-direction, N
F_z = Force acting on tyre in z-direction, N
θ_{max} = Maximum rotation angle of wheel-snow contact, rad.

2.2.7 Calculation of resultant torque

In the model, the components of resultant torque acting on the wheel axle are the torque due to compaction, shearing and flow of snow, as well as the internal torque of the tyre due to deformation. It should be noted that in reality, several other components also exist.

The deformation torque T_{r0}, i.e. torque due to internal motion resistance, is determined by multiplying the measured motion resistance, acting against the direction of travel, on hard surface by the deformed radius over lugs. As mentioned earlier, the surface, along which snow flows, is modelled as flat and inclined. The torque T_f induced by the flow resistance is determined by multiplying the flow resistance with the perpendicular distance from the centre of the wheel to the centre of the plane of flow.

The determination of the torque generated by the compaction pressure is simplified by converting the pressure to act on the undeformed radius r of the wheel. This is accomplished by first calculating the perpendicular distance from the centre of the wheel and the line of action of pressure $\bar{p}$. Then pressure $\bar{p}$ is moved along the line of action so, that it acts on the undeformed radius r, and the angle between the pressure and the radius is used for calculating the tangential component. The resultant torque is given by Equation 57.

$$T = r^2 \cdot \int_{\theta_{cs}}^{\theta_{max}} \int_{0}^{b_{co}(\theta)} p(\theta) \cdot \frac{s_M(\theta)}{r} \, dx \, d\theta \ldots + T_\tau + T_f + T_{r0} \qquad (57)$$

where $s_M(\theta)$ = Perpendicular distance from the line of action of pressure to wheel axle, m
T = Torque acting on tyre axle, N m.
T_f = Torque induced by the flow resistance of snow, N m
T_{r0} = Torque induced by the internal motion resistance of tyre, N m

Finally, when the model is used for determining motion resistance, the conditions for a towed wheel must be fulfilled. In practice this means, that the entry angle and slip are varied until F_z is equal to the vertical wheel load and T is equal to zero.

2.2.8 Calculation of the following passes

For the first pass in snow, the snow-tyre interaction was modelled by using a straight contact surface cross section instead of the true elliptical cross section. The straight surface was assumed to have the outer radius of the ellipse. In reality only a fraction of snow is compressed to the extent suggested by the model. On the following pass, the tyre is travelling in the snow compressed during the previous pass. The depth of the compressed snow on the following pass is likely to be greater than the minimum compressed thickness of the preceding pass. In addition to the aforementioned difference in cross section form, which is firstly due to the remoulding action of the trailing edge of the contact path and secondly the snow collapsing into the rut bottom from its side walls after the passing tyre on the previous pass and in front of the passing tyre on its present pass. Thirdly, the following pass may not have exactly same course as the previous one. Some of the factors having an effect on the snow depth of the following pass are random in nature.

In order to take these factors into account when determining the snow depth for the following pass, the average distance between the modelled elliptical tread surface cross section and the a-axis of the ellipse across the compressive width is calculated (Equation 58) and subtracted from the b-axis of the ellipse (Equation 59). The difference $diff_b$ in b-direction of the ellipse is then added to the final length of compressed snow cover (s_{sf}, see Figure 2, p. 19) to get the snow depth s_{sn} for the following pass (Equation 60). The length of compression

that the snow material has experienced, when the following pass starts to compress it further, is determined by subtracting $diff_b$ from the length of compression on the previous pass at $\theta\tau$ (Equation 61).

$$b_{avg} := \frac{\int_0^{\frac{b_{2\pi}(\theta_{max})}{2}} y_{el}(x, \theta_{max})\, dx}{\frac{b_{2\pi}(\theta_{max})}{2}} \tag{58}$$

$$diff_b := b - b_{avg} \tag{59}$$

$$s_{sn} := s_{sf} + diff_b \tag{60}$$

$$s_{cop} := s_{co}(\theta_\tau) - diff_b \tag{61}$$

where b_{avg} = Average perpendicular distance between ellipse circumference and a-axis at $\theta=\theta_{max}$, m
$diff_b$ = Snow depth and compression length adjustment for the following pass, m
s_{cop} = Length of compression on the previous passes, m
s_{sn} = Snow depth on the following pass, m
s_{sf} = Final length of compressed snow cover, m
$y_{el}(x,\theta)$ = y co-ordinate of ellipse, m.

The contact path on the following passes is mainly in the $2 \cdot \pi$ region, where compression width of the tyre is assumed constant already on the first pass. To speed up the execution of the model, variable compression width $b_{co}(\theta)$ was therefore replaced by constant compression width b_{coc} for the following passes. Hence, forces acting in z- and y-directions as well as torque could be calculated by single integration as follows:

$$F_z = b_{coc} \cdot \int_{\theta_{cs}}^{\theta_{max}} r_R(\theta) \cdot p_z(\theta)\, d\theta + F_{\tau z} \tag{62}$$

$$F_y = b_{coc} \cdot \int_{\theta_{cs}}^{\theta_{max}} r_R(\theta) \cdot p_y(\theta)\, d\theta + F_{\tau y} + F_f + F_{r0} \qquad (63)$$

$$T = b_{coc} \cdot r^2 \cdot \int_{\theta_{cs}}^{\theta_{max}} p(\theta) \cdot \frac{s_M(\theta)}{r}\, d\theta \ldots + T_\tau + T_f + T_{r0} \qquad (64)$$

where b_{coc} = Constant compression width of tyre, m.

2.3 Model operation

The operation of the model starts by feeding in the data on snow cover (including measured mechanical behaviour), tyre data (including deflection behaviour and parameters), forward speed and wheel normal load, in addition to setting initial values for wheel slip and entry angle (See model flowchart in Appendix 1, p. 100). The model then calculates wheel geometry and kinematics, compaction and flow resistance pressure as well as corresponding tyre widths. Finally resultant torque, vertical force and horizontal force are calculated. If resultant vertical force is equal to wheel load and the resultant torque is zero within desired tolerances, a solution for the pass in question is reached. Otherwise, slip and/or entry angles are manually given new values, and the execution of the programme is repeated until an acceptable solution is reached. An accepted solution consists of input values of entry angle and slip, and output values of sinkage, final length of compressed snow cover and motion resistance. If a further pass is to be calculated, the programme gives values for initial snow depth and state of compression for the next pass. Slip and entry angle must be given new initial values manually.

The rolling radius r_0 used in the model is determined as the zero torque condition rolling radius measured during the empirical test runs on compacted shallow snow of low-density on frozen sand. In the above mentioned measuring conditions motion resistance is low and the tyre can be assumed to operate near zero slip and under rubber-snow friction conditions, and the normal load is supported by both the carcass and the lugs. Using the selected zero torque condition results in fixing the zero point of the slip scale and including the influence of snow deformation in slip values. The method should result in a good approximation of rolling radius on snow covered ground if compared to measurements made on concrete or on deformable sand.

3 MATERIAL AND METHODS

3.1 Introduction

To test the mobility model described in Chapter 2, a set of empirical data was collected. Since one of the main objectives of the present work was to examine the effect of snow properties on mobility, the mobility measurements were conducted outdoors in snow bins filled with one single snow type on each occasion. Considerable quantities of snow material would have been needed for tests with a real forest machine tyre, inevitably resulting in large time consumption in snow handling. Taking into consideration the unstable nature of snow, it was decided to use tyres of diameter 0.425 m in the tests to minimise time expenditure per snow type.

The mobility studies, with the associated plate load and shear strength tests, were conducted in six different snow types, called mobility test snow types M1 to M6 as referred to later. In order to make a difficult task easier, the effect of grain bonding and age of snow were overlooked, and classification of snow was based mainly on its physical properties. Selected layers of the natural snow cover, at different stages of metamorphism, were extracted through the course of the winter manually by shovel and laid in the bins. A series of six consecutive test runs with an instrumented towed scale model axle was conducted in each snow type to find out the mobility parameters and the effect of snow properties on them.

In addition to mobility tests, rubber-snow interface friction and flow resistance of snow were assessed. These tests were carried out in two additional sets of snow types, namely friction test snow types Fr1 to Fr4 and flow resistance test snow types Fl1 to Fl5. Snow material for friction and flow tests was collected according to the same principles as for the mobility test snow material. All snow types are numbered in the order of increasing density.

Study arrangements, as well as the measuring of mobility and snow parameters, are described in detail in the following chapters.

3.2 Selection, sampling and handling of snow

Since the effect of snow properties on mobility was of prime interest, studying mobility in natural snow cover, normally consisting of several snow types, was excluded. Layers of the natural snow cover, consisting of snow types M1 to M6, were utilised instead.

First, a vertical profile of the natural snow cover was exposed by shovelling. Clearly separable layers were identified visually and one layer was chosen to be examined. Since the field study was carried out throughout the course of

winter, several snow types could be selected. These ranged from recently fallen snow from the top of the snowpack (M1), through to layers of fine- (M2) and medium-grained (M3 and M4) old snow from the centre of the snowpack and medium- and coarse-grained wet spring snow from the bottom of the snowpack (M5 and M6) (See photos in Figure 5, p. 44). Snow possibly overlying the top of the layer of interest was shovelled off, and the snow to be used in the experiments was shovelled into 50 dm^3 buckets. The natural structure of the snow was thus broken into smaller aggregates. Particular attention was paid not to include any irregularities, such as ice or aggregates of the neighbouring snow layers, in the snow to be removed. Occasional irregularities or foreign aggregates were removed manually.

Next, the collected snow material was either tipped into the bins, or subjected to the measurements described in Chapter 3.3. The snow sampled for property measurements was taken from the same location and treated similarly as the snow in the bins for mobility studies. Finally, the snow in the bins was trimmed by either dragging a piece of plywood along the top of the bin (snow depth 0.15 m), or with a shovel equipped with runners to keep the desired distance from the ground (snow depths 0.05 m and 0.10 m).

3.3 Measuring of snow properties

The selection of measurements to be performed was aimed to include all the important snow properties thought to have an effect on mobility, that could be assessed with reasonable effort and time expenditure in field conditions. Some of the measurements were intended to be applicable to operational use in solving mobility-related questions, whilst others were of more complex nature. All measurements were performed during the single loading cycle. The accuracy of the measurements is given in Chapter 3.5, p. 42.

Snow temperature was measured with a semiconductor temperature probe connected to a datalogger. The probe was pushed into the snow material either in the bin, or in the bucket containing the snow for the assessment of properties.

Density was measured by two means. Firstly, a rectangular (dimensions length 0.148 m, width 0.135 m, height 0.05 m, dimensions are given in the same order throughout the text) box with removable sliding lid was employed. The volume of the box was 1.0 dm^3 . When measuring, the lid was removed, and the box was filled by tipping snow in the same way as when filling the bins. The excess snow was trimmed by sliding the cover back on, and the box was cleaned externally with a brush. Finally the box was weighed with a laboratory or spring scale. The method is called snow scale later in the text.

Secondly, density, together with the free water content of snow, was assessed with a microwave snow probe, the Snow Fork (Snow Fork Measures...). The probe measures the resonant frequency, attenuation, and bandwidth of the fork-shaped antenna pushed into the snow material. The principle of the measurement is explained in detail in Tiuri et al. (1984) and Sihvola and Tiuri (1986). Density and free water content are determined on the basis of the real and imaginary part of relative dielectric constant of snow, according to Equations 65 to 70 (Snow Fork...). The operating principle is based on theory, but the constants were empirically determined by calibrations in snow (Tiuri et al., 1984).

For snow fork measurements, the snow was tipped from one bucket into another, so as to replicate the filling of the mobility snow bins. The bucket was lifted on top of the natural snow cover in order to eliminate the mineral ground from interfering with the measurement. Ten measurements in vertical direction were performed per bucket. Snow scale measured density was used in determining free water content to improve the accuracy of the measurement.

$$\varepsilon' := \left(\frac{f_{air}}{f}\right)^2 \tag{65}$$

$$B_{air} := 0.02 \cdot (f - 56) \tag{66}$$

$$\varepsilon'' := \frac{B - B_{air}}{f} \cdot \varepsilon' \tag{67}$$

$$w_{vol} := -0.06 + \sqrt{0.06^2 + \frac{\varepsilon''}{0.0075 \cdot f}} \tag{68}$$

$$\rho_f := -1.2142857 + \sqrt{1.2142857^2 - \frac{1 + 8.7 \cdot w_{vol} + 70 \cdot w_{vol}^2 - \varepsilon'}{0.7}} + w_{vol} \tag{69}$$

$$w := \frac{w_{vol}}{\rho_f} \tag{70}$$

where B = Bandwidth in snow, MHz
B_{air} = Bandwidth in air, MHz
f = Resonant frequency in snow, MHz
f_{air} = Resonant frequency in air, MHz
w = Free water content of snow, %wgt
w_{vol} = Free water content of snow, %vol

ε' = Real part of relative dielectric constant of snow
ε'' = Imaginary part of relative dielectric constant of snow
ρ_f = Snow density assessed by snow fork, kg m^{-3}.

Grain size and grain shape were assessed by first photographing in-situ, and measuring later indoors. The method shortened the in-situ time and presumably increased accuracy. Snow from the sample bucket was taken with a spoon and placed on a sheet of clear plastic attached to a camera tripod. A millimetre scale was placed on the plastic holder to appear in the photos. The aim was to get a uniform one-layer sample. This was accomplished by tapping the spoon as the sample was being tipped to the holder, and vibrating the holder by tapping hence spreading the specimen. The specimen was lit by a flash aimed $\pi/4$ rad from below. The magnification varied from 1.5x to 2.0x, according to the grain size.

The grain photographs were converted into computer images, and Image-Pro Plus Version 1.0 image processing software (Image... 1993) was employed for measuring. Grains were measured manually along the main axis (largest dimension), in the direction perpendicular to it, and twice crosswise at an angle of $\pm \pi/4$ rad to the main axis. This allowed for the assessment of the greatest and smallest dimension, the average dimension, the relation of the standard deviation of the dimensions to the average of the dimensions, used for describing the heterogeneity of the measures (inverse of roundness), as well as the length-to-width ratio of the grain. The thickness of the grain in the perpendicular direction to the plane of measurements could not be assessed with this method.

The magnification of the images varied from 11x to 48x, according to the grain size. Pixel resolution varied correspondingly from 0.036 mm/pixel to 0.009 mm/pixel. Visual distinguishing between grains in aggregates was often difficult, as a result of which only grains with reliably definable borderlines were selected for measurement.

The pressure-sinkage relationship (Bekker 1969) was measured by performing a plate loading test in a closed snow bin. The bin dimensions were 0.50 m · 0.50 m · 0.15 m, whilst the lid had a hole for plate access. Upon filling the bin, the lid was removed and the snow sample was tipped in, and subsequently trimmed with a sheet of plywood. After closing the lid, an electric motor driven penetrometer (Sirviö 1994), equipped with plates 0.07 m and 0.11 m in diameter, was placed on top of the bin, and the plates were driven into the snow sample through the hole. The penetrometer was equipped with electric measuring of plate load and sinkage.

Shear strength was assessed with a direct shear test (Craig 1992). The sample container of the direct shear device was a cylinder with length of 0.168 m and diameter of 0.100 m. The piston compressing the sample against the closed end of the cylinder, and thus producing the normal pressure, was loaded by a separate pneumatic cylinder. The sample cylinder was cut at 0.025 m from the bottom end. The shearing was accomplished by displacing the lower part in a radial direction with an electric motor driven screw drive. The pressure of the pneumatic cylinder, shearing force, as well as piston and shear displacements were measured electrically. Upon testing, the snow was taken from the sample bucket with a cup, and tipped to the sample container of the direct shear device. Two to three normal pressure levels ranging from 55 to 195 kPa at the start of the test were used for each snow type. The effect of decreasing shear area on normal pressure during the test was taken into account when determining the true normal pressure on the shear surface.

The assessment of the effect of snow properties on rubber-snow interface static friction was based on earlier unpublished data by the author. Rubber-snow interface friction was measured with bevameter (Ala-Ilomäki 1991). The snow sample handling procedure and the snow bin were similar to those used in the plate loading test described previously. A smooth butyl rubber-covered annulus was rotated on the snow sample for one rotation. Normal pressures, accomplished by applying weights on the bevameter structure, of 42 kPa, 65 kPa, and 88 kPa were used. The annulus was rotated hydraulically and the corresponding torque was measured electrically. The maximum friction after the start of rotation was used to exclude the effect of the possible freezing of the interface (Conant and Liska 1960).

The flow resistance of snow was measured by pushing a rubber-coated half ellipsoid along a linear trajectory in a snow bin. The half ellipsoid axis dimensions, a=0.060 m and b=0.035 m, were similar to those of the modelled cross-section of the tyre. The bin dimensions were 1.50 m · 0.30 m · 0.30 m. The top and the rear end (in the direction of travel of the half ellipsoid) of the bin were open. The half ellipsoid was attached to a rod via a load cell, which sensed the flow resistance. The rod was guided to ascertain linear trajectory and was actuated manually. The maximum rod travel was 1 m.

Two flow resistance test procedures were used. Firstly, measurements were performed with three different velocity levels, and secondly, with velocity decreasing from maximum to zero. Flow resistance measurements were conducted on an occasion separate to the main body of the measurements. Due to limited resources, only snow density as well as ambient and snow temperature were measured. Furthermore, the same snow sample was used per snow type for the ten measurements. After each measurement, the structure of the sample was loosened by first shovelling it from the bin into a bucket, and then tipping it back into the bin.

3.4 Mobility test rig

The mobility test rig, i.e. the mobility equipment built for the study, consisted of an instrumented cart with a towed axle, guide car, and support frame (Figure 4). The frame was connected to an agricultural tractor via an A-frame and a three point linkage mounted timber skidding winch. The tractor, while remaining stationary itself, pulled the guide car along the top of the stationary support frame via the cable of the winch at an average speed of 0.42 m s^{-1}. The speed for each test run was assumed constant, since the resisting force on the cable was relatively low, and the cable on the drum was fixed so, that it was wound on the same layer throughout the length of the test track.

A stiff axle, with wheels of 0.425 m diameter, was attached to the cart with roller bearings. Friction losses due to the bearings were considered negligible (Gieck and Gieck 1990). The cart served as a platform for the ballast weights used for loading the axle. At the front of the cart was an instrumented tow bar. The tow bar had two coaxial steel tubes, one welded to the frame of the cart, the other pivoted to the supporting vertical post of the guide car. Brass slide journals were inserted between the tubes and lubricated to reduce friction. The tubes were connected together via a HBM U 9 load cell (Kraftaufnehmer... 1988), which thereby transmitted the force exerted in pulling the axle. The coaxial construction of the tow bar together with the knuckle eye couplings at both ends of the cell eliminated transverse forces from loading the cell. Axle rotation was measured with an inductive proximity switch pulsed by a chain sprocket with 19 teeth. The accuracy of the performed measurements is given in Chapter 3.5, p. 42.

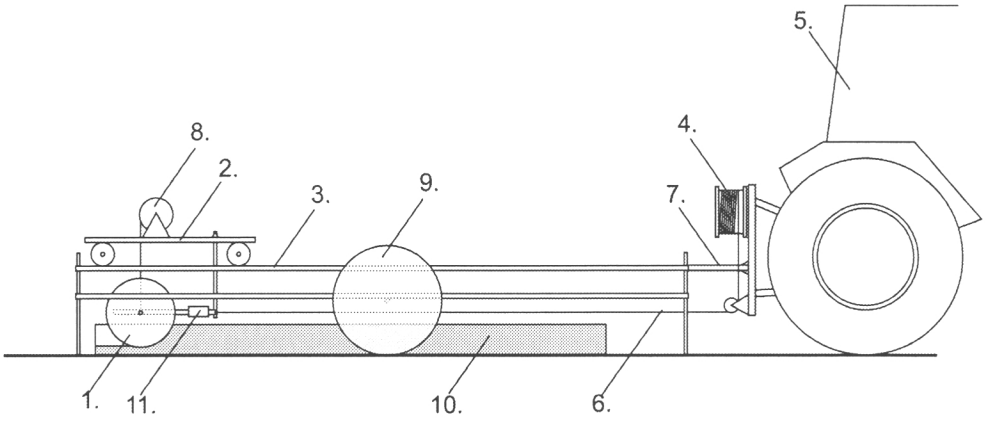

Figure 4. Schematic figure of the mobility test rig. 1=Cart axle and wheels, 2= Guide car, 3=Support frame, 4=Skidding winch, 5=Agricultural tractor, 6=Winch cable, 7=Connecting A-frame, 8=Winch for lifting the axle, 9=Wheels for transporting the test rig, 10=Snow bins, 11=Load cell.

Since forestry applications were of prime interest, tires with tread design typically used in logging machiney tyres were chosen. Hence, Trelleborg 4.00-8 4 P.R. tyres with manufacturer's tread pattern design code 63 (Agricultural...) were mounted on the axle. The tyres were of cross ply construction, and had a typical tractor drive tyre tread pattern with lugs forming a chevron. The dimensions of the lugs were 75 mm · 12 mm · 12 mm, they were angled at 45° and over lapped in the centre of the tread. The measured unloaded radius over lugs was 212.5 mm, whilst unloaded section width was 120.0 mm, and the unloaded section height was 95.0 mm. The tyres were inflated to 200 kPa. Tyre deflection was measured on loose sand and on frozen ground, the first used for operation in snow, and the latter for test track profile measurements. Deflected weighted radius measured on loose sand (r_d) was 194.6 mm with the applied axle load. Rolling radius was determined under zero net torque condition (Upadhyaya et. al, 1988) on loose sand (r_0=200.2 mm), frozen sand (r_0=204.1 mm) and frozen sand covered by snow (r_0=194.7 mm). The latter was determined as an average of the passes which supposedly had the slip closest to zero (passes 5 in 0.05 m and passes 4 to 6 in 0.10 m of M1 snow), and a zero torque condition rolling radius (r_0) for use later.

The ballast weights on the cart were located so that the centre of gravity was exactly above the axle. Thus, there was no vertical load at the end of the tow bar. The axle weight of the cart was 2.6 kN on all test drives. The resulting theoretical average wheel-soil contact pressure with sinkage of 0.15·r, as determined according to Terrängmaskinen (1981), was 50 kPa, which is at the lower end of the range typically encountered with forest machinery.

The support frame was rested on two wheels, which enabled the system to be transported between test tracks. Each four corners had adjustable support legs to improve stability during the experiments. The top of the support frame served as a pair of rails for the guide car. The tow bar of the cart was connected to the guide car via an adjustable vertical post. The support frame was connected to the skidding winch by means of an A-frame. The winch cable was hooked to the tow bar of the cart.

One snow bin, measuring 2.5 m · 0.5 m · 0.15 m, for both cart wheels was set on the ground. The test drives covered a 1.8 m section in the centre of the bins. The bins were of wooden construction and had no bottom, i.e. the ground was levelled so, that the walls formed a tight fit against it to hold the snow inside. The guide car, riding on top of the support frame, was equipped with a winch for lifting the cart axle off the ground. This enabled the axle to be returned airborne to the beginning of the test track after each pass. Multiple passes could thus be performed without the return disturbing the snow in the wheel ruts.

The support frame was levelled to horizontal to serve as the reference of all the vertical position measurements. The height of the support frame was determined by measuring the distance from the corners to the ground surface manually with a measuring tape. The distance from the guide car to the cart axle and, respectively, to the tow bar-vertical post -pivot, was measured with cable extension linear position transducers. The ground profile of the test track was measured by pulling the cart along the bare test track (snow depth=0). The drive on bare track gave data on the vertical location of the wheel axle in respect to the support frame along the track, and the location of the track surface could then be determined by adding the deflected wheel radius to the axle location. The same measuring principle was used in determining the vertical location of the lowest point of the wheel when operated in snow. As the vertical location of the track surface and lowest point of the wheel were known, the final length of compressed snow cover (s_{sf}, see Figure 2 on p. 19) under the wheel could be determined.

Pulling speed per test run, both in snow and bare track, was assumed to be constant. The resisting force on the cable was considered relatively low, and the cable on the drum was fixed so, that it was wound on the same layer throughout the length of the test track. Average speed per each test run was thus determined by starting and stopping the measurement at pre-determined points, and calculating the speed on the basis of travelled distance and the automatic recording of elapsed time. The position along the test track was then determined from average speed and elapsed time. The test arrangements allowed for geometrical corrections, as well as axle vertical location and the related data to be calculated.

In summary the following mobility model variables could be verified with the mobility rig measurements:

- wheel slip
- wheel sinkage
- final length of compressed snow cover (s_{sf}, see Figure 2 on p. 19)
- motion resistance.

3.5 Data acquisition, instrumentation and accuracy

Data acquisition in mobility measurements, the measurement of snow compressive and shear strength, as well as ambient- and snow temperature, was based on Campbell CR10 datalogger (CR10... 1990). A datalogger, rather than a microcomputer, approach was chosen for the data acquisition system because it could withstand both temperatures below freezing and substantial humidity, as well as occasional mechanical shocks, all present in field study conditions.

The datalogger provided the supply voltage for the transducers and sampled the output voltages at user-programmed rates. The data collected by the datalogger was down-loaded onto a portable PC. In order to maximise reliability, all the datalogger-based measurements were started and stopped with a manually operated switch.

The sampling rates of the measurements were chosen by taking into account the rather limited memory capacity of the datalogger. The result was quite satisfactory, however. The most critical rate was that of the motion resistance measurement, which was about four times the estimated resonant frequency of the test axle. Table 1 gives an overview of the datalogger-based measuring instruments and their accuracy, as well as the sampling rates used. The accuracy given in Table 1 is that of datalogger-transducer measuring chain, and thus it may be limited by the accuracy of the transducer or the resolution of the datalogger. If the accuracy is limited by the accuracy of the transducer as announced by the manufacturer, the corresponding source of information is given. In the case of the strain gauge transducers, manufacturer's accuracy data was given as a percentage of the nominal capacity. If the resolution of the datalogger is limiting the accuracy, or if the transducer is calibrated separately for a limited range of input, or if the transducer is made in-house by the Finnish Forest Research Institute (FFRI), the calibration method given by Doebelin (1990, pp. 55 to 58) was used in determining accuracy. The effect of temperature deviation from the reference temperature on sensitivity of the transducers was corrected according to manufacturer's specifications, when available, or determined empirically. The zero or no-load readings of the transducers were recorded in conjunction with each test.

Determination of wheel slip was based on time per one revolution and distance travelled. Average slip per snow type and number of pass was determined as an average of consecutive overlapping revolutions. The use of 19 consecutive pulses equal to one wheel revolution, improved the accuracy in the determination of slip. The absolute error of wheel slip, determined according to the guidelines presented in Doebelin (1990, pp. 58 to 67), was in the order of ± 0.05.

The microwave snow probe (Snow fork) was manufactured by a Finnish engineering agency, Insinööritoimisto Toikka. According to manufacturer's data, the liquid water content measurement range is 0 to 10 % vol with accuracy of ±0.15 % vol, and the density measurement range is 0 to 600 kg m^{-3}, with accuracy of ±2.5 kg m^{-3} (Snow Fork Measures...).

The resolution of the laboratory scale, used in weighing the snow scale box whilst defining snow density, was 0.1 g, but the accuracy in determining the content of the box was somewhat poorer, due to the snow residues on the box structures. The laboratory scale was, therefore, read to the closest g. Spring

scales, with resolution of ±5 g, were utilised in weighing the friction test and flow test snow samples.

Table 1. An overview of the datalogger-based measuring instruments and their accuracy (SG= strain gauge, FFRI=Finnish Forest Research Institute).

Measuring device	Variable(s)	Trans-ducer	Make and model	Accuracy (source or method)	Sampling rate, Hz
Temperature probe	Snow- and ambient temperature	Integrated-circuit sensor	National Semicond. LM 35	±0.5°C (LM 35... 1992)	0.5
Mobility rig	Motion resist. in snow	SG load cell	HBM U 9	±30 N per wheel (Doebelin 1990)	16.0
	Motion resist. on bare track			±9 N (Doebelin 1990)	16.0
	Axle rotation angle	Inductive proximity switch	Honeywell 921 LC5	±0.33 rad (Doebelin 1990)	16.0
	Axle height	Cable extension linear pos. transducer	FFRI	±0.66 mm (Doebelin 1990)	16.0
	Tow bar height			±0.35 mm (Doebelin 1990)	0.5
Snow compression tester	Compressive force	SG load cell	Kyova LM-100KA	±9.81 N (Load Cells... 1991)	32.0
	Compression depth	Inductive proximity switch	Honeywell 921 LC5	±1.5 mm (Doebelin 1990)	32.0
Snow shear tester	Shear force	SG load cell	DS 546 QD	±2.48 N (Z-Folded...)	32.0
	Shear displacement	Linear potentio-meter	Midori LP-200F	±0.3 mm (Precision... 1993)	32.0
	Sample height			±0.3 mm (Precision... 1993)	32.0
	Compressive air pressure	SG pressure transducer	DS LP 632	±6.4 kPa (Transducers...)	32.0
Bevameter	Snow-rubber friction	SG torque transducer	HBM T 4A	±0.5 Nm (Torque/Sqrew... 1987)	4.0
Snow flow resistance tester	Resisting force	SG load cell	DS 535 QD	±0.06 N (Transducers...)	32.0
	Linear position	Cable extension linear pos. transducer	FFRI	±1.01 mm (Doebelin 1990)	32.0

3.6 Field study sequence and loading speed of snow

After selecting the snow type to be studied, the field study proceeded in the following sequence. The measurements per each snow type were completed during one day. First, the mobility study equipment was set up on gravel field. In the mid-spring, when snow types 5 and 6 were examined, the gravel field was flooded, and the mobility study equipment had to be set up on asphalt. The properties of frozen gravel, on which the earlier tests were made, and asphalt were assumed to be similar enough for the purpose of the study. The assumption was based on several facts. Firstly, the wheels did not ideally contact with the ground. Secondly, the wheels were towed, so the ground-rubber friction did not play such an important role as would have been the case with a powered axle. Moreover, the difference in the friction properties between the surfaces was considered a lesser problem, than the presence of a layer of water. The support frame was levelled with a sprit level by adjusting the support legs. After levelling, the frame to ground distance at the four corners of the frame was measured.

After the equipment had been set-up, the scale of the position transducers was fixed at two separate positions by recording the reading with both the datalogger and measuring tape. In addition the zero reading of the load cell was recorded. The speed of the winch cable was set by adjusting the tractor engine speed with the help of a tachometer. Thereafter, track profile and motion resistance on bare track were measured.

Snow from the selected layer was extracted and the bins were filled. Then, a set of six consecutive passes per snow type was performed.

Finally, the properties of the studied snow type were determined, as described in Chapter 3.3. The loading speed used in determining the mechanical properties of snow together with the speed of loading induced by the test axle wheels are presented in Table 2. In the case of rubber-snow interface friction and snow shearing, the loading speed by the test axle varies.

Table 2. Typical loading speeds induced by the test axle wheels and the measuring devices.

Type of loading	Typical loading speed, m s^{-1}	
	Test axle wheel	Measuring device
Compression	0.2	0.021
Flow	0.42	0 to 4
Interface friction	0 to 0.47	0.042
Shearing	0 to 0.015	0.0024

3.7 Data processing and analysis

Part of the data from the measurements was treated by simply calculating the averages of the variables by snow type. This group included variables describing snow grain properties and snow density as well as free water content. Averages by snow type and by test drive or testing of sample were calculated in the case of snow and ambient temperature. Averages by test drive were calculated for the motion resistance of the axle. Motion resistance per one wheel was then obtained by dividing the axle motion resistance by two.

Owing to the displacement transducers of the mobility equipment, measuring the vertical location of the tow hitch and the axle, the relative angles of the various components of the mobility rig could be determined and their effect through geometry on the measured variables corrected. The horizontal frame structure of the mobility testing equipment, levelled prior to testing was used as reference. Likewise, the slope of the test track was taken into account in the calculation of motion resistance. Fourier transform (Kreyszig 1988, Mathcad... 1995) was used for filtering the effect of high frequency variations ($f > 10$ Hz), due to tyre lug pattern and the varying small irregularities of the ground surface, when determining the longitudinal profile of the test tracks. The filtering frequency was determined by multiplying the number of lugs per tyre by the rotational speed of the tyre.

A second group of data consisted of measurements, where a selected model was to be fitted. This was accomplished mainly by using the Nlin or Reg Procedures of SAS/STAT statistical software (SAS/STAT... 1994). This group included data from the pressure-sinkage test, shear strength test, rubber-snow interface friction test and snow flow resistance test. Models for the data from the first two tests were fitted separately for each snow type, whereas the two latter tests were performed in separate snow material, and a general model was therefore formed. With some snow types, there was considerable variation between the replications in pressure-sinkage and shear strength tests. Therefore, some outlying replications had to be excluded from the data in order to fit the models with reasonable results or to meet the convergence criterion of the statistical software. The number of replications given in Tables 8 and 9 (p. 48 and 50) is the actual number included in the fitting of the models.

The predictions of the mobility model were compared to the data of the empirical experiment. The sensitivity of the model was examined by changing the values of selected input parameters by ±5 % and determining the effect on the output variables wheel sinkage (z) and motion resistance coefficient (μ_r). The magnitude of the change was chosen according to the estimated accuracy in determining zero torque condition rolling radius. The reference values were

from the first pass in 0.15 m layer of M1 and M6 type snow. The selected input parameters were:

- snow properties: compressive strength (p-z relationship)
  maximum shear strength
  free water content
  density

- tyre properties: zero condition rolling radius
  tyre deflection
  tyre width and cross section ellipse a-axis.

4 Results

4.1 Ambient temperature and physical snow properties

During the mobility studies and the associated plate load and shear strength tests, measured ambient temperature varied from -7.5 to 5.5 °C whilst snow temperature ranged from -9.0 to 0.5 °C (Table 3).

Table 3. Measured ambient and snow temperature in mobility, plate load and shear strength tests.

Variable	Test	Snow type					
		M1	M2	M3	M4	M5	M6
Ambient temperature, °C	Mobility	-2.0	-5.5	-7.5	-1.5	3.5	1.0
	Plate load	-2.5	0.0	-2.0	-1.5	2.0	1.0
	Shear strength	0.5	-5.0	-2.5	-3.0	5.5	1.0
Snow temperature, °C	Mobility	-5.0	-9.0	-4.0	-6.0	-1.0	-1.0
	Plate load	-6.0	-8.5	-4.0	-3.5	-1.0	-1.0
	Shear strength	-3.5	-9.0	-3.5	-3.5	0.0	0.5

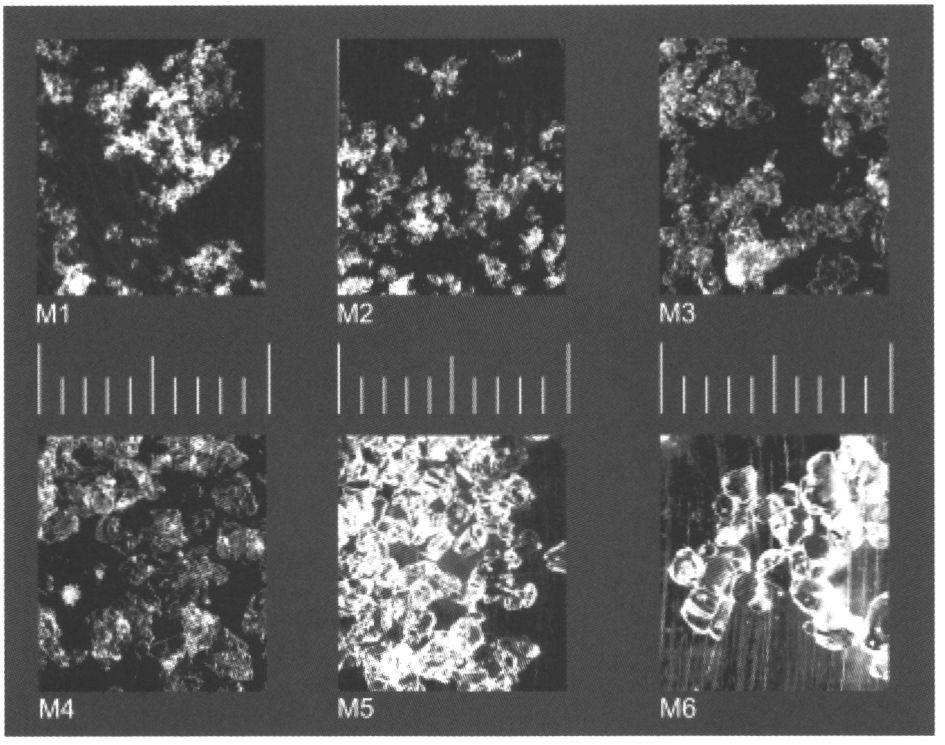

Figure 5. Grains from samples of snow types M1 to M6. Scale of photographs presented are to the mm.

The photographs of grains from samples of snow types M1 to M6 (Figure 5) give an overall idea of the variation in grain size and form between the different mobility snow types. Snow density was measured by both a snow scale and the microwave snow fork. In the following, the term 'snow density' or 'density' refers to snow scale measurements, unless otherwise stated. The density of the mobility snow types M1 to M6 varied from 230 to 491 kg m^{-3}, free water content from 1.5 to 9.8 % wgt, and average grain dimension from 0.24 to 1.21 mm. In snow type M5, the antenna of the snow fork was damaged and the readings were therefore not considered reliable. Since the ambient and snow temperature, as well as the physical properties of snow types M5 and M6 were relatively similar, the approximated free water content of 10 % wgt was used in the analysis for M5. Approximately five fold variation was experienced in grain dimensions between the snow types, whereas the variation in grain shape was much smaller. An overview of the physical properties of mobility snow types is given in Table 4.

Table 4. Physical snow properties in mobility, plate load and shear strength tests.

Variable	Statistic	Snow type					
		M1	M2	M3	M4	M5	M6
Density (scale), kg m^{-3}	$\bar{x}$	230	313	337	348	466	491
	s	11	16	9	10	17	16
	n	10	10	10	10	10	10
Density (fork), kg m^{-3}	$\bar{x}$	226	273	273	294	..	422
	s	39	20	27	14	..	63
	n	10	39	49	47	..	44
Free water content, % wgt	$\bar{x}$	2.7	1.5	2.6	3.1	..	9.8
	s	1.8	0.7	0.8	0.8	..	1.3
	n	10	39	49	47	..	44
Average grain dim., mm	$\bar{x}$	0.26	0.24	0.66	0.58	0.68	1.2
	s	0.06	0.09	0.24	0.18	0.24	0.4
	n	67	191	82	155	284	220
Greatest grain dim., mm	$\bar{x}$	0.34	0.32	0.92	0.80	0.86	1.4
	s	0.11	0.14	0.36	0.32	0.34	0.4
	n	67	191	82	155	284	220
Smallest grain dim., mm	$\bar{x}$	0.19	0.17	0.50	0.44	0.52	1.0
	s	0.06	0.07	0.22	0.16	0.22	0.4
	n	67	191	82	155	284	220
Hetero-geneity of measures, %	$\bar{x}$	22.7	23.5	25.1	23.1	19.3	13.0
	s	13.6	12.2	14.0	12.9	9.6	6.5
	n	67	191	82	155	284	220
Length-to-width of grain	$\bar{x}$	1.93	2.00	2.03	1.90	1.71	1.43
	s	0.81	0.87	0.91	155	0.53	0.31
	n	67	191	82	155	284	220

The snow fork under predicted density, when compared to snow scale measurements (Figure 6). Linear regression model for snow density, assessed by snow scale, and the corresponding statistics are presented in Equation 72 and Table 5.

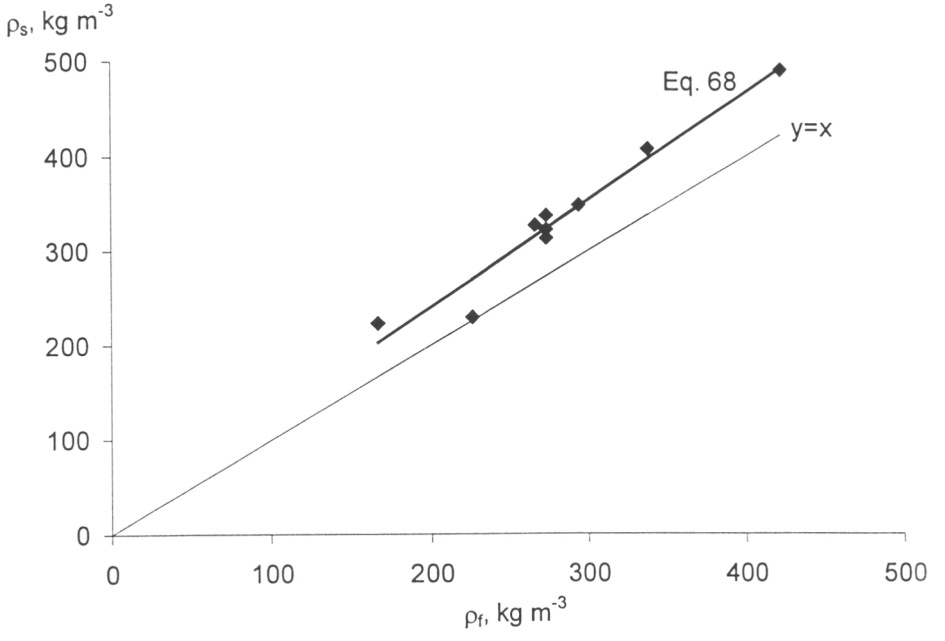

Figure 6. Average snow scale measured density ρ_s as a function of average snow fork measured density ρ_f.

Table 5. The statistics of snow scale density vs. snow fork density model.

Statistic	Parameter	
	a_ρ, kg m^{-3}	b_ρ
Estimate	13	1.136
Std. err.	28	0.096
T	0.48	11.9
Prob > |T|	0.6430	0.0001
	Model	
n	9	
Adj. R^2	0.95	
RMSE, kg m^{-3} *	19	

* Root Mean Square Error = $\left[\sum_{i=1}^{n}\left(y_i-\hat{y}_i\right)^2 \Big/ (n-k)\right]^{0.5}$

$$\rho_s = a_\rho + b_\rho \cdot \rho_f \quad (72)$$

where a_ρ, b_ρ = parameters
ρ_f = snow density assessed by snow fork, kg m^{-3}
ρ_s = snow density assessed by snow scale, kg m^{-3}.

Rubber-snow interface friction tests were conducted in conditions with ambient temperature ranging from -5.0 to 3.0°C and snow temperature ranging from -6.0 to -4.0°C. Density of the friction test snow types Fr1 to Fr4 varied from 223 to 327 kg/m^3, free water content from 1.0 to 2.9 % wgt, and average grain dimension from 0.33 to 0.70 mm. The snow fork data on snow type Fr2 was lost, and the free water content could therefore not be assessed. In the friction analysis of Fr2, the free water content of Fr4 was used, since the snow types had fairly similar physical properties and they were tested during the same day. Conditions in the rubber-snow interface friction tests are presented in Table 6.

Table 6. Conditions in the rubber-snow interface friction tests.

Variable	Statistic	Snow type			
		Fr1	Fr2	Fr3	Fr4
Ambient temp, °C	$\bar{x}$	-5.0	2.5	-0.5	3.0
Snow temp., °C	$\bar{x}$	-6.5	-8.0	-5.0	-4.5
Density (scale), kg m^{-3}	$\bar{x}$	223	287	323	327
	s	16	19	10	17
	n	65	50	21	50
Density (fork), kg m^{-3}	$\bar{x}$	167	..	273	266
	s	37	..	19	25
	n	191	..	42	67
Free water content, % wgt	$\bar{x}$	2.9	..	2.3	1.0
	s	1.1	..	0.7	0.7
	n	191	..	42	67
Average grain dim., mm	$\bar{x}$	0.33	0.39	0.70	0.46
	s	0.11	0.12	0.30	0.20
	n	223	168	152	212
Greatest grain dim., mm	$\bar{x}$	0.48	0.50	0.92	0.59
	s	0.20	0.18	0.40	0.27
	n	223	168	152	212
Smallest grain dim., mm	$\bar{x}$	0.24	0.30	0.54	0.37
	s	0.08	0.10	0.26	0.17
	n	223	168	152	212
Hetero-geneity of measures, %	$\bar{x}$	27.0	18.6	22.0	18.0
	s	14.9	9.8	10.4	8.7
	n	223	168	152	212
Length-to-width of grain	$\bar{x}$	2.06	1.68	1.81	1.64
	s	0.80	0.50	0.52	0.42
	n	223	168	152	212

The standard deviation and sample size of the datalogger-based temperature measurements are dependent on the sampling frequency, and are therefore not presented in Table 6. Generally, snow temperature when performing a test on a snow type was essentially constant, and standard deviation was within the measuring error.

A third set of snow types was formed from the flow resistance test snow types Fl1 to Fl5 (Table 7). The density of this group of snow types ranged from 120 to 470 kg m^{-3}. Ambient temperature during the tests varied from -4.5 to 1.0°C, and snow temperature from -4.0 to -0.5°C.

Table 7. Conditions in the flow resistance tests.

Snow type	Variable			
	Ambient temperature, °C	Snow temperature, °C	Density (scale), kg m^{-3} (n=10)	
	$\bar{x}$	$\bar{x}$	$\bar{x}$	s
Fl1	-4.5	-4.0	120	7
Fl2	-3.5	-4.5	310	11
Fl3	-2.5	-2.5	390	8
Fl4	0.0	-1.0	470	18
Fl5	1.0	-1.0	470	11

4.2 Mechanical snow properties

4.2.1 Pressure-sinkage relationship

The model selected for describing the pressure-sinkage relationship is presented in Chapter 2.2.3 (p. 23). Roughly four to six fold variation of pressure as a function of sinkage between the snow types was measured in the plate loading tests (Figure 7, Table 8 and Appendix 2 on p. 101). The pressure-sinkage relationship of the most compressible snow types M1 to M4 was rather similar, whereas the least compressible group was formed by snow types M5 and M6. The modelled maximum sinkage of the most compressible snow types was about 1.5 times that of the least compressible snow types.

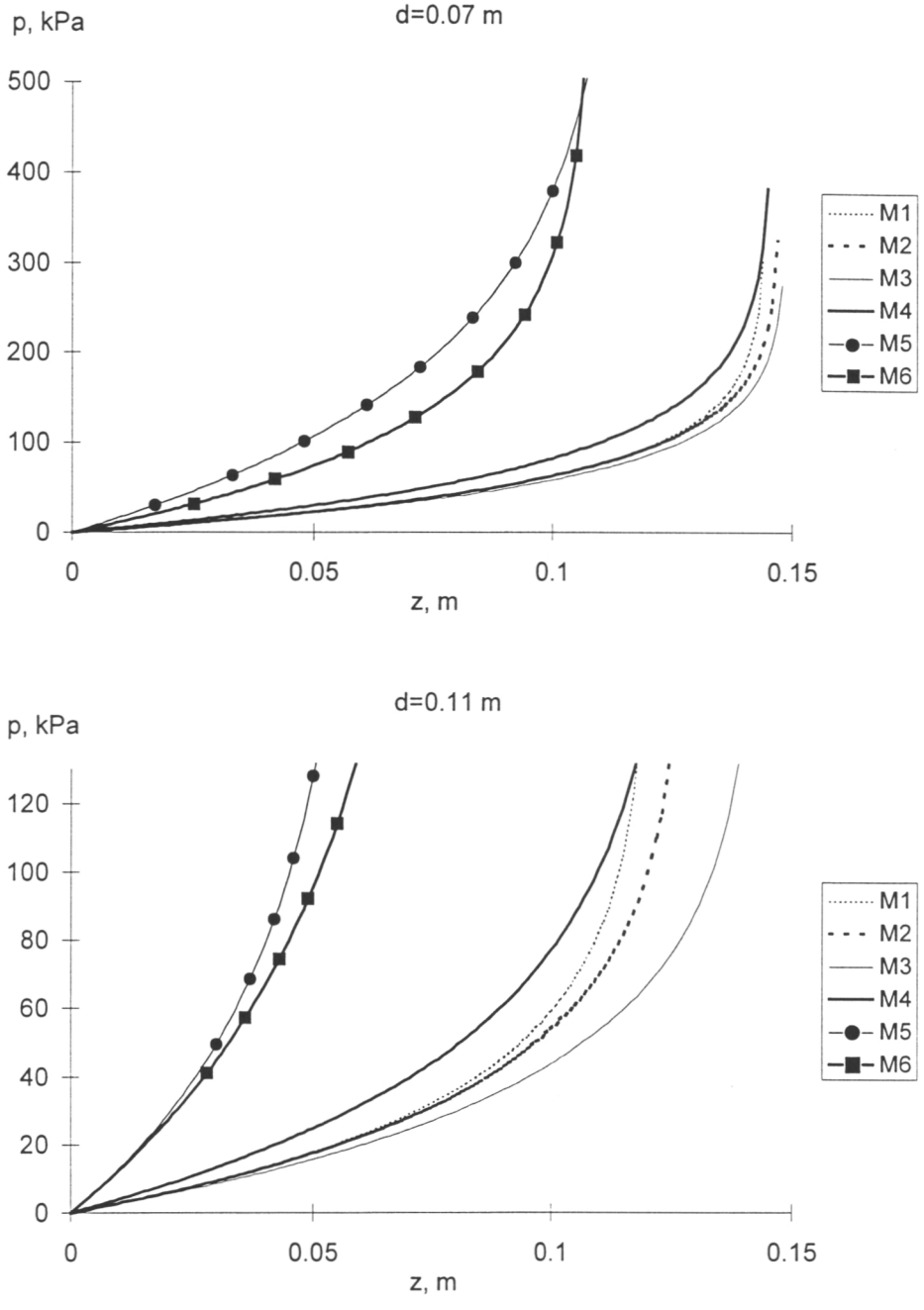

Figure 7. Modelled pressure (p) vs. sinkage (z) relationship with plate diameters 0.07 m and 0.11 m for snow types M1 to M6, when initial snow depth is 0.15 m.

Table 8. Parameter estimates of pressure-sinkage models for snow types M1 to M6.

Snow type	Plate diam., m	No. of replica-tions	Parameter				RMSE, kPa	n
			p_w, kPa		z_w, m			
			Estimate	Asymptotic std. err.	Estimate	Asymptotic std. err.		
M1	0.07	5	53.32	0.65	0.144	$0.09 \cdot 10^{-3}$	24.72	929
	0.11	5	33.17	0.50	0.120	$0.41 \cdot 10^{-3}$	8.41	824
M2	0.07	10	55.70	0.59	0.147	$0.09 \cdot 10^{-3}$	22.89	996
	0.11	10	35.30	0.54	0.128	$0.40 \cdot 10^{-3}$	10.38	881
M3	0.07	5	52.16	0.46	0.149	$0.04 \cdot 10^{-3}$	19.18	956
	0.11	5	36.42	0.58	0.143	$0.59 \cdot 10^{-3}$	8.82	974
M4	0.07	4	71.04	0.57	0.146	$0.17 \cdot 10^{-3}$	12.69	851
	0.11	3	49.22	1.14	0.126	$1.09 \cdot 10^{-3}$	7.66	543
M5	0.07	3	156.74	3.52	0.108	$1.10 \cdot 10^{-3}$	12.92	310
	0.11	4	71.77	3.01	0.060	$1.21 \cdot 10^{-3}$	9.16	335
M6	0.07	3	119.54	2.26	0.108	$0.68 \cdot 10^{-3}$	17.94	554
	0.11	2	90.22	9.59	0.077	$4.78 \cdot 10^{-3}$	12.40	192

4.2.2 Shear strength of snow

The model proposed by Oida (1979) (Equation 73) was used for describing the relationship of shear stress and shear displacement, since it allowed for the hump in shear strength at certain shear displacement, which is typical of the behaviour of snow in shearing. First, Oida's equation was fitted for each studied snow type and normal stress to determine the maximum shear strength (Table 9). The estimates of the other parameters were not utilised, since shear strain was omitted in the mobility model.

$$\tau = \tau_{max} \cdot K_r \left[1 - \frac{\sqrt{1 - K_r} \cdot \left(1 + \frac{\sqrt{1 - K_r} - 1}{K_r} \right)^{\frac{j}{K_w}}}{\sqrt{1 - K_r} \cdot \left(1 - \frac{2}{K_r} \right) + \frac{2}{K_r} - 2} \right] \cdot \left[1 - \left(1 + \frac{\sqrt{1 - K_r} - 1}{K_r} \right)^{\frac{j}{K_w}} \right] \quad (73)$$

where j = Shear displacement, m
K_w = Shear displacement at τ_{max}, m
K_r = Ratio of residual shear strength to maximum shear strength
τ = Shear strength, Pa
τ_{max} = Maximum shear strength, Pa.

Table 9. Parameter estimates of Oida's models for maximum shear strength of snow types M1 to M6 (*= assessed visually on the basis of the data).

Snow type	Normal pressure, kPa	No. of replica-tions	τ_{max}, kPa		n
			Estimate	Asymptotic std. err.	
M1	70	4	38.2	0.4	1616
	125	2	95.0	1.0	817
	180	3	119.0	1.4	1194
M2	60	5	34.3	0.5	893
	90	4	56.8	1.4	676
	125	4	82.1	1.6	667
M3	120	5	54.0	0.3	1471
	185	5	87.6	0.5	1255
M4	55	4	24.0	0.3	926
	125	4	65.0	0.6	913
	185	5	103.5	0.7	1157
M5	75	2	138*	-	-
	135	3	225*	-	-
	195	3	500*	-	-
M6	65	6	66.4	0.2	2474
	100	4	116.4	0.6	1619
	125	5	162.0	0.5	2641

Secondly, either a modified Coulomb's model (Equation 74) or an empirical model by the author (Equation 75) was fitted separately for each snow type to describe the relationship of maximum shear strength to normal stress in the normal pressure range of the data. Coulomb's model, fitted to the data of the dryer snow types, was modified in the sense, that apparently negative values of cohesion, represented by term a_τ, were allowed in the range of experimental data. This was motivated by the fact, that the data was lacking in low normal pressure observations, and non-linear behaviour was therefore possible. In the case of parameter a_τ less than zero, the model was fitted without the cohesion term in the normal pressure range below the data, since the structure of the snow was initially broken and cohesion was thus assumed zero.

$$\tau_{max} = a_\tau + p \cdot \tan(\phi) \tag{74}$$

$$\tau_{max} = b_\tau \cdot \exp(c_\tau \cdot p_n) \tag{75}$$

where a_τ, b_τ, c_τ = Parameters
p_n = Normal pressure, Pa
ϕ = Angle of internal friction, rad.

Three groups can be distinguished among the snow types when shear strength measurement results are examined (Table 9, Table 10, Figure 8 and Appendix 3 on p. 107). Snow types M3 and M4 had the least shear strength, followed by the group formed by snow types M1 and M2 with an angle of internal friction roughly one third higher. Non-linear behaviour of shear strength as a function of normal pressure was experienced with the group of the highest shear strength, snow types M5 and M6. Since the physical properties of snow types M5 and M6 were relatively similar, the shear strength of M6 at normal pressures in excess to 125 kPa was assumed to behave in a manner similar to M5, although no data was available. The maximum shear strength of this group was typically two to three times higher than the strength of types M1 and M2.

The behaviour of snow type M5 showed signs of strain hardening, as demonstrated by McClung (1977), and the shear displacement at maximum shear strength was high. Difficulties were encountered in assessing the maximum shear strength of snow type M5. In the first set of tests, its shear stress increased continuously up to shear strain of 0.03 m. In the second set, the maximum shear displacement of the testing equipment was insufficient for Oida's model to be fitted, although in some measurements the shear stress already started to flatten out. The maximum shear strength was assessed visually on the basis of the second set of data.

Table 10. Parameter estimates of general models for maximum shear strength of snow types M1 to M6.

Snow type	Normal pressure, kPa	Parameter				RMSE, kPa	n
		ϕ, rad	a_τ, kPa	b_τ	c_τ		
		Estimate (Std. err.)		Estimate (Asymptotic std. err.)			
M1	$0 \le p_n < 70$	0.519 (.)	- (-)	- (-)	- (-)	-	-
	$70 \le p_n < 180$	0.632 (0.100)	-7.8 (22.9)	- (-)	- (-)	7.9	3
M2	$0 \le p_n < 60$	0.519 (.)	- (-)	- (-)	- (-)	-	-
	$60 \le p_n < 125$	0.634 (0.008)	-9.6 (0.7)	- (-)	- (-)	0.4	3
M3	$120 \le p_n < 185$	0.426 (0.003)	- (-)	- (-)	- (-)	0.6	2
M4	$55 \le p_n < 185$	0.457 (0.021)	- (-)	- (-)	- (-)	2.3	3
M5	$75 \le p_n < 195$	- (-)	- (-)	49.1 (12.9)	0.012 ($1.5 \cdot 10^{-3}$)	26.4	3
M6	$65 \le p_n < 125$	- (-)	- (-)	26.8 (3.4)	0.015 ($1.1 \cdot 10^{-3}$)	21.4	3

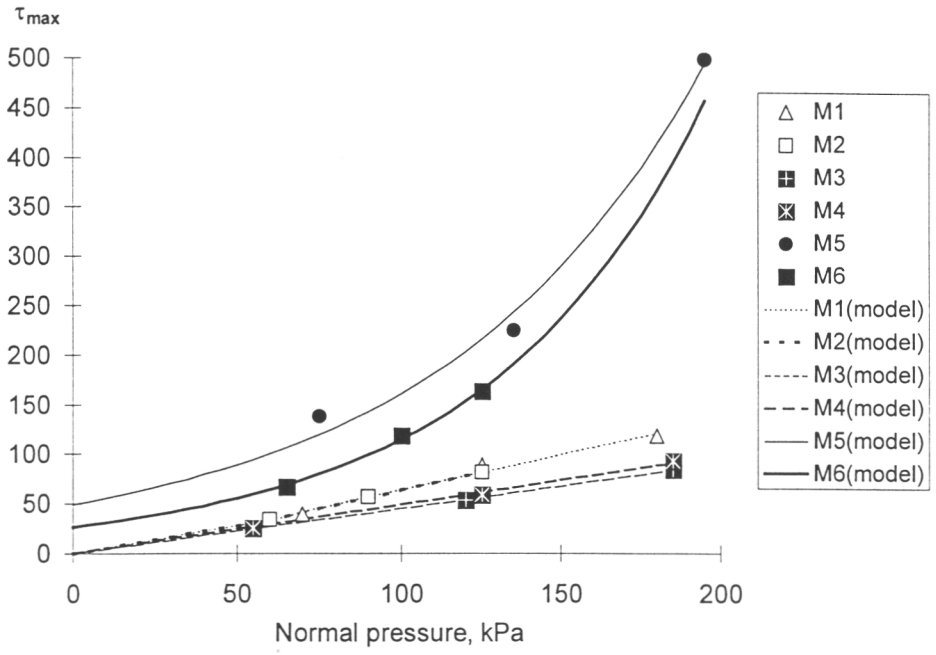

Figure 8. Measured and modelled (Equations 74 and 75) maximum shear strength τ_{max} of snow types M1 to M6 .

4.2.3 Rubber-snow interface friction

The rubber-snow interface static friction was defined as the maximum value in the friction vs. rotation angle curve after the rotation had begun. The dependence of the rubber-snow interface static friction coefficient on normal pressure and snow properties was described with an empirical model by the author (Equation 76). Parameter a_μ defines the friction coefficient at zero normal pressure, whereas parameter b_μ defines the rate of the friction coefficient decline with increasing normal pressure. The model was first fitted separately for each snow type to obtain estimates of the parameters. Thereafter, the dependence of the parameters a_μ and b_μ on snow properties was modelled.

$$\mu = a_\mu \cdot \exp\left(b_\mu \cdot p_n\right) \tag{76}$$

where a_μ, b_μ = Parameters.

The model (Equation 76) parameter estimates for each snow type are presented in Table 11. For snow types Fr3 and Fr4 the maximum friction coefficient was

set to 1 (a_μ=1), and therefore only parameter b_μ was fitted. Had the maximum value not been fixed at 1, which is considered as a reasonable maximum for rubber-snow friction coefficient, the fitting algorithm would have resulted in unrealistically high values.

Table 11. Parameter estimates of rubber-snow interface static friction coefficient models for snow types Fr1 to Fr4.

Parameter		Snow type			
		Fr1	Fr2	Fr3	Fr4
a_μ	Estimate	0.192	0.277	1.000*	1.000*
	Asymptotic std. err.	0.007	0.006	.	.
b_μ	Estimate	$-5.18 \cdot 10^{-6}$	$-8.54 \cdot 10^{-6}$	$-11.0 \cdot 10^{-6}$	$-11.0 \cdot 10^{-6}$
	Asymptotic std. err.	$5.39 \cdot 10^{-7}$	$3.72 \cdot 10^{-7}$	$3.22 \cdot 10^{-7}$	$1.94 \cdot 10^{-6}$
RMSE		$2.5 \cdot 10^{-3}$	$2.0 \cdot 10^{-3}$	0.018	0.107
n		3	3	3	3

*=pre-determined value

Equations 77 and 78 present the general static friction coefficient model (Equation 76) parameters as a function of snow free water content and density. In forming the general static friction coefficient model, snow type M6 was included in the data (n=5) with estimated values of a_μ=0.15 and b_μ=$-9.00 \cdot 10^{-7}$. This proved to be necessary in order to make the model behave realistically even with high values of snow density and free water content. Therefore, the model parameters were selected merely using Excel spreadsheet software, since determining them through a statistical procedure would be somewhat misleading. The parameter estimates for Equations 77 and 74 are given in the following:

Parameter	Estimate
$p_{\mu 1}$	-0.234
$p_{\mu 2}$	$1 \cdot 10^{-5}$
$p_{\mu 3}$, $kg^{-1}\,m^3$	$-5 \cdot 10^{-4}$

$$a_\mu = \exp\left(p_{\mu 1} \cdot w\right) \tag{77}$$

$$b_\mu = p_{\mu 2} \cdot \exp\left(p_{\mu 3} \cdot \rho \cdot w\right) \tag{78}$$

where a_μ, b_μ, $p_{\mu 1}$, $p_{\mu 2}$, $p_{\mu 3}$ = parameters
w = free water content of snow, % wgt
ρ = snow density, kg m^{-3}.

When Equation 76 with the selected parameters was applied to the mobility study snow types (Figure 9), snow type M2 exhibited the highest friction coefficient, which with low normal pressures was roughly seven times higher than the coefficient of types M5 and M6. These coefficients were nearly always equal and almost independent of normal pressure. The behaviour of friction coefficient of snow types M1, M3 and M4 was very similar, the values of the coefficient being slightly below those of M2.

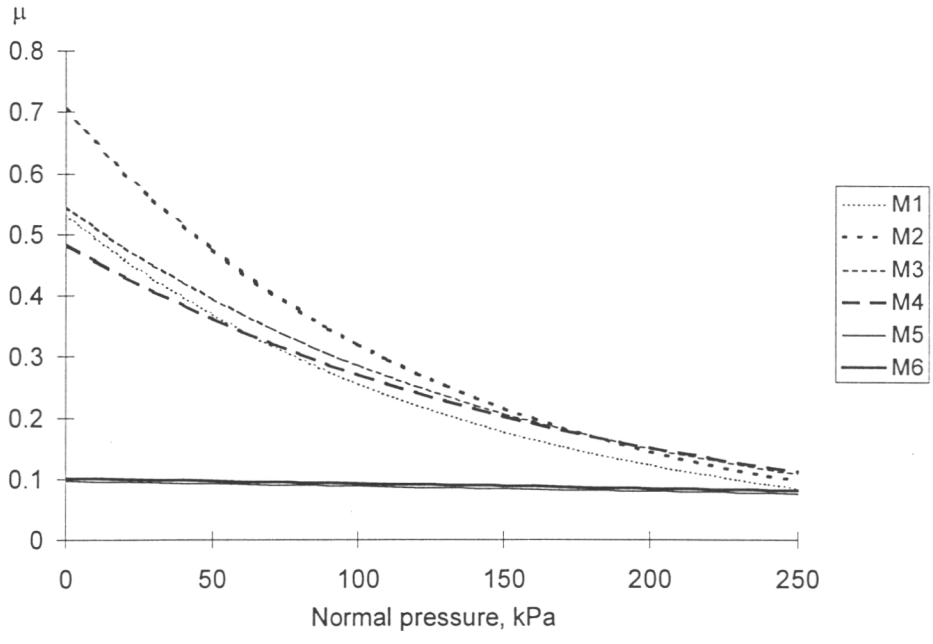

Figure 9. Coefficient of static friction μ for the rubber-snow interface in snow types M1 to M6 according to Equation 76.

4.2.4 Flow resistance of snow

The empirical flow resistance model of snow by the author is presented in Equation 79. The first term of the model defines the resistance pressure at zero velocity, and the second term determines the effect of velocity on pressure. First, the average value of pressure with a velocity of less than 0.5 m s^{-1} was determined separately for each snow type. Then, the dependence of the

obtained average values on snow properties in the whole data with a velocity of less than 0.5 m s^{-1} was modelled, resulting in estimates of a_f and b_f. Finally, the model, with obtained estimates of a_f and b_f, was fitted to the complete flow resistance data (Appendix 4, p. 113) to determine parameters k_f and n_f.

$$p_f = a_f \exp(b_f \rho) + k_f \rho \cdot v^{n_f} \quad (79)$$

where a_f, b_f, k_f, n_f= Parameters.

In flow resistance trials, the maximum velocity varied from 1.8 to 4.0 m s^{-1}. The flow resistance model parameter estimates are presented in Table 12. The parameter estimates of a_f and b_f ($v < 0.5$ m s^{-1}) were used in the model, when determining the parameters k_f and n_f.

Table 12. Parameter estimates of the general flow resistance model (*=values from model p_f ($v<0.5$ m s^{-1})).

Parameter		Model	
		p_f ($v<0.5$ m s^{-1})	p_f ($v \geq 0.5$ m s^{-1})
a_f	Estimate	2920	2920*
	Asymptotic std. err.	1650	.
b_f, m^2 s^{-2}	Estimate	$2.76 \cdot 10^{-3}$	$2.76 \cdot 10^{-3}$*
	Asymptotic std. err.	$1.32 \cdot 10^{-3}$	.
k_f, m s^{-1}	Estimate	-	0.230
	Asymptotic std. err.	-	0.222
n_f	Estimate	-	1.68
	Asymptotic std. err.	-	1.38
RMSE, kPa		2.17	2.15
n		5	1508

In the mobility study flow resistance was determined almost entirely by the velocity independent term of Equation 79. The model resulted in the following values of flow resistance pressure:

Snow type	Flow resistance pressure, kPa
M1	5.5
M2	6.9
M3	7.4
M4	7.6
M5	10.6
M6	11.3

4.3 Wheel mobility

4.3.1 Introduction

In the following, the modelled (Equations 6 to 64 and Appendix 1 on p. 100) performance of the wheel is compared to the measured values, the first being referred to as model or modelled values. The model was run on a PC with 266 MHz Pentium 2 processor and 64 MB RAM. With calculation tolerance of Mathcad set at 1, the approximate execution time of the main body of the program for the first pass was three hours, and for the following passes 10 minutes. Before this, two angles had to be solved with tolerance set to 0.0001, this took approximately 5 minutes. The solution per snow type and number of pass had to be iterated manually, which required up to eight trials. The allowed deviation from the equilibrium per wheel was 20 N in vertical force and 1.0 N m in torque.

As the mobility model did not have procedures for determining the compressive width of tyre at $2 \cdot \pi$ region $b_{2\pi}(\theta)$ on the first pass, the constant compressive width of tyre b_{co} on the following passes, and the parameter $c_{f\tau}$ used in determining the variables derived from snow shearing in the flow region, these remained as empirical parameters. When calculating the results to be presented in the following, tyre parameter $b_{2\pi}(\theta)$ was set at 0.06 m, b_{co} at 0.08 m, $c_{f\tau}$ at 0.66, p_{da} at 0.37, and p_{db} at 0.75. Motion resistance is given as a motion resistance coefficient μ_r, which is determined as motion resistance force divided by the wheel normal load.

4.3.2 Wheel sinkage

Wheel sinkage could be measured reliably only on the first pass, where sinkage was determined on the basis of the initial snow depth and the wheel ride height. Wheel sinkage on passes 2 to 6, however, proved to be impossible to determine reliably on the basis of the measurement data, since the snow depth in the rut could not be assessed reliably. This was mostly due to snow falling into wheel rut from the snowpack walls immediately in front of and behind the passing wheel, and secondly the remoulding effect of the trailing edge of the tyre. Manual measuring of snow depth before each pass would have solved these problems except the problem arising from snow falling in before the wheel, but it proved to be impossible to perform these measurements with reasonable accuracy.

Measured and predicted wheel sinkage on the first pass in snow types M1 to M6 is presented in Figure 10. The accuracy of the prediction was quite good, and the model duplicated the rank between the snow types, with the exception of snow types M4 and M6. Wheel sinkage in relation to snow cover depth was greater than that of plate sinkage.

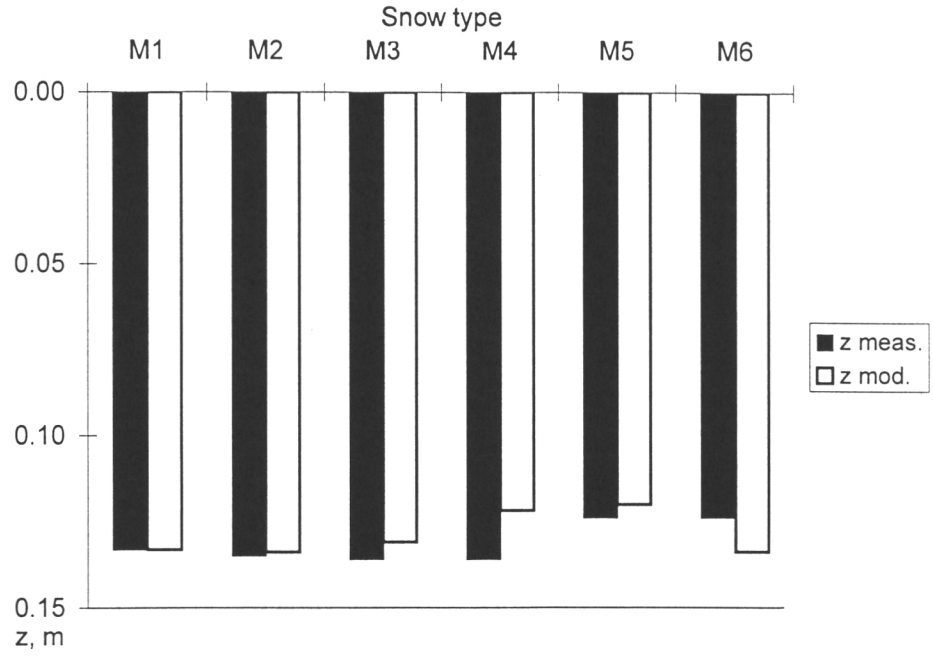

Figure 10. Modelled and measured wheel sinkage z on the first pass in snow types M1 to M6 with initial snow depth s_{si}=0.15 m.

Figure 11 presents the modelled behaviour of wheel sinkage on passes two to six in snow types M1 to M6. Sinkage decreased consistently with the increasing number of passes. The asymptote value was generally reached on pass five, with the exception of snow type M6 (pass four) and snow type M4 (not reached during six passes). Snow types M5 and M6 were distinguished by lower sinkage on the second pass followed by a more gradual decline in sinkage values on the following passes. Snow type M2 demonstrated the highest sinkage on the second pass, which was also the case on the first pass in Figure 10.

Figure 11 also shows modelled wheel sinkage on passes two to six in snow type M1 with an initial snow depth of 0.10 m. Here, the asymptote value was reached already on pass three. In snow type M1 with initial snow depth 0.05 m, modelled wheel sinkage was only marginally lower than initial snow depth already on the first pass (Figure 12).

Figure 12 shows modelled and measured wheel sinkage on the first pass in snow type M1, when the initial snow depth varies from 0.05 to 0.15 m. The model over estimated the sinkage increasingly with decreasing initial snow depth.

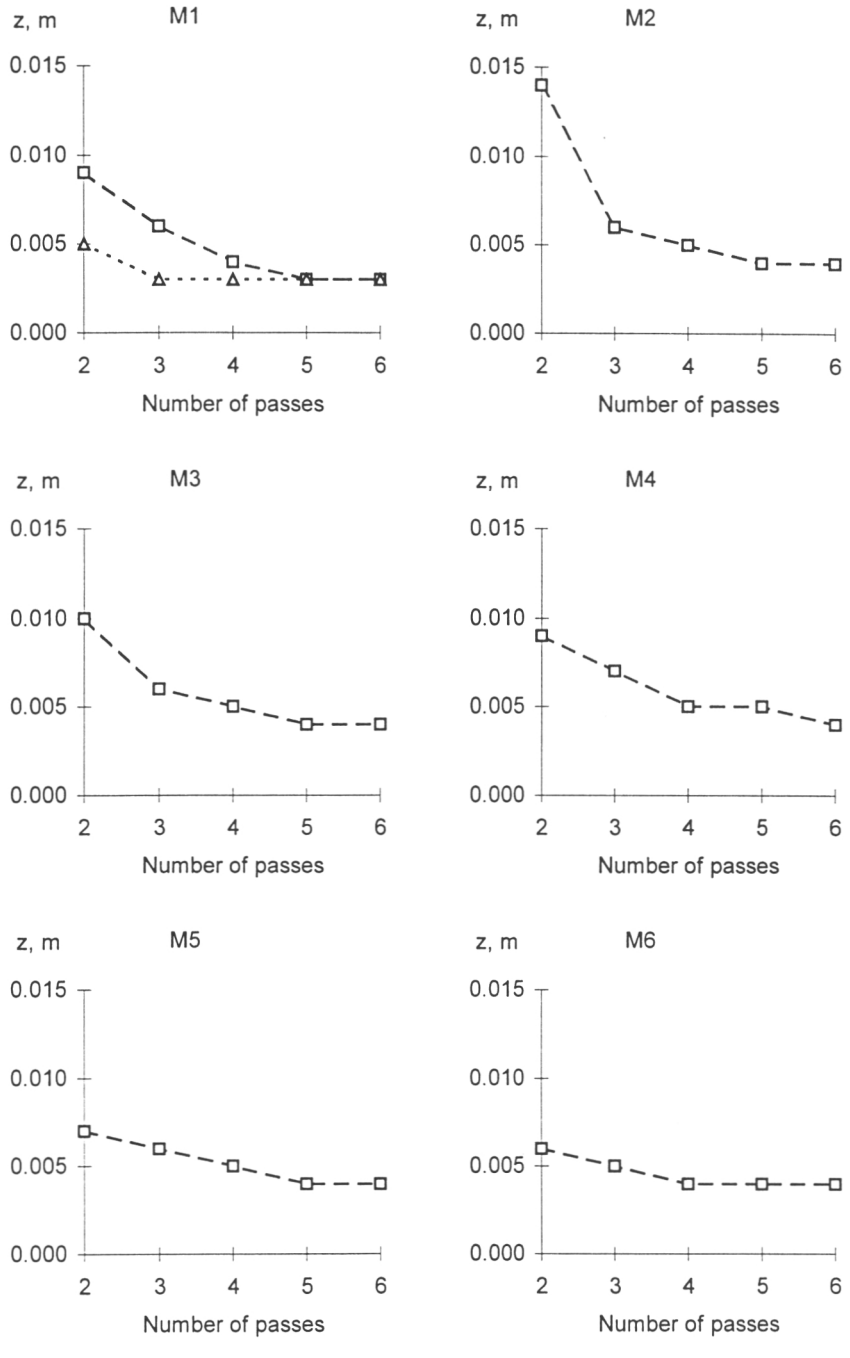

Figure 11. Modelled wheel sinkage z on passes two to six in snow type M1 with initial snow depth s_{si}=0.10 m (triangle markers, dotted line) and s_{si}=0.15 m (square markers, dashed line), as well as snow types M2 to M6 with initial snow depth s_{si}=0.15 m (square markers, dashed line).

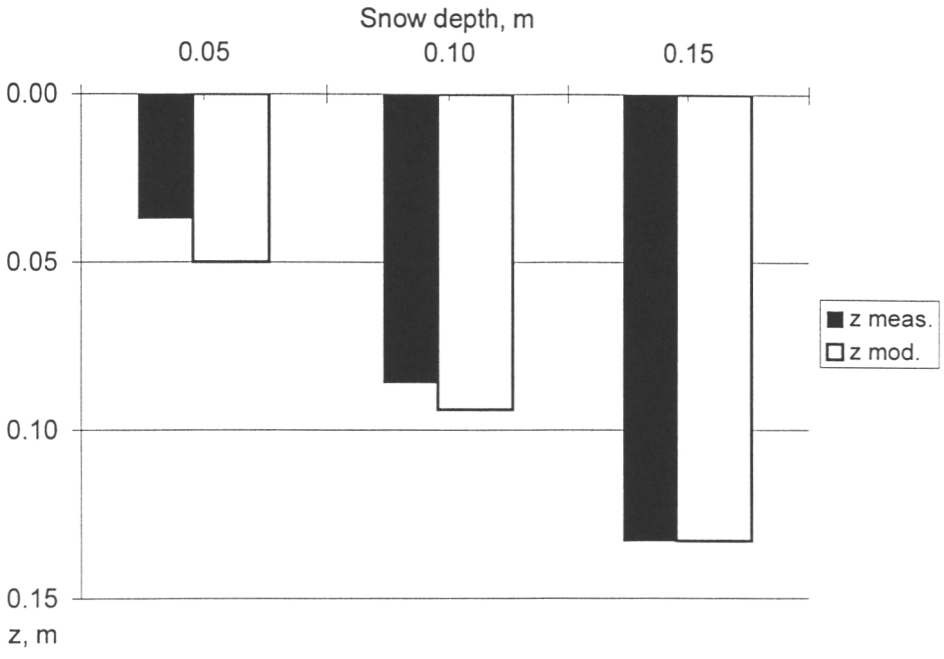

Figure 12. Measured and modelled wheel sinkage z on the first pass in snow type M1, when initial snow depth s_{si} varies from 0.05 to 0.15 m.

4.3.3 Final length of compressed snow cover

Since the ride height of the axle was measured directly and the vertical location of the ground surface was determined for each track, the final length of compressed snow cover (See Figure 2 on p. 19) could be determined for each pass of the test axle.

The final length of compressed snow cover as a function of the number of passes with a snow depth of 0.15 m is presented for snow types in Figure 13. The model results for final length of compressed snow cover showed a consistent decline with the increasing number of passes, whereas the measured final length of compressed snow cover remained fairly constant for all snow types throughout the passes. Hence, the measured and model results generally agreed on one pass only. With snow type M6, the model and measured results showed a similar trend, but also here the deviation was remarkable. In some cases the measured final length of compressed snow cover increased from the previous passing to the following.

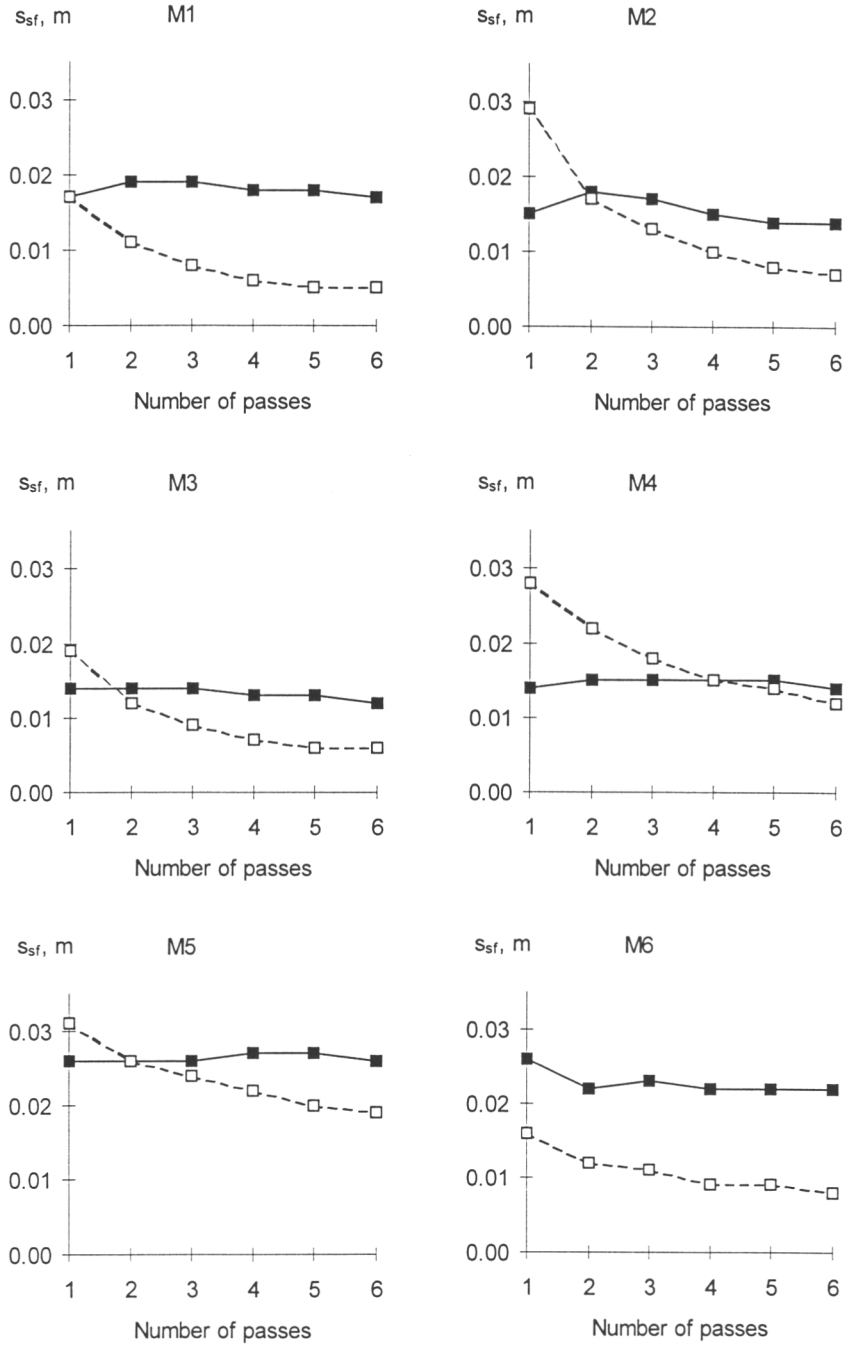

Figure 13. Modelled (dashed line, empty markers) and measured (solid line, filled markers) final length of compressed snow cover s_{sf} in snow types M1 to M6, when initial snow depth s_{si}=0.15 m.

The model results for final length of compressed snow cover in varying depths of snow type M1 were below the measured values (Figure 14). With snow depth 0.05 m, the final length was negligible already on the first pass.

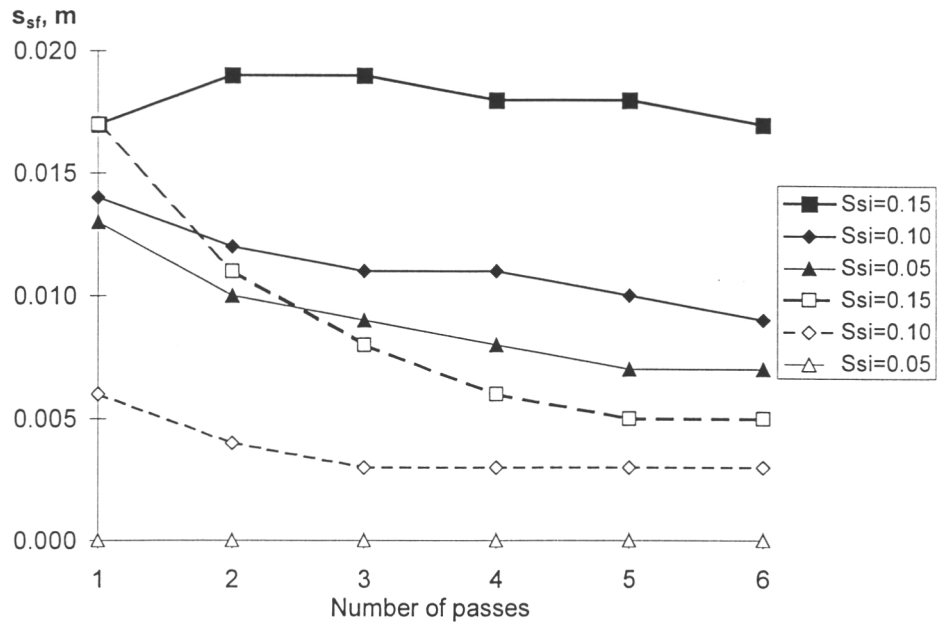

Figure 14. Modelled (dashed line, empty markers) and measured (solid line, filled markers) final length of compressed snow cover s_{sf} in snow type M1 , when initial snow depth s_{si} varies from 0.05 to 0.15 m.

In snow type M1, measured values of the final length of compressed snow cover in initial snow depths of 0.05 and 0.10 m showed a steady decrease with the increasing number of passes. This contrasted with the behaviour of the final length of compressed snow cover with snow depth 0.15 m, where an increase from the first passing to the second was evident, whilst the decrease after the second pass more gradual.

4.3.4 Motion resistance, wheel slip and wheel operation sectors

Motion resistance on the bare track was determined as an average of the six measurements on different test tracks, the average value was 0.04. As mentioned earlier, the model result for motion resistance consists of the calculated resistance due to snow and the measured resistance on bare track, taken for the internal motion resistance of the tyre.

The motion resistance model results for snow types M1 to M6, are presented together with the measured values in Figure 15. The behaviour of the modelled resistance was consistent for all snow types. The motion resistance on the first pass was clearly higher than on following passes, the resistance on passes 2 to 6 declined gradually towards an asymptote. The model over predicted the motion resistance of the first pass on all snow types except M5. With increasing number of passes, the predicted values of motion resistance with snow types M1, M2, M5 and M6 corresponded quite well to the measured values, despite some slight under prediction. With snow types M3 and M4 the model results showed gross under prediction on passes 2 to 6.

The behaviour of measured motion resistance in snow with varying properties and increasing number of passes can be divided into three groups (Figure 15). The first group, formed by snow types M3 and M4, was characterised by the slow decline of motion resistance with increasing number of passes. The asymptote value was probably relatively high, but was not reached during the first six passes. The group of wet and dense snow types M5 and M6 was characterised by a relatively high initial value for motion resistance and its rapid decline with the increasing number of passes. The asymptote value, which was considerably lower than that of the previous group, was reached already on the fourth pass. The third group was formed by snow types M1 and M2, which had the least density. The behaviour of motion resistance of the third group was between the first two groups.

Figure 16 presents motion resistance as a function of the number of passes in snow type M1 for snow depths of 0.05, 0,10 and 0.15 m. The model over predicted motion resistance on the first pass with snow depths 0,10 and 0.15 m, whereas the prediction in 0.05 m snow was more accurate. On passes 3 to 6 in 0.10 m snow and passes 2 to 6 in 0.05 m snow, motion resistance was formed entirely by the internal motion resistance of the tyre. The general form of the curves of predicted motion resistance is in accordance with the curves formed by the measured values. Measured values for depths of 0.05 and 0.10 m were practically equal after and including pass 2, whereas motion resistance in a snow depth of 0.15 m was consistently higher. The asymptote value in snow depths 0.05 and 0.10 m was also achieved earlier. As can be seen in Figure 16, motion resistance was not directly proportional to snow depth.

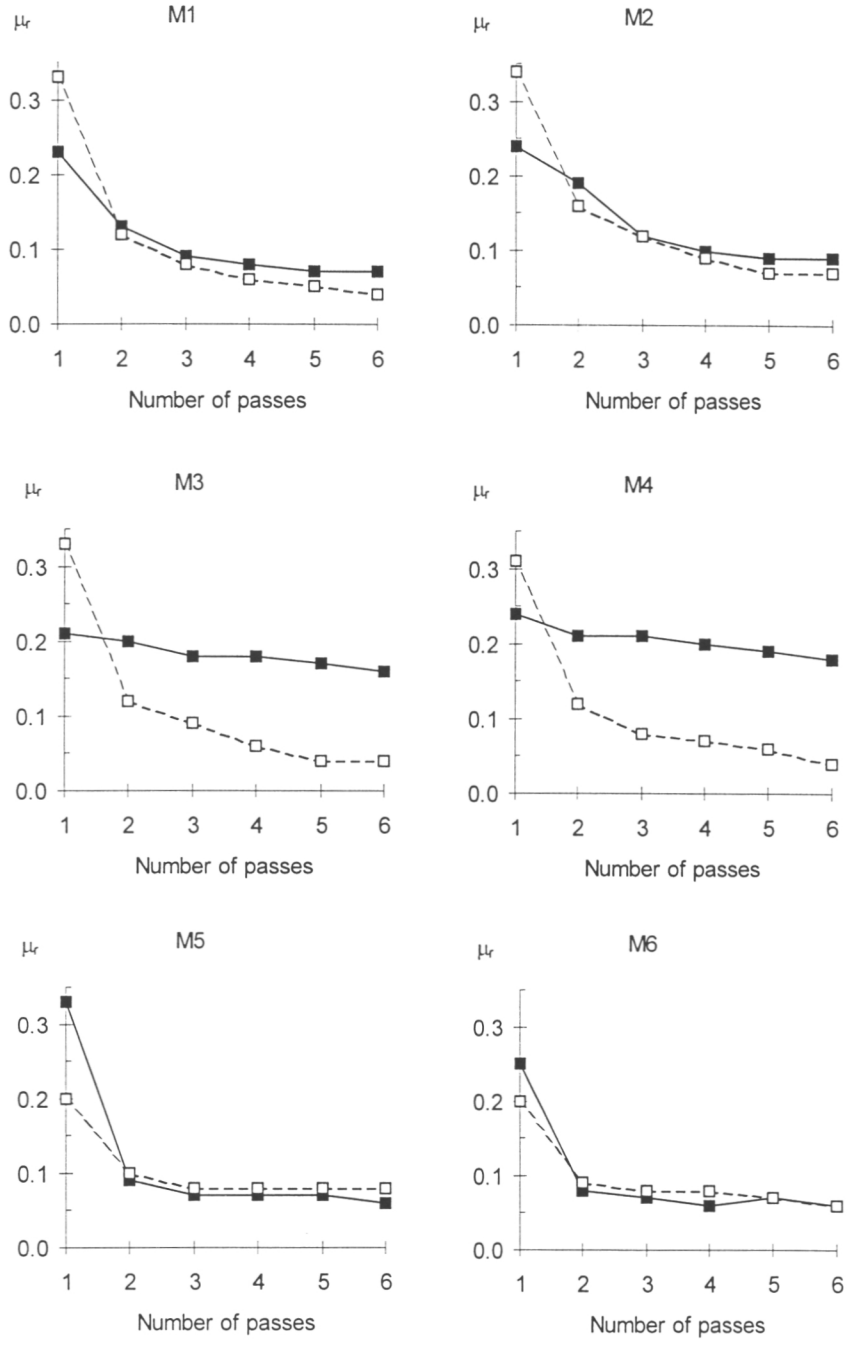

Figure 15. Modelled (dashed line, empty markers) and measured (solid line, filled markers) motion resistance coefficient μ_r in snow types M1 to M6, when initial snow depth s_{si}=0.15 m.

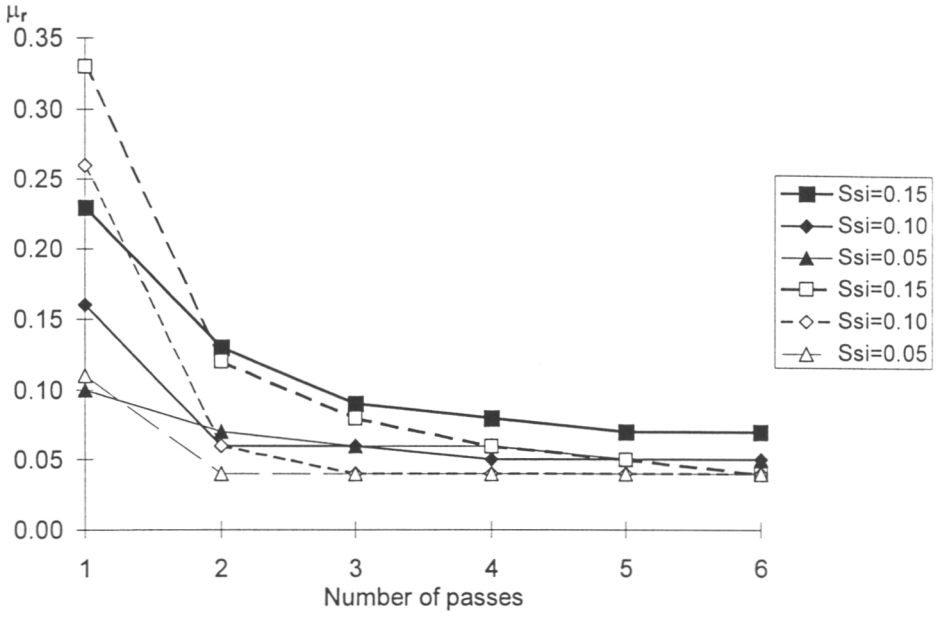

Figure 16. Modelled (dashed line, empty markers) and measured (solid line, filled markers) motion resistance coefficient μ_r in snow type M1, when initial snow depth s_{si} varies from 0.05 to 0.15 m.

Given constant angular and forward velocity, the magnitude of wheel slip is dependent on the determination of the length of wheel circumference and the resulting rolling radius. Here, the slip scale was fixed by using a zero torque condition radius r_0 measured on frozen sand covered by compacted M1 snow, since the rolling radius determined under a zero net torque condition on loose or frozen sand would have resulted in positive slip values for the last passes in the study conditions. 4 to 10 overlapping revolutions were used in determining the average slip per pass.

Since negative slip is dealt with later, the terminology utilized deserves further clarification. 'Slip value' refers to the actual negative or positive figure, whereas 'slip' refers to the magnitude of the relative movement of the contact surfaces, i.e. the absolute value of the figure. A decreasing slip value thus means a smaller negative figure, and decreasing slip means approaching zero from the negative or from the positive.

Modelled slip, calculated with zero torque condition radius r_0, is given in Figure 17. The value of modelled wheel slip in 0.15 m initial snow depth on first pass was highest in snow types M3 and M4, and it remained relatively constant for following passes. Wheel slip values for snow types M5 and M6 were the

lowest on the first pass, and the highest thereafter. Slip values of snow types M1 and M2 were slightly below types M3 and M4. The measured slip values especially in snow types M5 and M6, but also in M3 and M4, behaved in a manner similar to modelled slip (Figure 18).

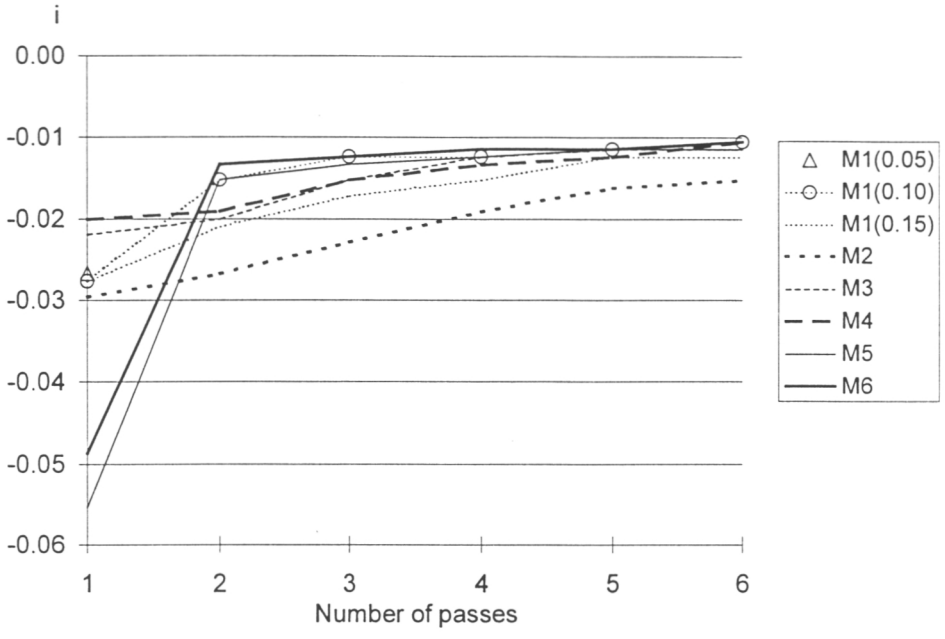

Figure 17. Modelled wheel slip i for zero torque condition rolling radius r_0. M1: Initial snow depth s_{si} (m) given in brackets, M2 to M6: s_{si}=0.15 m.

On the first pass, the measured slip value in snow type M5 at a depth of 0.15 m was the lowest. The measured slip in 0.05 and 0.10 m deep layers of M1 snow was the lowest, as was the motion resistance. Generally, the measured slip values with snow depth of 0.15 m were lower than the modelled ones. However the trend in modelled and measured values with increasing number of passes is similar. The measured values demonstrated some fluctuation between consecutive passes.

Modelled wheel operation was based on the flow and compressive area of the tyre tread. The corresponding sectors on wheel circumference, defined as central angles, are given in Table 13. The sectors were defined by the entry angle θ_e, the angle of compression start θ_{cs} and the trailing angle of rotation θ_{max}, the average value of the last being 6.583 rad.

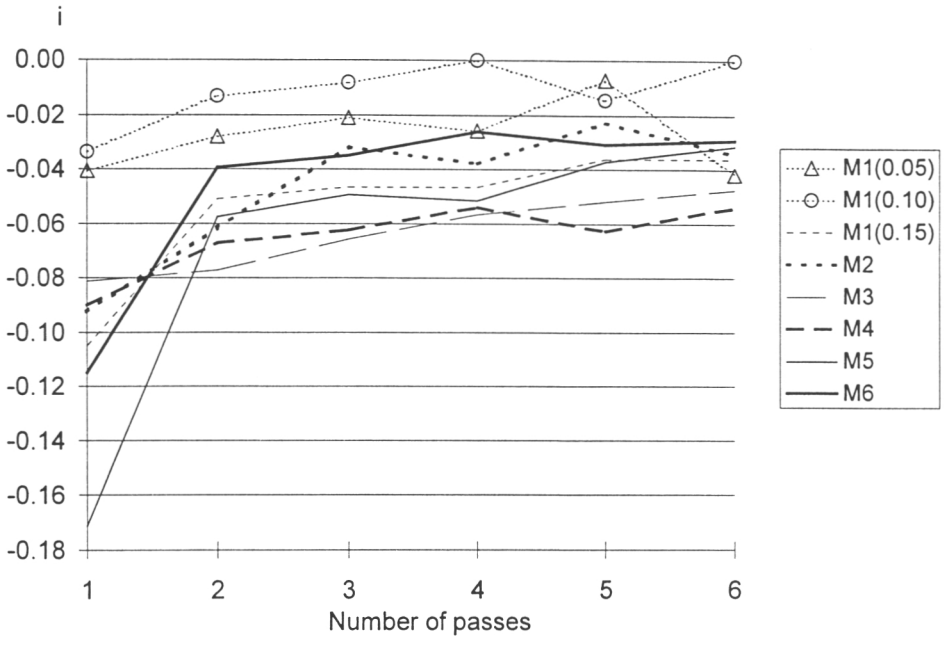

Figure 18. Measured wheel slip i for zero torque condition rolling radius r_0. M1: Initial snow depth s_{si} (m) given in brackets, M2 to M6: s_{si}=0.15 m.

Table 13. Modelled flow and compressive sectors of the test wheel with initial snow depth of 0.15 m.

No. of pass	M1	M2	M3	M4	M5	M6
	Flow sector, rad *Compressive sector, rad*					
1	0.078 *1.484*	0.000 *1.501*	0.064 *1.486*	0.105 *1.398*	0.094 *1.398*	0.603 *0.970*
2	0.027 *0.695*	0.000 *0.784*	0.017 *0.715*	0.041 *0.685*	0.163 *0.535*	0.168 *0.519*
3	0.072 *0.611*	0.006 *0.696*	0.066 *0.623*	0.075 *0.620*	0.169 *0.512*	0.173 *0.497*
4	0.095 *0.571*	0.042 *0.638*	0.097 *0.570*	0.096 *0.579*	0.174 *0.495*	0.177 *0.484*
5	0.115 *0.538*	0.068 *0.597*	0.114 *0.541*	0.108 *0.558*	0.176 *0.486*	0.180 *0.476*
6	0.121 *0.528*	0.083 *0.573*	0.118 *0.536*	0.122 *0.535*	0.179 *0.478*	0.180 *0.476*

Snow type M2 was distinguished by the narrowest flow sector, whereas the flow sector of M6 was clearly widest on the first pass. This, together with the differences in flow resistance pressure (See p. 60), resulted in flow resistance having the following share of snow-induced motion resistance in 0.15 m snow depth on the first pass, where variation between the snow types was at its greatest:

Snow type	Share of flow resistance, %
M1	2.7
M2	0.0
M3	3.0
M4	5.2
M5	52.5
M6	67.0

4.3.5 Model sensitivity

The relative effect of ±5 % change in selected input parameter values on the output variables wheel sinkage (Δz) and motion resistance coefficient ($\Delta \mu_r$) on the first pass in 0.15 m layer of M1 snow and M6 snow (ρ(M6) in the figures), is presented in Figures 19 and 20. Parameter and output variable values from the first pass in the 0.15 m layer of M1 and M6 type snow were used as a reference. In the mobility model, snow density only has a direct effect on flow resistance. The share of flow resistance in M1 snow is relatively small, therefore the sensitivity of the model to snow density on the first pass was also studied in M6 type snow.

Predicted wheel sinkage was most sensitive to changes in the compressive strength of snow and tyre width, whereas the free water content of snow had a lesser effect (Figure 19). The absolute value of the relative effect of tyre deflection was only about 0.5 %. Changes in the values of the rest of the tested input variables had very little or no effect.

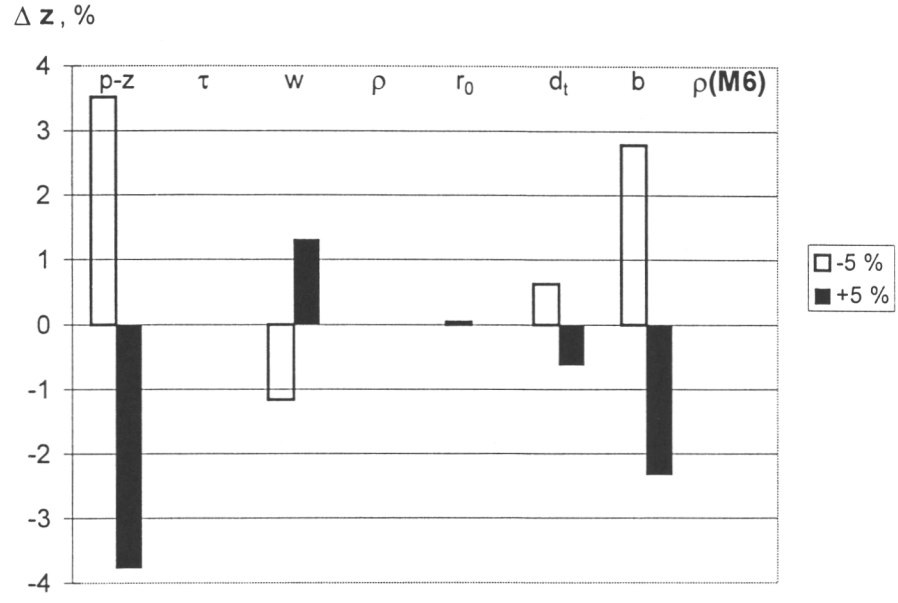

Figure 19. The relative effect of ±5 % change in selected input parameters on model output variable wheel sinkage (Δz) on the first pass in 0.15 m layer of M1 snow and M6 snow (ρ(M6)). Input parameters: p-z=compressive strength, τ=shear strength, w=moisture content, ρ=density, r_0=zero condition rolling radius, d_t=tyre deflection, b=tyre width and ellipse a-axis.

In M1 snow, the predicted motion resistance coefficient (Figure 20) was most sensitive to changes in tyre width and the water content of snow, the effect of compressive strength of snow was smaller. The absolute effect of ±5 % change in the values of other tested input variables on predicted motion resistance coefficient was less than 1 %. In M6 snow, the absolute effect of snow density was clearly higher than in M1 snow.

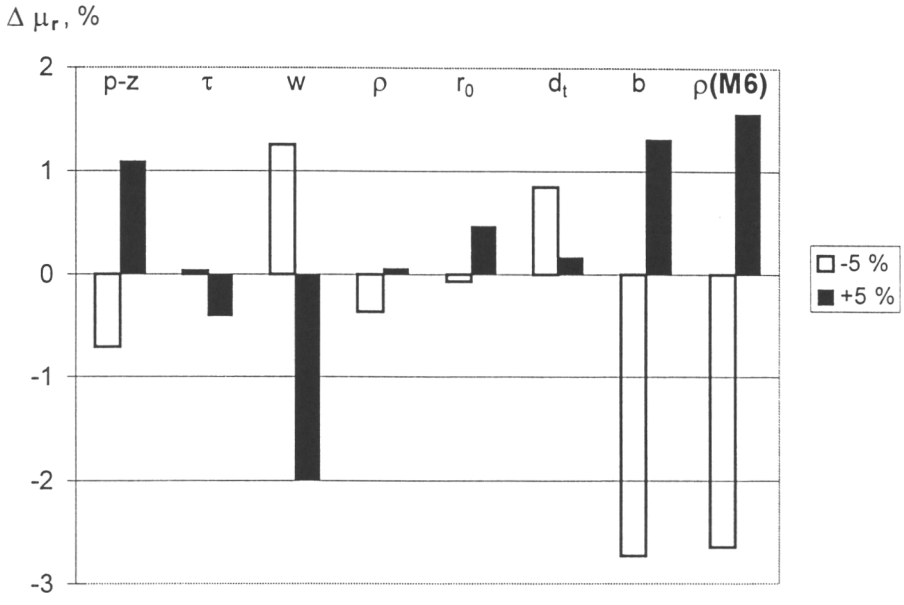

Figure 20. The relative effect of ±5 % change in input parameters on model output variable motion resistance coefficient ($\Delta\mu_r$) on the first pass in 0.15 m layer of M1 snow and M6 snow (ρ(M6)). Input parameters: p-z= compressive strength, τ=shear strength, w=moisture content, ρ=density, r_0=zero condition rolling radius, d_t=tyre deflection, b=tyre width and ellipse a-axis.

5 Discussion

5.1 Test arrangements

In order to discover the effect of snow properties on wheel mobility, the experiments were conducted in snow layers consisting of a single snow type at a time. The snow types had to be extracted from the natural snow cover and placed in snow bins or sample containers for the experiment. These facts have two significant consequences. Firstly, the snow material did not correspond to the natural snow cover due to its homogeneity and, secondly, the structure of the snow material was disturbed during extraction and handling. The latter was done partly to ensure uniform properties for each snow type in different tests. The properties of the snow material were thus determined from the samples which had undergone all the necessary phases of the extraction and handling process, and therefore describe the properties of the material in which the mobility trials were conducted. In determining the flow resistance, the same snow sample was used throughout the testing of each snow type, which had some effect on the properties of the sample during the test. Comparing the data obtained in the course of replications per snow type did not cause noticeable effects on the results, partly since here one complete set of tests took only about half an hour per snow type.

The studying of each snow type was carried out during one day. The delay from the first trials of the day to the last was hence several hours, except for friction coefficient and flow resistance measurements, as mentioned earlier. Knowing the unstable nature of snow, the properties of the snow types inevitably changed during the delay. The magnitude of the change is uncertain, but it likely did not affect the measured variables within the measuring accuracy. The effect of the time delay was at its greatest whilst ambient temperature was around 0°C. This was at least partly counteracted by the fact, that the snow type of interest was located at the bottom of the natural snow cover, well isolated from the variations of ambient temperature. Since a fresh sample was acquired for each type of test, the sample temperature did not vary greatly during the day.

The determination of snow grain dimensions by photographing and subsequent computer image analysis was a successful solution. The method was less time consuming and very likely more accurate than in-situ determination. Further reduction in time consumption could be achieved by automating the image analysis phase. Subjective sample selection and measuring only in two dimensions are some of the drawbacks of method.

The snow fork used for measuring snow density and free water content proved to be a useful tool. The density measurement is fairly accurate (Table 2, p. 45), when compared to snow scale measurements, which also contain a certain error. The snow fork under estimated the density, in accordance with the author's

previous experiments (Ala-Ilomäki et. al. 1989), whereas Kendra et al. (1994) found the measuring principle to over predict density. Obviously there is room for further instrument development. The constant term in Equation 67 (p. 37) was not statistically significant, yet previous experience (Ala-Ilomäki et. al. 1989) supported keeping it in the model. Unfortunately a reliable and fast control method for measuring the free water content was not available, yet the measuring principle of the device seems to be able to determine free water content more accurately than density (Kendra et al., 1994). The accuracy of the estimate for free water content was further improved by using density measured with snow scale in Equation 66 (p. 37). Due to antenna damage, an estimated free water content of 10 % wgt was used for snow type M5, but this was not likely to cause a great error in mobility prediction.

The ability to duplicate real loading conditions is an important factor when defining the validity of the measurement methods for mechanical soil properties (Shoop 1989). The loading speed of the measurement device should preferably be in the same order of magnitude as that of the real loading situation. The measuring methods applied here for snow simplified the real loading conditions, and the difference in loading speed varied from zero to ten fold, the measurements of fundamental pressure-sinkage relationship demonstrating the greatest difference. The low loading speed in snow shearing may be responsible for the experienced strain hardening of M5 and the occasional irregularities in the data of M1. Generally, a greater number of replications would have helped in reliable determination of the mechanical properties.

Another aspect of measuring material properties is the nature of loading. In reality, multiple wheel passes result in cyclic loading of snow, whereas in the present study snow properties were measured under a single loading cycle. The effect of cyclic loading is bound to vary according to the physical properties of snow, ambient temperature, time delay between the cycles as well as the type of loading and the combination of the loading types in a real situation.

To study the behaviour of the wheel snow interaction an instrumented test axle was run in snow bins filled with several snow types. Since the radius of test axle wheels was roughly 0.2 to 0.5 times the radii of wheels normally used in forest machinery, the test may also be considered a scale model test. The similitude of soil-machine systems has been discussed by Freitag et al. (1970), Schafer et al. (1973), Wismer et al. (1976). The criteria for evaluating the quality of a scale model presented in Wismer et al. (1976) for pneumatic wheels on soft soils are applied in rating the test axle. The velocity of the test axle was scaled appropriately, if compared to 18.4-34 forest machine tyre (diameter 1.68 m, width 0.47 m, The Driving... 1994) with a typical off-road transportation velocity of 1 m s^{-1}. The choice of width-to-diameter ratio in the diameter class of the test axle tires was rather limited. Nevertheless, the width-to-diameter ratio of the test axle tires closely corresponds to that of the 18.4-34 forest

machine tyre, whereas for example the width-to-diameter ratio of more modern 600/65-34 tyre is greater. The size of snow particles remained constant, the effect of which must be more pronounced than that of water molecules in testing a vessel scale model. Nevertheless, the model can be considered an adequate 1:4 scale model of a 18.4-34 forest machine tyre.

At this stage the aim was not to develop a completely true model but to examine the effects of snow properties and behaviour with respect to interaction with the wheel. Therefore, savings in time expenditure were emphasised in designing the field study in order to minimise the changes in snow properties during the testing of one snow type. Wheels of relatively small diameter were hence used.

Another important difference in wheel operating conditions, besides the uniform snow layer, was that the wheels were travelling in snow bins, which may have an effect on wheel and snow behaviour (Gee-Clough 1979). The side walls of the bins offered support and set ultimate limits for the lateral displacement of the snow. The width of the tyres was, however, only one fourth of the width of the bin. Based on the pressure-sinkage test results, the confining effect of the side walls was likely to be small. Overall, it should be noted that the results of the conducted experiments are not necessarily directly applicable to operation in natural snow cover.

5.2 Ambient temperature and physical snow properties

The ambient temperature varied during the field study from -7.5 to 5.5 °C, whilst snow temperature ranged from -9.0 to 0.5°C. The measured snow temperature of 0.5°C in shear strength tests of snow type M6 may be erroneous. The sensors were calibrated at 0°C, and the positive reading may thus be due to heat conduction via the sensor cable. However in the temperature range covered in the study, snow properties change radically (Mellor 1975). Variations in snow temperature during the testing in each snow type could not be avoided, and hence they may have had an effect especially on the results of snow types M5 and M6, as described in Chapter 4.2 (p. 52). Overall, the data covered a rather wide range of variation in snow properties. The fact is, however, that the study would have benefited from data measurement in colder temperatures. Snow temperature was dependent on ambient temperature hence. If the study were to be completed in the planned time frame there was no opportunity to examine a broader range of temperatures.

The snow material was chosen to cover a maximum possible range of density, free water content in addition to grain size and shape. All snow types were numbered in the order of increasing density. In brief,

- M1 was fine-grained, recently fallen snow with low density and low free water content, collected from the top of the snowpack
- M2 was fine-grained, old snow with medium density and low free water content, collected from the centre of the snowpack
- M3 and M4 were medium-grained, old snow types with medium density and low free water content, collected from the centre of the snowpack
- M5 was medium-grained, old snow with high density and high free water content, collected from the bottom of the snowpack
- M6 was coarse-grained, old snow with high density and high free water content, collected from the bottom of the snowpack.

The variation in the physical properties of snow types M1 to M6 can be considered to cover most of the duration of a typical Finnish winter. Compared with the data of Sirén et. al. (1987), covering the density of natural snow cover throughout the winter, the data lacked snow material with density below 200 kg m^{-3}. This may be due to the handling procedure applied in this study. The handling may have altered the shape and size of the grains of the least dense snow types, breaking down the subtle structure of the crystals. Also, snow material with greater density, greater grain size and roundness can be found, yet only during a short period of time in the late spring.

Due to the prevailing ambient temperature, the data did not include snow with zero free water content. Free water content was measured with the snow fork only, therefore the apparent lack of dry snow may also be due to the measuring error of the fork. The weather conditions did not allow for data in the free water content range of 5 to 7 % wgt, either. The Snow Fork antenna was damaged during the measurements in M5, but the use of free water content of 10 % wgt for M5 was not likely have caused a great error. Likewise, the free water content estimate for snow type Fr2 can be considered realistic.

The variation in grain size was approximately proportional to that of density, whereas the results showed less variation in grain shape. Sample selection, snow properties and the interpretation of the computer images had a strong influence on the grain size and shape measurement results. The natural structure of the snow was broken during the handling of the sample, but the remaining aggregates consisted of one to several snow grains. In some cases, obtaining a sample with separate or visually separable grains was difficult, and the amount of visually separable grains in the computer image varied greatly. Sometimes it was impossible to differentiate between one large grain or several smaller grains, and therefore the most reliably interpretable grains were selected.

5.3 Mechanical snow properties

The measurement of the mechanical properties of the snow types was conducted in extracted and processed snow. Therefore, the results did not include the cohesive or initial bonding strength of undisturbed natural snow. The effect of the disturbed structure was likely to be least in rubber-snow interface friction measurements. Generally the initial strength of snow is low compared to the strength values encountered with test axle mobility, which are achieved through substantial compression. The initial strength can not be overlooked, though, since it is likely to be an important component in wheel motion resistance in hard snow. The ambient conditions and study methodology did not allow for this type of snow to be studied.

Pressure-sinkage results exhibited considerable variation between snow types. The results formed two groups, whereas data between these would have been more desirable. The error of the pressure-sinkage models was acceptably small, although the behaviour of snow types M5 and M6 caused some uncertainty. The behaviour of the pressure-sinkage relationship resembled that reported by Muro (1984) for fresh snow, although the relation of maximum sinkage to initial snow depth was 30 to 100 % higher than Muro's values. According to the results of Abele (1975) for undisturbed snow and Yong and Metaxas (1985) for zero day old snow, loading speed does not have a strong influence in compressive strength. The difference in the loading speed of measured and real compression in this study is therefore, not likely to be a remarkable source of error in the mobility model.

The relation of shear stress and normal pressure of snow types M1 to M4 with the applied strain rate in the range of applied normal pressure obeyed Mohr-Coulomb failure criterion. Muro (1984) found similar results for dry snow in vane-cone shear tests however, Yong and Harrison (1978) mention the inherent inapplicability of Mohr-Coulomb theory as failure criterion for snow. In the present study it was also not found valid for snow types M5 and M6. Determining the shear strength was especially difficult for snow type M5. This may have been due to the high ambient temperature, or perhaps the strain hardening experienced may be typical for snow with properties similar to M5. The shearing behaviour of snow types M5 and M6 might have been different with a greater shear strain rate.

Asymptotic standard error in fitting Oida's model for each snow type and normal pressure was small. No sharp hump in shear strength vs. shear displacement could be detected. In many cases the hump was almost non-existent. Fitting the modified Coulomb's model for snow type M1 resulted in a relatively large model error. The inclusion of parameter a_τ, representing cohesion in Equation 69 (p. 37) describing the relationship of maximum shear strength to normal stress, can be questioned on the basis of the large asymptotic

standard error. However the large errors of the model for M1 are most likely to be due to the limited data, and the general non-linear behaviour of snow properties supports the inclusion of parameter a_τ.

The model fitted to describe the relationship of maximum shear strength of M5 and M6 to normal stress (Equation 70, p. 37) was formed on the basis of the data. In general, the form of the model fits the data better than a linear model would have. In Equation 70, parameter b_τ can be interpreted as a cohesive term. Since the physical properties of M6 were relatively close to those of M5, similar non-linear behaviour was assumed probable also at high normal pressure. The shearing behaviour of M5 differed from the other snow types and determining the maximum shear strength on each normal pressure level was not straightforward. Evaluating the accuracy of the model is thus difficult, yet the values of maximum shear strength are not very far from those of M6.

In the mobility model, the shear strength to normal pressure models were applied on the range of zero to maximum pressure encountered. They were thus utilised below the range of data, yet the results of Muro (1984) suggest, that the behaviour is likely to be close to the model also for low normal pressures.

Shear strength measurements are subject to differences in measuring methods and devices. Increasing shear strength and a complete change in shearing behaviour with varying strain rate have been reported (de Montmollin 1982, Perla et al. 1982). Increasing sample size has been found to decrease observed shear strength (Sommerfeld et al. 1976, Perla et al. 1982). The measurements of McClung (1977) for avalanche prediction purposes were performed with normal stress and but the strain rate was remarkably low in comparison to the present study, therefore the high strength values are most likely not comparable with the values obtained here. Other studies include Mundl et al. (1997) who measured the shear strength of pre-compressed snow with direct shear apparatus, yet with unknown strain rate. In addition Muro's (1984) results for vehicle mobility prediction were obtained with two different methods, but both are different from the method utilised here, and the strain rate for wet snow was not given. The shear annulus measurements reported in Osborne and Alger (1989) and Blaisdell et al. (1990) were made with a smooth rubber annulus, which actually measures the rubber-snow interface friction and their results are therefore treated as interface friction later.

The measured angle of internal friction of snow types M1 to M4 was 20 to 150 % higher than the angle of internal friction of fresh and dry snow (ρ=184 kg m^{-3} and 199 kg m^{-3}, snow temperature –5°C) measured by Muro (1984) with a vane cone. Had a Mohr-Coulomb model been fitted to the data of M5 and M6, the resulting angles of internal friction would have been 1.01 and 1.25 rad, well below shear ring measured 1.33 rad given by Muro (1984) for

fresh snow (w=1 % wgt, ρ=228 kg m^{-3}, snow temperature 0°C) and close to the shear box measured 1.05 to 1.22 rad by Mundl et al. (1997) for pre-compressed (ρ=500 kg m^{-3}) natural snow. The assumption of zero cohesion for snow types M1 to M4 was in accordance with Muro's (1984) low values of cohesion (1 to 2 kPa). Cohesion and the angle of internal friction in the study of Harrison (1981), obtained in dry snow with density from 100 to 300 kg m^{-3} correspond well to the values obtained for snow types M1 to M4 in the present study. Unfortunately, no description of the study method is given. The angle of internal friction calculated from the instrumented vehicle traction data of Blaisdell et al. (1990) was roughly 50 % lower than what was measured in this study, and cohesion in the order of magnitude of snow types M5 and M6.

Shear strength appeared to be a rather complex function of density, grain size and form, free water content in addition to temperature. Therefore constructing a general, rather than snow type specific, model of shear behaviour was not possible on the basis of limited data. The high free water content together with high temperature of snow types M5 and M6 resulted in the greatest shear strength amongst the studied snow types. These snow types also had the highest initial density. On the other hand, M1 and M2 with the smallest grain size, demonstrated the highest shear strength among snow types M1 to M4. In Blaisdell et al. (1990), the shear strength measured with the instrumented vehicle increases with increasing density, whereas a similar trend for fresh snow in Muro (1984) is not obvious. The effect of grain size is not obvious in either of these studies.

The rubber-snow interface friction model is the least reliable among the models describing the mechanical properties of snow presented in this study. The errors of the models fitted to the data of snow types Fr1 to Fr3 are acceptably small, but the root mean square error of the model for Fr4 is fairly large. Models for Fr3 and Fr4 were constructed with the assumed maximum friction coefficient of 1. This may be valid for the present mobility model application, yet coefficients greater than 1 have been reported on rubber-ice interface friction (Roberts and Richardson 1981). There was a lack of available data with large free water content with regards to friction. Therefore snow type M6, with assumed model parameter values, needed to be included in the data. This makes the evaluation of the validity and accuracy of the final model difficult.

The present findings suggest that increase in normal pressure, temperature, free water content and density together with grain size decrease the coefficient of rubber-snow interface friction. In the literature describing rubber-snow or rubber-ice interface friction, increasing values of normal pressure (Conant and Liska 1960, Järvinen and Makkonen 1987), temperature in the region of the present study (Conant and Liska 1960, Roberts and Richardson 1981, Blaisdell 1983a, Järvinen and Makkonen 1987), free water content (Osborne and Alger 1989), and density (Osborne and Alger 1989, Blaisdell et al. 1990) have been

reported to decrease the coefficient of friction. Additionally, the sliding friction coefficient of steel (Ericksson 1949) and plastic runners (Palosuo 1981) on snow has been found to decrease with increasing grain size. In addition lower friction as snow crystals wear and become more rounded has been reported (Klein 1947).

The differences in measured values of flow resistance pressure were smaller than expected. This suggests that, besides density, internal and interface friction properties play an important role in determining flow resistance. In addition the model of snow flow resistance would have benefited from the examination of a greater number of snow types examined. In its present form, the model generally behaves logically, yet it exhibits large error terms which results in over or under prediction when applied to certain snow types. Due to the relatively small values of resistive pressure and small cross-sectional area of the flow region, the flow model is not a remarkable source of error in the mobility model on the first pass in snow types M1 to M4, whereas in M5 and M6 its importance is crucial (See p. 72). In test drives, Richmond (1995) reported drag resistance of approximately 750 N, due to vehicle parts ploughing in deep snow of 160 kg m^{-3} density, at a velocity of 2 m s^{-1}. Assuming a cross-sectional area of 0.18 m^2 on the basis of vehicle and snow depth data, the corresponding resistive pressure would be 4.2 kPa, which is close to the value of 5.7 kPa, calculated with Equation 79 (p. 60).

The flow resistance model can be assumed to be valid for the first pass. On the following passes, snow has already been processed by the previous passes of the wheel, which most probably will significantly change the properties of wet snow in respect to flow resistance. Tests for replicating this in flow resistance would have been complicated. Mere compaction of the snow sample between succeeding measurements would have been possible, but in many cases it would have resulted in an insufficient snow depth in the sample bin. Due to methodological difficulties, the present approach was used as a first attempt to deal with the phenomena.

5.4 Wheel mobility

5.4.1 Wheel sinkage

Due to the compressible nature of snow, sinkage on the first pass is much greater than on the following passes. Modelled and measured sinkage can be compared on the first pass only, as an appropriate measuring method was lacking in the present study. The model prediction for sinkage on the first pass was quite accurate. In snow depth of 0.15 m, sinkage can be predicted also with the plate sinkage method (Wong 1989) using the results of the 0.11 m diameter plate. Especially for snow types M5 and M6, the mobility model gives a more accurate estimate for sinkage than the plate method (z_w in Table 8, p. 54).

Wheel sinkage exceeds plate sinkage, which indicates part of the snow in contact with the wheel is not being compressed by the wheel, but flowing past along the tyre surface.

Sinkage calculation in the CRREL shallow snow mobility model (Blaisdell et al. 1990, Richmond et al. 1990) is based on the assumption that the entire snow mass in contact with the wheel is compressed from the initial depth to the final length. This is defined by the maximum or critical density (Yong and Fukue 1977) in confined compression as a function of maximum exerted ground pressure. In Richmond (1995), a slightly higher value of final density is used. The error of the models in the conditions of the test axle study is compared to the presented model in Table 14.

Table 14. Error of the proposed model, Blaisdell et al. (1990) (Eq. A7, final density 500 kg m^{-3}) and Richmond (1995) (Eq. 1 and 7) in wheel sinkage calculation for the first pass of the test axle.

Snow type	Snow depth, m	Model error, %		
		Proposed	Blaisdell et al. (1990)	Richmond (1995)
M1	0.15	0	-39	-33
M1	0.10	9	-37	-31
M1	0.05	35	-27	-20
M2	0.15	-1	-58	-50
M3	0.15	-4	-64	-55
M4	0.15	-10	-66	-58
M5	0.15	-3	-92	-79
M6	0.15	8	-98	-84

The under prediction of the models by Blaisdell et al. (1990) and Richmond (1995) is considerable. This suggests, that part of the snow is indeed not compressed by the wheel, and that the compression by the wheel can be considered unconfined. In the data presented by Richmond et al. (1990), sinkage prediction error is not as pronounced, yet the model has a tendency for remarkable under prediction. In general, measured sinkage in relation to initial snow depth was approximately 10 to 90 % greater in this study than in Richmond et al. (1990) and Richmond (1995) for a towed wheel of the instrumented vehicle of CRREL (Blaisdell 1983b). This could be due to different tyre geometry as the type used in this study had a greater radius-to-width ratio and most likely a greater share of tyre width occupied by rounded shoulders.

On the following passes, sinkage can be examined in the light of the model results only. Sinkage decreases rapidly with increasing number of passes, and approaches the asymptote value, which is reached on the fourth pass at the

earliest. The asymptote value of sinkage suggests, that the wheel will finally be riding on top of a layer of snow compressed to critical density, at least in snow types M1, M2, M5 and M6. On the basis of motion resistance results, the real sinkage may be close to the modelled values, excluding snow types M3 and M4, where sinkage will likely be higher.

Measured wheel sinkage in relation to the initial snow depth increases with increasing snow depth whilst model error increases with decreasing snow depth. This may be due to the fact that plate load tests were carried out in a snow depth of 0.15 m only, and the obtained parameters p_w and z_w were used in predicting the pressure-sinkage relationship in a manner similar to the case of cycloidal compression (Equations 30 to 37, p. 25 and 26). For example, the measured ratio of the sinkage asymptote z_w to initial snow depth in 0.15 m snow was also used to predict the sinkage asymptote in 0.10 and 0.05 m layers. The relative difference in snowpack depths is greater than that encountered with regards to vertical vs. cycloidal compression in the 0.15 m snow layer, hence the assumptions may no longer be valid.

5.4.2 Final length of compressed snow cover

The final length of compressed snow cover (See Figure 2 on p. 19) was measured indirectly through the axle ride height, test track ground surface height and the measured tyre deflection. The measured values are, however, quite reliable, since the error of the base measurements is small.

The rank in measured final length of compressed snow cover between the snow types bears resemblance to the corresponding values in plate load tests. The values of final length of compressed snow cover remained surprisingly steady throughout the succession of passes in each snow type. Sometimes a rise in final length was measured as the number of passes increased. Very gradually declining values of final length could be expected, since the major part of compression is accomplished on the first pass. Increasing values of final length suggest that snow falls into the wheel rut as the wheel passes or that the structure is disturbed by the trailing edge of the tyre.

The trend in mobility model predictions of the final length of compressed snow cover was not duplicated by the measured values, excluding snow type M6. The difference is partly due to the modelled wheel geometry and the operating principle of the model. The circumference of the tyre was always modelled as a segment of a circle and additional sinkage was always needed to support the wheel load, which resulted in a steadily decreasing final length. Collapsing snow from the side walls into the wheel rut was not directly included in the model, since besides being dependent on snow properties, it was of random nature. Most compressing is accomplished on the first pass and the final length

of compressed snow cover can be assumed to remain fairly constant, and therefore even small amounts of snow falling into the rut may change the trend of the final length notably. The loosening of the structure of snow by the trailing edge was partly covered by adding the snow depth and decreasing the length of accomplished compression for the following path.

The trend of measured values of the final length of compressed snow cover in snow type M1 follows model predictions fairly well with an initial snow depth of 0.10 m, yet there is a considerable difference between the measured and modelled values. With an initial snow depth of 0.05 m, the modelled final length is already negligible on the first pass, resulting in considerable error in the level of the values in addition to an erroneous trend. In snow depth of 0.15 m, the measured behaviour of final length of compressed snow cover differs totally from the modelled one. This is most likely due to snow collapsing into the wheel rut. The snow depth data of M1 support the this theory. With an initial snow depth of 0.15 m, the final length increases from the first to second pass, and thereafter stays fairly constant. With the shallower snow covers the final length declines steadily with increasing number of passes, since the probability of collapsing is likely to be lower and the amounts of collapsing snow smaller.

5.4.3 Motion resistance, wheel slip and wheel operation sectors

According to mobility model results, the variation in the combination of snow properties in the range of the experimental data had relatively little effect on the magnitude of motion resistance. The model results are in reasonable accordance with the measurements on the first pass. The model also predicted motion resistance reasonably well for snow types M1, M2, M5 and M6 through all passes. However the model performance in predicting the motion resistance in snow types M3 and M4 was poor.

The mobility model generally over estimated the motion resistance on the first pass. This may be due to the simplifications in the form of the compressing surface cross-section and the equal starting angle of compression throughout the compressive region. Excluding snow types M3 and M4, the error of the model on subsequent passes was small. The model assumptions for snow compression most likely did not correspond to the real behaviour of snow types M3 and M4.

The difference in measured motion resistance between the snow types on the first pass was surprisingly small. This may be caused by the differences in the properties of the snow types, and the resulting differences in the wheel-snow interaction. Snow with high compression strength needs less compression to support the wheel than more easily compressible snow. Since high

compression strength was associated with a low rubber-snow friction coefficient, the compression of these snow types started on higher values of contact angle, where the y-component of the compression pressure was small. Higher compression strength thus resulted in more efficient compression. The contact area, where the assumed flow resistance was present, was correspondingly greater, since the amount of wheel sinkage did not differ to a great extent. The measured difference in flow resistance pressure values was only two fold, but together with the increase in cross-sectional area they made a remarkable difference in the value of flow resistance. As a result, the motion resistance of the two snow types may well be nearly equal. The motion resistance coefficient values for the first pass by Richmond et al. (1990) for the towed front wheels of the instrumented vehicle of CRREL, with comparable initial snow depth-to-wheel radius -ratio and snow density from 190 to 200 kg m^{-3}, were approximately 13 % lower than the values measured in the 0.15 and 0.10 m layers of M1 snow in this study.

The difference in the behaviour of motion resistance between the snow types on the following passes was considerable. The number of pass, when the asymptote value of motion resistance was reached, reflects the differences in snow behaviour well. The behaviour of snow types M5 and M6 could be expected, due to compression results in hard and well bonded snow. In addition snow types M1 and M2 behaved according to expectations, needing a greater number of passes to develop a hard surface. The decline of motion resistance of snow types M3 and M4 was, however slower than expected. It was felt that the snow bonded poorly, and thus slowly declining motion resistance may be caused by repeated work by the wheel in the snow mass with no remarkable increase in density or strength. No measured property of snow types M3 and M4 explains the observed behaviour of motion resistance, although their shear strength was the lowest. A test of cyclic compression and shearing could have explained the behaviour of M3 and M4, as well as revealing interesting differences between the snow types in general.

In snow type M1 with varying initial snow depth, the modelled values of motion resistance are reasonably close to the measured values, whilst motion resistance increased notably with the increase of initial snow depth. On the first pass the model over estimates the motion resistance, though only marginally with an initial snow depth of 0.05 m. The validity of model results on the following passes with an initial snow depth of 0.05 m is questionable since the modelled final length of the compressed snow layer is already close to zero on the first pass, this disagrees with the measured values.

Richmond (1995) measured the motion resistance coefficients on passes 1 to 4 with the CRREL instrumented vehicle in initial snow depth-to-wheel radius -ratio and density (ρ= 230 to 250 kg m^{-3}) closely corresponding to the 0.10 and 0.05 m layers of M1 snow in the present study. The values by Richmond are

very close to the values measured in this study on all but the third pass on snow comparable to the 0.10 m layer of M1 snow, where the value by Richmond is more than double. Obviously the value in question is erroneous, since it is twice as big as the value of the preceding and the following passes.

The error in motion resistance prediction in the conditions of the test axle study of models Blaisdell et al. (1990), Richmond (1995) and the model proposed in this paper is compared in Table 15. As can be noted, the error of Blaisdell et al. (1990) is excessive, and the largest error of the model proposed here is only slightly bigger than the error of the best prediction of Blaisdell et al. (1990). Models proposed by Richmond are based on linear regression of the data collected with the CRREL instrumented vehicle. Richmond's models work well with the test axle data, and the prediction of Richmond's Equation 3 is on average more accurate than the prediction of the proposed model.

Table 15. Error of the proposed model, Blaisdell et al. (1990) (Eq. A1, final density 500 kg m^{-3}) and Richmond (1995) (Eq. 2 and Eq.3) in wheel motion resistance calculation for the first pass of the test axle.

Snow type	Snow depth, m	Model error, %			
		Proposed	Blaisdell et al. (1990)	Richmond (1995), Eq. 2	Richmond (1995), Eq. 3
M1	0.15	43	160	-38	-28
M1	0.10	63	157	-26	-20
M1	0.05	10	126	-11	-10
M2	0.15	42	99	-31	-17
M3	0.15	57	106	-20	-2
M4	0.15	29	71	-30	-14
M5	0.15	-39	-60	-54	-46
M6	0.15	-20	-74	-45	-36

As mentioned previously, the level of slip values is dependent on the chosen rolling radius. Therefore, comparison of measured and modelled slip, determined with the same radius is of prime interest here. Modelled wheel slip on the first pass was dependent on the shear strength of snow on the $2 \cdot \pi$ region of the tyre and the torque induced by compression and flow resistance. The high shear strength of snow types M5 and M6 was able to counteract to slip near the trailing edge on passes 2 to 6. On passes 2 to 6, M5 and M6 type snow was hard and able to support the wheel, additional compaction did not cause great torque, and hence the value of slip rose close to its final level already on the second pass. According to the performed iterations for each snow type and the number of pass, modelled motion resistance was inversely proportional to the value of wheel slip.

Modelled slip in snow types M3 and M4, which had the lowest shear strength, was close to the final value already on the first pass. Snow types M1 and M2 exhibited considerable compaction through the first passes and shear strength above types M3 and M4. Their wheel slip values are below those of M3 and M4, but especially the values of M1 approach to the final value more rapidly.

Measured wheel slip values were generally lower than modelled ones, and the difference between snow types and depths was greater. The fluctuations of the values of consecutive passes largely reflect the accuracy of the measuring method, as does the order of the slip values in the 0.05 and 0.10 m layers of M1 snow. The rapid decrease of modelled slip as a function of the number of passes in snow types M5 and M6 was verified by the experimental data, as was the relatively slow decline of wheel slip in M3 and M4 snow. The relatively consistent measured slip in M3 and M4 supports the assumption of poor bonding with increasing number of passes. In the modelled values on passes 2 to 6, similar behaviour was merely due to low shear strength, since the model did not take into account snow properties in cyclic loading.

Owing to the high rubber-snow interface friction coefficient, snow type M2 exhibited the widest compressive sector and a non-existing flow sector on passes 1 and 2. The low interface friction coefficient of snow type M6, together with compressibility higher than that of M5, resulted in the widest flow sector and the narrowest compressive sector on the first and second passes. Generally, flow resistance was a decisive component of the motion resistance in M5 and M6 on the first pass, whereas it was of little importance in the other snow types.

5.4.4 Model sensitivity

The model was not very sensitive to ±5 % change in the value of any tested single input parameter, when tested on the first pass in 0.15 m of M1 snow. Amongst the parameters, the model was most sensitive to the changes in compressive strength and moisture content of snow in addition to tyre width.

In the model, density directly affected only flow resistance. Therefore, its effect in M1 snow, where the flow sector was relatively narrow, was small. This is in contrast to many empirical mobility models, where snow density often the most important or the sole parameter describing snow properties. The relative effect of density on the first pass in M6 snow, where flow resistance plays an important role, was greater than that of any single studied variable in M1.

In reality, snow properties are cross correlated, and changing just one parameter is contrary to the natural behaviour of snow properties. For example greater

density of natural snow usually means greater grain size and compressive strength, and it may mean greater shear strength, greater moisture content and a lower interface friction coefficient as well.

5.4.5 Wheel-snow interaction

According to the mobility model results, the variation in the combination of snow properties in the range of the experimental data had relatively little effect on the magnitude of motion resistance. This must be partly due to the fact that the snow properties in natural snow covers are cross-correlated, and the changes in snow properties in the course of metamorphism will have opposite effects on motion resistance. For example, according to the sensitivity analysis (Chapter 4.3.5, p. 72), increase in compressive strength increases motion resistance, but in reality it is often accompanied by increased free water content, having an opposite effect.

The variation in snow properties did, however, have a substantial effect on the mechanism of the wheel-snow interaction in the form of the friction coefficient determining the flow and compressive regions of the tyre, sinkage being ultimately defined by the pressure-sinkage relationship. The division into regions, together with the magnitude of flow resistance pressure, had a remarkable effect on the composition of motion resistance. On the first pass, the share of flow resistance of snow-induced motion resistance varied from 0% (M2) to 67% (M6).

Motion resistance increased notably with an increase in initial snow depth. The model predicted motion resistance reasonably well for snow types M1, M2, M5 and M6. The model, however, performed poorly in predicting the motion resistance of snow types M3 and M4. Overall, the motion resistance predictions were surprisingly accurate if compared to the accuracy of predictions of the final length of compressed snow cover. This contradiction is examined in the following.

Wheel slip was one of the key factors determining motion resistance, since it directly affected the direction of the compressive pressure, and hence the relative magnitude of its y- and z-components. The earlier compression start results in a relative increase in the y-component resulting in less efficient compression. Due to its effect on the orientation of pressure, the torque equilibrium for a given entry angle was achieved through adjusting the slip.

The pressure-sinkage relationship together with rubber-snow interface friction had a strong influence on model results. Both compressive strength and the friction coefficient of snow type M2 were higher than those of M1, resulting in a notable difference in the final length of compressed snow cover. The

measured difference between the snow types was both much smaller and inverse. The modelled motion resistance was higher for snow type M2, since an earlier starting angle of compression resulted in less efficient compression and a lower slip value.

The most important difference in the mechanical properties of snow types M5 and M6 were the lower compressive and shear strengths of M6. Since the friction coefficients of the snow types are nearly equal, compression is bound to start at a nearly equal angle of rotation, given constant sinkage. As a result of lower compressive strength, snow of M6 type in reality has to be compressed further to support the wheel. This, in turn results, in higher sinkage, a lower final length of compressed snow cover and a wider flow sector than in the case of M5 type snow. The compression of M6 is accomplished in a direction more vertical than that of M5, resulting in a lower horizontal force component contributing to motion resistance. The positive torque induced by the flow resistance is capable of maintaining a higher slip value in M6 than in M5. These factors may contribute to the difference in motion resistance between M5 and M6 on the first pass.

The concept of snow flow and flow sectors, although physically meaningful, is not entirely sound on latter passes especially in wet snow and at near zero temperatures. Theoretically, the snow may not be compressed by the wheel in the flow region, but the mechanism of failure must be due more to the nature of the fracture. Due to the lugs, the snow is likely to be compressed on a sector wider than proposed by the model. Lugs probably also widen the compressive sector on the first pass.

In photographs of chalk dust marked snow by Richmond (1995), snow in front of the wheel is compressed along curved paths and the snow near the side walls of the tyre is displaced further from the tyre in a lateral direction. Interestingly, snow directly under the tyre also undergoes compaction in a lateral direction along a curved path. Richmond (1995) notes, that displacement of snow near the top of the cover is small compared to deeper layers, this suggests that the deeper layers are more decisive for motion resistance. This is generally in agreement with the findings of the present study for the drier snow types. In M5 and M6, the surface layer is equally important as must also be the case in hard snow.

Measured motion resistance on the first pass showed very little variation between the snow types. It is possible that the vehicle-snow interaction mechanism, suggested for the tracked snow vehicle by Brown (1981) is also at least partly valid for wheel operation. It was found that dense snow experiences relatively little compression, due to its initial density being close to critical density, and it subsequently absorbs relatively little energy. The behaviour of the final length of compressed snow cover and wheel sinkage

compared to motion resistance for the snow types supports the assumption when M5 and M6 are compared with the other snow types.

On the following passes the variation in motion resistance was remarkable. The mechanical properties of the snow type form the basis for the build up of motion resistance. Especially the behaviour in compression on the first pass and in cyclic compression appear to be important properties. In the case of snow types M5 and M6 with initial snow depth of 0.15 m, the measured motion resistance decreased strongly from the first pass to the second, after which it stayed nearly constant. This suggests, that snow is being compressed to a stage where it supports the loading from the test axle wheel on the first pass, and the resistance on the following passes is due to the internal resistance of the tyre and the sinkage of the lugs.

The final length of the compressed snow cover of snow types M3 and M4 remained very constant, which could indicate fairly small amounts of snow collapsing into the rut. Remarkably, only very gradual decline was experienced in motion resistance. One possible cause for the behaviour in M3 and M4 could be the poor bonding of the snow material in compression, and subsequent loosening of the structure in the region of positive slip at the trailing edge of the tyre, which is possibly combined with snow falling into wheel rut.

In addition to the mechanical properties of the snow material, the behaviour of the wheel-snowpack system played an important role in determining the mobility of the test axle wheels. For example, for snow types M1 and M2 with an initial snow depth of 0.15 m, a rise in the final length of compressive snow cover was detected on the second pass. Since the motion resistance decreased with increasing number of passes, the behaviour of final length could be due to snow falling into the wheel rut as the wheel passes. The behaviour of final length and motion resistance in snow type M1 with varying snow depth also indicates snow collapsing into the rut, with more the higher the side walls. Collapsing can be of a more random nature as well, in the case of the wheel not following the rut precisely on subsequent passes. Even in that case, more snow collapses with higher side walls. Remarkably, snow can fall into the rut both in front of and behind wheel axle line on the following passes. The collapse of snow into the wheel rut has also been reported by Richmond (1995).

5.5 Future research and development needs

The basis of the present model is complicated, and many approximations and simplifications regarding snow loading and behaviour were imposed. Some issues, such as the behaviour of snow in the $2 \cdot \pi$ region, the role of tread in determining the friction condition and the flow mechanisms, could not be modelled based on physical principles, but instead empirical tyre parameters were needed. In the course of the study, it became obvious, that the empirical parameters presented are not constant but they change according to snow depth and snow properties. Separate data would be needed to validate the parameters, but it would be better if the model did not require them. Some possibilities are discussed later.

Simplification of the model to utilize a rectangular tyre cross-section would result in uniform snow behaviour across the tread, yielding a single true compression start angle and constant compressive width of the tyre throughout the compressive sector. An empirical study with a smooth tyre with rectangular cross-section, and a wider spread of snow properties, would then reveal the validity of present cycloidal compression and snow flow principles.

An elliptical cross section could be approximated by dividing the tread into a series of belts with varying inclination. A compression start angle would vary between, but not within, the belts, making 3-d approximation possible. In addition the role of the tyre tread pattern should be added to the model. Finally, the elliptical tyre cross-section with variable compression start angle could be introduced to the model, necessitating hardware and software capable of dealing with the increased complexity.

The flow resistance function should be re-formulated as function of the previous loading. The mechanism of snow fracture could be utilized to describe snow behavior in the $2 \cdot \pi$ -region of the tyre. The error of the model was as its greatest in snow types M3 and M4, where the collapsing of snow into the wheel rut was one possible explanation. The phenomena should be examined closer, and a function should be built into the model.

Although the measuring equipment was adequate for the purpose of the study, the need for further development became obvious in the course of the work. Regarding the mobility study equipment, the aim was to keep the system as reliable as possible. Therefore, a datalogger based measuring system was utilized, which imposed limitations with regards to memory capacity. Automated starting and stopping of data collection at each test drive, or even further, measurement of travel distance would enhance the accuracy in determining the location on the test track. A rotation measurement device with better resolution would be needed to improve the accuracy of the determination of wheel slip. In order to determine wheel sinkage after the first pass, ultrasonic

transducers could be utilized to measure the location of the snow layer surface in wheel rut immediately before and after the wheel.

The biggest shortcoming in defining snow properties was the lack of data in cyclic loading. The behaviour in cyclic loading is another possible explanation for the model results in snow types M3 and M4.

The precise definition physical snow properties would call for 3-d measurements of grain size and form.

5.6 Concluding remarks

The main aims of this work were to examine the effect of selected snow cover properties on the mobility parameters of a towed wheel, to form a model describing the interaction of the towed wheel and snow and to study the feasibility of a microwave sensor for determining the free water content and density of snow for vehicle mobility analysis.

The mobility model and field test were simplifications of the real wheel-snow interaction in the sense, that the snow cover consisted of only a single snow type. This type of test arrangement was needed to determine the differences due to snow cover properties alone. In reality, snow cover normally consists of more than one snow type, the vertical location and properties of which determine wheel mobility. In the mobility model, simplifications were extended beyond the structure of snow to wheel geometry and snow loading as well. Some phenomena were treated with empirical parameters.

In the field tests with constant snow depth, the effect of snow properties on motion resistance on the first pass was small, but the behaviour of the resistance on the following passes differed between the snow types. Also, snow properties had a notable effect on other examined mobility parameters. The effect of snow depth on mobility parameters in M1 type snow was clear. In conjunction with the field tests, the microwave sensor was found to be an extremely useful tool for measurements of snow density and free water content. The accuracy of the density measurement is sufficient, supposing that the bias will be solved. The accuracy of free water content measurements could not be controlled.

Compressive strength, shear strength, interface friction and the flow resistance of snow were measured and used as input variables in the constructed mobility model, which was based on cycloidal compression of a uniform snow layer. With measured snow properties as input variables, the mobility model yielded realistic values for mobility parameters. The basis of the mobility model can be assumed to be realistic, and the measured properties of snow seemed to have an

effect on mobility. The role of the starting angle of compression, determined by the coefficient of rubber-snow interface friction, was important. The lack of function for cyclic loading was a shortcoming in the model.

As expected, the hypothesis of increasing motion resistance with increasing snow depth was supported on the basis of modelled and empirical results. However, contrary to expectation, motion resistance was not directly affected by the state of metamorphosis and grain size.

A model is always a compromise between fidelity to the real system and operability. In the present study, this also became obvious since the execution time was reduced from three hours on the first pass to 10 minutes on the following passes merely due to single integrals replacing double integrals. In its present form, the model for the first pass is more suitable for office work. Providing computing power is not a limitation, a more sophisticated tyre model would benefit the model, such as proposed by Abd El-Gawwad et al. (1999).

The behaviour of snow outside the compressive region and the cyclic loading of snow, as well as the role of tyre tread pattern and the behaviour of snowpack adjoining the wheel should be addressed in future work. The main value of the work was, that it gave a valuable insight into wheel-snow interaction, which would have been very difficult to reach merely on the basis of empirical data. On the other hand, empirical data was of great importance in defining the missing links in the model.

References

Abd El-Gawwad, K. A., Crolla, D. A., Soliman A. M. A. & El-Sayed, F. M. 1999. Off-Road Tyre Modelling I: The Multi-Spoke Tyre Model Modified to Include the Effect of Straight Lugs. Journal of Terramechanics, Vol. 36, No. 1., pp. 3-24. ISSN 0022-4898.

Agricultural Tyres. Trelleborg Industri AB, Trelleborg, Sweden. Product Catalogue. 20 p.

Ala-Ilomäki, J. 1986. Harvennushakkuisiin soveltuvan maastokuljetuskaluston liikkuvuus lumessa. (In Finnish). M.Sc. Thesis, University of Helsinki. 156 p.

— 1991. Ajoneuvon kulkualustan mekaanisten ominaisuuksien mittausmenetelmän kehittäminen. (In Finnish). 32/Mdd248/89 loppuraportti. MATINE, Helsinki, Finland. 5 p.

— , Hallikainen, M., Saarilahti, M. & Toikka, M. 1989. Microwave Snow Sounding for Trafficability Analysis. Subzero Engineering Conditions Conference Proceedings, pp. 145-150. Society of Automotive Engineers, Inc., Warrendale, PA, USA. ISBN 0-89883-84-8.

Abele, G. 1975. Compressibility Characteristics of Undisturbed Snow. ISTVS 5th International Conference Proceedings, Vol. 2, pp. 379-399.

Arfken, G., 1970. Mathematical Methods for Physicists. Second Edition. Academic Press. 815 p. ISBN 0-12-059832-9.

ASAE Standard: ASAE S296.3, Uniform Terminology for Traction of Agricultural Tractors, Self-Propelled Implements, and Other Traction and Transport Devices. In: ASAE Standards 1995, 42nd Edition, pp. 119-121. ISBN 0-929355-65-2.

Bader, H. 1962. The Physics and Mechanics of Snow as a Material. U. S. Army Cold Regions Research and Engineering Laboratory, Hanover, New Hampshire, USA. 79 p.

Bajpai, A. C., Mustoe, L. R. & Walker, D. 1989. Engineering Mathematics. Second Edition. John Wiley & Sons. 714 p. ISBN 0-471-92283-8.

Baladi, G. Y. & Rohani, B. 1984. Development of a Soil-Wheel Interaction Model. Proceedings of 8th International Conference of ISTVS, Vol. 1, c/o CRREL, Hanover, NH, USA. pp. 33-60.

Bekker, M. G. 1969. Introduction to Terrain-Vehicle Systems. University of Michigan Press, Ann Arbor, MI, USA. 846 p.

Blaisdell G. L. 1981. Predicting Wheeled Vehicle Motion Resistance in Shallow Snow. CRREL Special Report 81-30. U.S. Army Cold Regions Research and Engineering Laboratory, Hanover, NH, USA. 18 p

— 1983a. Driving Traction on Ice and Snow With All-Season and Mud-And-Snow Radial Tires. CRREL Report 83-27. U.S. Army Cold Regions Research and Engineering Laboratory, Hanover, NH, USA. 22 p.

— 1983b. The CRREL Instrumented Vehicle: Hardware and Software. CRREL Report 83-3. U.S. Army Cold Regions Research and Engineering Laboratory, Hanover, NH, USA. 75 p.

— 1987. Trailing-Tire Motion Resistance in Shallow Snow. Proceedings of 9th International Conference of ISTVS, Vol. 1, c/o CRREL, Hanover, NH, USA. pp. 296-304.

— , Richmond, P. W., Shoop, S. A., Green, C. E. & Alger, R. G. 1990. Wheels and Tracks in Snow. Validation Study of the CRREL Shallow Snow Mobility Model. CRREL Special Report 90-9. U.S. Army Cold Regions Research and Engineering Laboratory, Hanover, NH, USA. 72 p.

Brown, R. L. 1981. An Analysis of Vehicle Power Requirements in Deep Snowpack. Journal of Terramechanics, Vol. 18, No. 3, pp. 169-181. ISSN 022-4898.

— 1989. Perspective on Mechanical Properties of Snow. Proceedings of the 1st International Conference on Snow Engineering, CRREL Special Report 89-6. U.S. Army Cold Regions Research and Engineering Laboratory, Hanover, NH, USA. pp. 502-503.

Conant, F. S. & Liska, J. W. 1960. Friction Studies on Rubberlike Materials. Rubber Chemistry and Technology, 33(1960), pp. 1218-1258.

Colbeck, S. C. 1982. An Overview of Seasonal Snow Metamorphism. Reviews of Geophysics and Space Physics, Vol. 20, No. 1, pp. 46-51.

— 1997. A Review of Sintering in Seasonal Snow. CRREL Report 97-10. U.S. Army Cold Regions Research and Engineering Laboratory, Hanover, NH, USA. 11 p.

CR10 Measurement and Control Module. 1990. Instruction Manual. Campbell Scientific Ltd., Shepshed, Leicestershire, UK. 298 p.

Craig, R. F. 1992. Soil Mechanics. Fifth Edition. Chapman & Hall. 427 p. ISBN 0-412-39590-8.

Doebelin, E. O. 1990. Measurement Systems: Application and Design. Fourth Edition. McGraw-Hill. 960 p. ISBN 0-07-017338-9.

Edens, M. Q. & Brown, R. L. 1993. The Relationship Between the Microstructure and Mechanical Properties of Snow. First International Conference on Winter Vehicle Mobility, CRREL Special Report 93-17. U.S. Army Cold Regions Research and Engineering Laboratory, Hanover, NH, USA. pp. 164-173.

Ericksson, R. 1949. Medens friktion mot snö och is. (In Swedish). Föreningen Skogsarbeten, Kunglige Domänstyrelsens Arbetstudieavdelning, Meddelande 34-35, 63 p.

Finnish Statistical Yearbook of Forestry. 1999. Finnish Forest Research Institute, Helsinki, Finland. 352 p. ISBN 951-40-1705-6.

Freitag, D. R., Schafer, R. L. & Wismer, R. D. 1970. Similitude Studies of Soil-Machine Systems. Transactions of ASAE, 13 (2), pp. 201-213.

Gee-Clough, D. 1979. The Effect of Wheel Width on the Rolling Resistance of Rigid Wheels in Sand. Journal of Terramechanics, Vol. 15, No. 4, pp. 161-184. ISSN 022-4898.

Gieck, K. & Gieck, R. 1990. Engineering Formulas. Sixth Edition. McGraw-Hill, Inc. 295 p. ISBN 0-07-023455-8.

Green, C. E., Grimes, K. & Blaisdell, G. 1989. Wheeled versus Tracked Vehicle Snow Mobility Test Program. ISTVS 3rd North American Meeting Proceedings, pp. 146-164.

Haarlaa, R. 1971. Maaston ja kuorman vaikutus metsätraktoreiden ajonopeuteen [Effect of Terrain and Load on the Driving Speed of Logging Tractors]. University of Helsinki, Department of Logging and Utilization of Forest Products, Research Notes No. 9. 88 p.

Harrison, W. L. 1981. Shallow Snow Model for Predicting Vehicle Performance. CRREL Report 81-20. U.S. Army Cold Regions Research and Engineering Laboratory, Hanover, NH, USA. 21 p.

Högnäs, T. & Silvennoinen, U. 1981. Bruunett Mini 578 F -kuormatraktorin lumikelpoisuus. (In Finnish). Metsähallituksen kehittämisjaosto, koeselostus No. 159. 19 p.

Image-Pro Plus Version 1.0 for Windows. Reference Manual. 1993. Media Cybernetics, Silver Spring, MD, USA. 390 p.

International Society for Terrain-Vehicle Systems Standards. 1977. Journal of Terramechanics, Vol. 14, No. 3, pp. 153-182.

ISTVS Committee on Snow Mechanic Research Coordination, 1978. Requirement for Identification and Characterization of Snow for Mobility Purposes. Proceedings of 6th International Conference of ISTVS, Vol. 3, c/o CRREL, Hanover, NH, USA. pp. 933-949.

Järvinen, E. & Makkonen, L. 1987. Lumen ominaisuuksien mittaaminen [Measurement of Snow Properties]. Technical Research Centre of Finland, Research Notes 759, 54 p.

Kendra, J. R., Ulaby, F. T. and Sarabandi, K. 1994. Snow Probe for In Situ Determination of Wetness and Density. IEEE Transactions on Geoscience and Remote Sensing, Vol. 32, No. , November 1994, pp. 1152-1159.

Klein, G. J. 1947. Snow Characteristics of Aircraft Skis. National Research Council of Canada, Aeronautics Report AR-2, 17 p.

Kolkki, O. 1969. Katsaus Suomen ilmastoon. (In Finnish). Ilmatieteen laitoksen tiedonantoja No. 18. 64 p.

Kraftaufnehmer mit DMS-System, U 9. 1988. (In German). Hottinger Baldwin Messtechnik GMBH, Darmstadt, Germany. Users Manual. 30 p.

Kreyszig, E. 1988. Advanced Engineering Mathematics. John Wiley & Sons, Inc. 1413 p. ISBN 0-471-62787-9.

LaChapelle, E. R. 1992. Field Guide to Snow Crystals. Reprint Edition, International Glaciological Society, Cambridge, 101 p.

Langham, E. J. 1981. Physics and Properties of Snowcover. In: Handbook of Snow, Edited by Gray, D. M. & Male, D. H., Pergamon Press Canada Ltd, pp. 275-337.

Leyton, L. 1975. Fluid Behaviour in Biological Systems. Oxford University Press. 235 p. ISBN 0 19 854126 0.

LM35/LM35A/LM35C/LM35CA/LM35D Precision Centigrade Temperature Sensors. 1992. National Semiconductor Corporation, National Semiconductor GMBH, Fürstenfeldbruck, Germany. Data Leaflet. 10 p.

Load Cells for Electronic Force Measurements and Weighing Applications. 1991. Kyowa Electronic Instruments CO., LTD., Tokyo, Japan. Product Catalogue No. 2005B. 20 p.

Mathcad. User's Guide. 1995. Math Soft Inc., Cambridge, MA, USA. 694 p. ISBN 0-942075-79-X.

McClung, D. 1977. Direct Simple Shear Tests on Snow and Their Relation to Slab Avalanche Formation. Journal of Glaciology, Vol. 19, No. 81, pp. 101-109.

Mellor, M. 1964. Properties of Snow. U. S. Army Materiel Command, Cold Regions Research & Engineering Laboratory, Hanover, New Hampshire. 105 p.

— 1975. A Review of Basic Snow Mechanics. Symposium. Mécanique de la neigee. Actes du colloque de Grindelwald, avril 1974. IAHS-AISH Publication No. 114. International Association of Hydrological Sciences, IAHS Press, Oxfordshire, UK. pp. 251-291

— 1977. Engineering Properties of Snow. Journal of Glaciology, Vol. 19, No. 81, pp 15-66.
de Montmollin, V. 1982. Shear Tests on Snow Explained by Fast Metamorphism. Journal of Glaciology, Vol. 28, No. 98, pp. 187-198.
Mundl, R., Meschke, G. & Liederer, W. 1997. Friction Mechanism of Tread Blocks on Snow Surfaces. Tire Science and Technology, TSTCA, Vol. 25, No. 4, pp. 245-264.
Muro, T. 1984. Shallow Snow Performance of Tracked Vehicle. Soils and Foundations, Vol. 24, No. 1, pp. 63-76. Japanese Society of Soil Mechanics and Foundation Engineering.
Osborne, M. D. & Alger, R. G. 1989. The Effects of Free Water Content of Snow on Mobility of Rubber Tired Vehicles -A Preliminary Study. ISTVS 3rd North American Meeting Proceedings, c/o CRREL, Hanover, NH, USA. pp. 225-233.
Oida, A., 1979. Study on equation of shear stress-displacement curves. Report No.5, Farm Power and Machinery Laboratory, Kyoto University.
Palosuo, E. 1981. Lumen raekoon vaikutus suksen luistoon [Relation Between Coefficient of Friction and Snow Grain Size for Plastic Skis]. In: X geofysiikan päivät Helsingissä 23-24.4.1981, Geofysiikan seura, Helsinki, pp. 89-95.
Perla, R., Beck, T. M. H. & Cheng, T. T. 1982. The Shear Strength Index of Alpine Snow. Cold Regions Science and Technology, 6(1982), pp. 11-20.
Precision Potentiometers. 1993. Midori Precisions CO., LTD. Product Catalogue. 16 p.
Richmond, P. W. 1995. Motion Resistance of Wheeled Vehicles in Snow. CRREL Report 95-7. U.S. Army Cold Regions Research and Engineering Laboratory, Hanover, NH, USA. 39 p.
— , Blaisdell, G. L. & Green, C. E. 1990. Wheels and Tracks in Snow. Second Validation Study of the CRREL Shallow Snow Mobility Model. CRREL Report 90-13. U.S. Army Cold Regions Research and Engineering Laboratory, Hanover, NH, USA. 39 p.
Roberts, A. D. & Richardson, J. C. 1981. Interface Study of Rubber-Ice Friction. Wear, 67(1981), pp. 55-69.
Salm, B. 1982. Mechanical Properties of Snow. Reviews of Geophysics and Space Physics, Vol. 20, No. 1, pp. 1-19.
SAS/STAT User's Guide. 1994. Version 6, Fourth Edition. Volume 2. SAS Institute Inc., Cary, NC, USA. 1739 p. ISBN 1-55544-376-1.
Schafer, R. L., Freitag, D. R. & Wismer, R. D. 1973. Distortion in the Similitude of Soil-Machine Systems. Journal of Terramechanics, Vol. 9, No. 2, pp. 33-63. ISSN 022-4898.
Shapiro, L. W., Johnson, J. B., Sturm, M. & Blaisdell, G. L. 1997. Snow Mechanics: Review of the State of Knowledge and Applications. CRREL Report 97-3. U.S. Army Cold Regions Research and Engineering Laboratory, Hanover, NH, USA. 35 p.
Shoop, S. A. 1989. Thawing Soil Strength Measurements for Predicting Vehicle Performance. ISTVS 3rd North American Meeting Proceedings, c/o CRREL, Hanover, NH, USA. pp. 165-182.
— & Alger, R. 1991. Snow Characterization for Traction Testing: A Survey of Techniques Used. First International Conference on Winter Vehicle Mobility,

CRREL Special Report 93-17. U.S. Army Cold Regions Research and Engineering Laboratory, Hanover, NH, USA. pp. 186-189.
Sihvola, A. & Tiuri, M. 1986. Snow Fork for Field Determination of the Density and Wetness Profiles of a Snow Pack. IEEE Transactions on Geoscience and Remote Sensing, Vol. GE-24, No. 5, pp. 717-721.
Silvennoinen, U. 1980. Talven 1980 lumikokeet. (In Finnish). Metsähallituksen kehittämisjaosto, koeselostus No. 149. 18 p.
— & Haarlaa, R. 1971. Metsätraktoreiden liikkuvuus lumessa [The Mobility of Logging Tractors on Snow]. Silva Fennica, Vol. 5, No. 2, pp. 145-167.
Sirén, M., Ala-Ilomäki, J. & Högnäs, T. 1987. Harvennushakkuisiin soveltuvan metsäkuljetuskaluston maastokelpoisuus [Mobility of Forwarding Vehicles Used in Thinnings]. Folia Forestalia 692. 60 p. ISBN 951-40-0784-0.
Sirviö, J. 1994. Moreenimaan kivisyyden ja väliaineen ominaisuuksien mittaaminen tunkeutumisvastusmittarilla. (In Finnish). M.Sc. Thesis. University of Helsinki. 53 p.
Snow Fork Measures the Density and the Liquid Water Content of Snow. Insinööritoimisto Toikka, Espoo, Finland. Sales brochure. 4 p.
Snow Fork. User's manual. Insinööritoimisto Toikka, Espoo, Finland. 20 p.
Sommerfeld, R. A., King R. M. & Budding, F. 1976. A Correction Factor for Roch's Stability Index of Slab Avalanche Release. Journal of Glaciology, Vol. 17, No. 75, pp. 145-147.
Terrängmaskinen. 1981. (In Swedish). Forskningsstiftelsen Skogsarbeten. 461 p. ISBN 91-7614-012-1.
The Driving Force Behind Logging. 1994. Nokia Tyres, Nokia, Finland. Product Catalogue. 8 p.
Tiuri, M. E., Sihvola, A. H., Nyfors, E. G. & Hallikainen, M. T. 1984. The Complex Dielectric Constant of Snow at Microwave Frequencies. IEEE Journal of Oceanic Engineering, Vol. OE-9, No. 5, pp. 377-382.
Torque/Screw Torque Transducers T 4A, T 4WA. 1987. Hottinger Baldwin Messtechnik GMBH, Darmstadt, Germany. Data Leaflet. 2 p.
Transducers and Systems. DS Europe SAS, Milan, Italy. Product Catalogue. 32 p.
Upadhyaya, S. K., Chancellor, W. J., Wulfsohn, D. & Glancey, J. L. 1988. Sources of Variability in Traction Data. Journal of Terramechanics, Vol. 25, No. 4, pp. 249-272. ISSN 0022-4898.
Wismer, R. D., Freitag, D. R. & Schafer, R. L. 1973. Application of Similitude to Soil-Machine Systems. Journal of Terramechanics, Vol. 13, No. 3, pp. 153-183. ISSN 022-4898.
Wong, J. Y. 1989. Terramechanics and Off-Road Vehicles. Elsevier. 251 p. ISBN 0-444-88301-0.
Yong, R N. & Fukue, M. 1977. Performance of Snow in Confined Compression. Journal of Terramechanics, Vol. 14, No. 2, pp. 59-82. ISSN 022-4898.
— & Harrison, W. L. 1988. On Vehicle Mobility in Snow-Covered Terrain - Problem Development and Requirements for Analysis. Journal of Terramechanics, Vol. 15, No. 4, pp. 223-235. ISSN 022-4898.
— & Metaxas, I. 1985. Influence of Age-Hardening and Strain Rate on Confined Compression and Shear Behaviour of Snow. Journal of Terramechanics, Vol. 22, No. 1, pp. 37-49. ISSN 022-4898.
Z-Folded Load Cells. DS Europe SAS, Milan, Italy. Data Sheet. 2 p.

Appendix 1. Flowchart of the Mathcad programme describing the interaction of towed wheel and snow

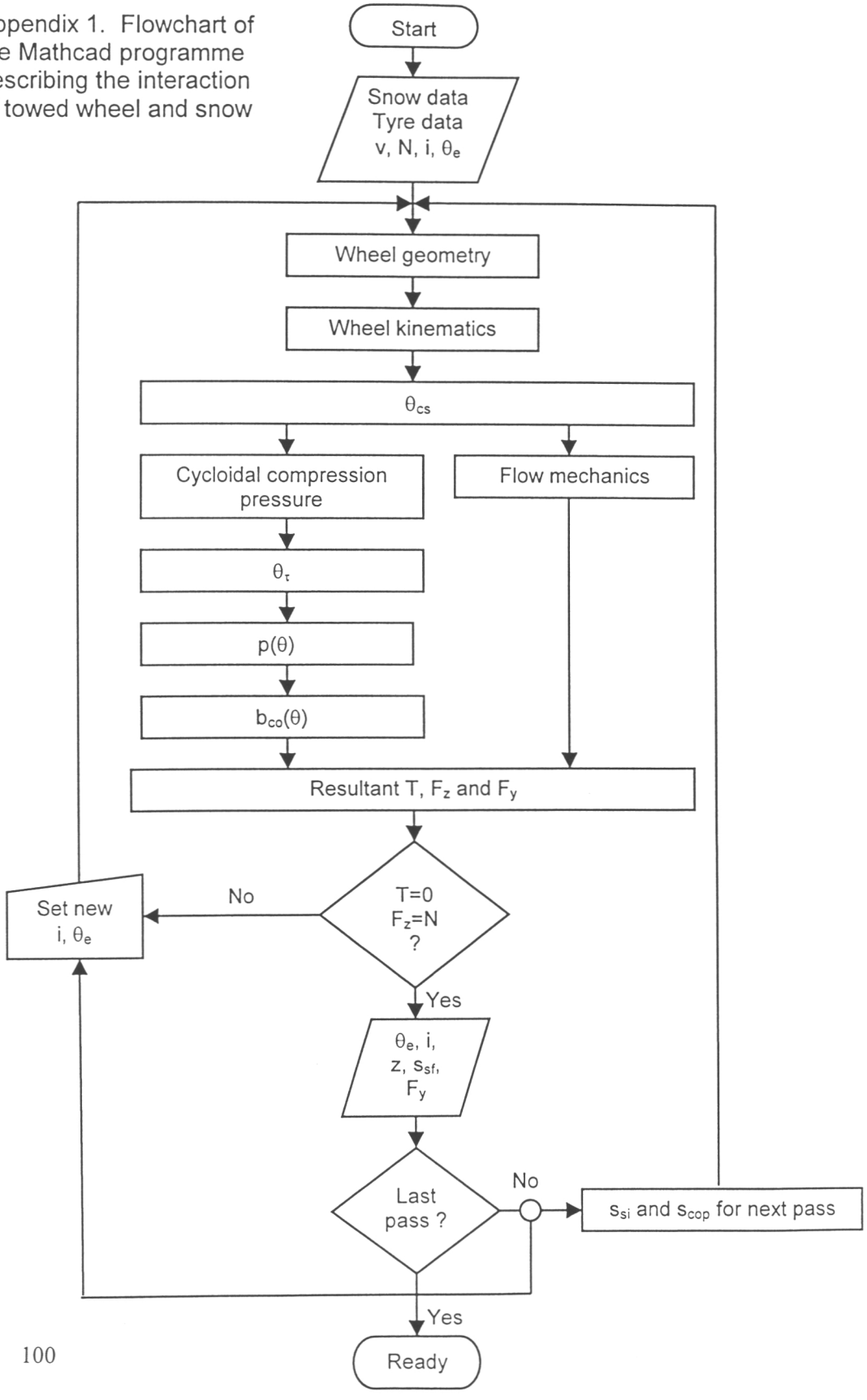

Appendix 2. Pressure (p) vs. plate sinkage (z) data and fitted models (Equation 30, p. 25 and Table 8, p. 54) for snow types M1 to M6 and plate diameters 0.07 and 0.11 m. Data not included in fitting the model is marked with circles (See Chapter 3.7 p. 46).

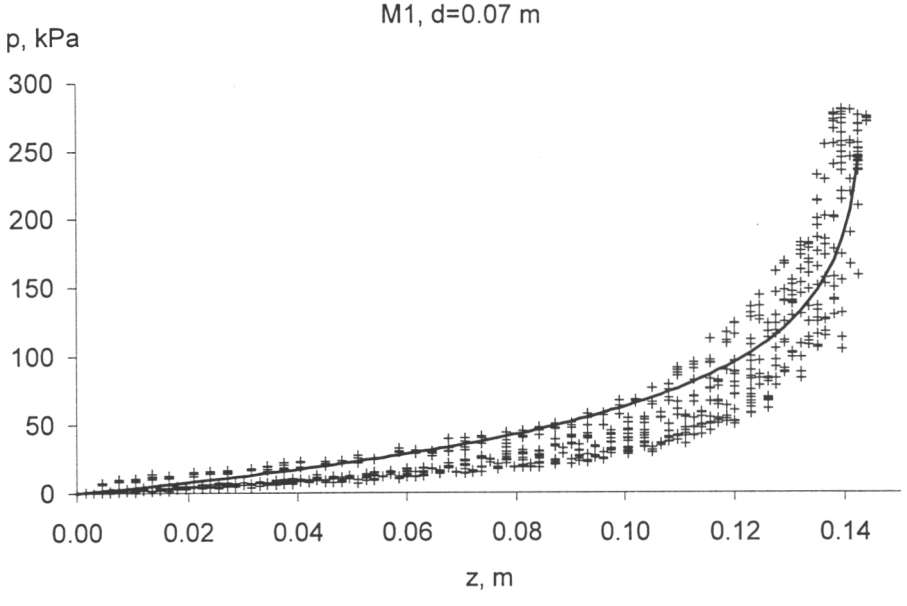

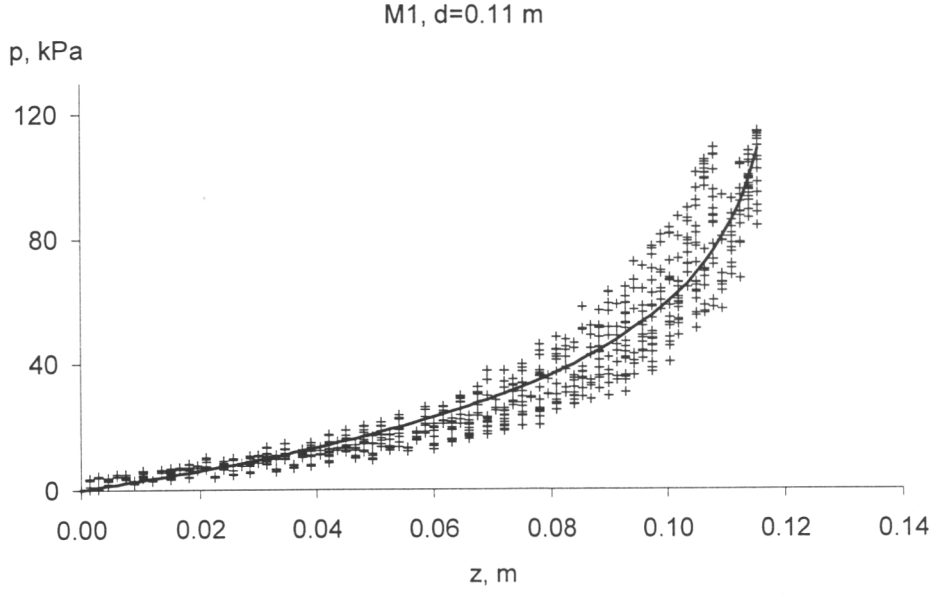

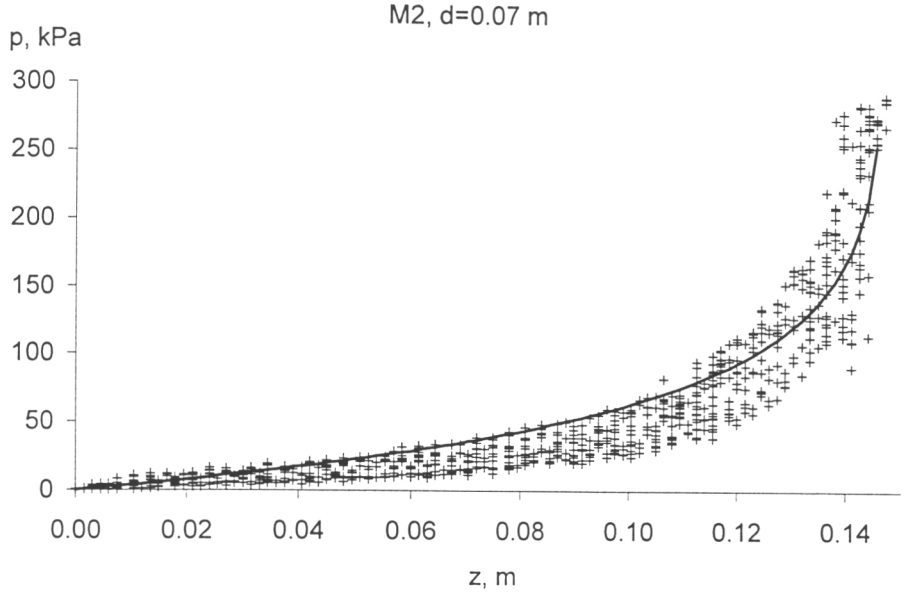
M2, d=0.07 m
p, kPa
300
250
200
150
100
50
0
0.00
0.02
0.04
0.06
0.08
0.10
0.12
0.14
z, m

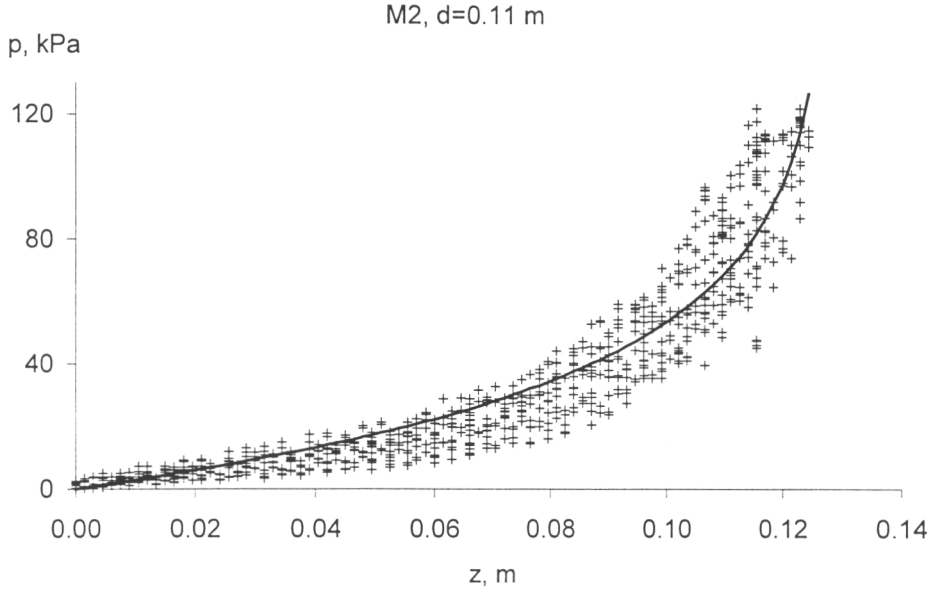
M2, d=0.11 m
p, kPa
120
80
40
0
0.00
0.02
0.04
0.06
0.08
0.10
0.12
0.14
z, m

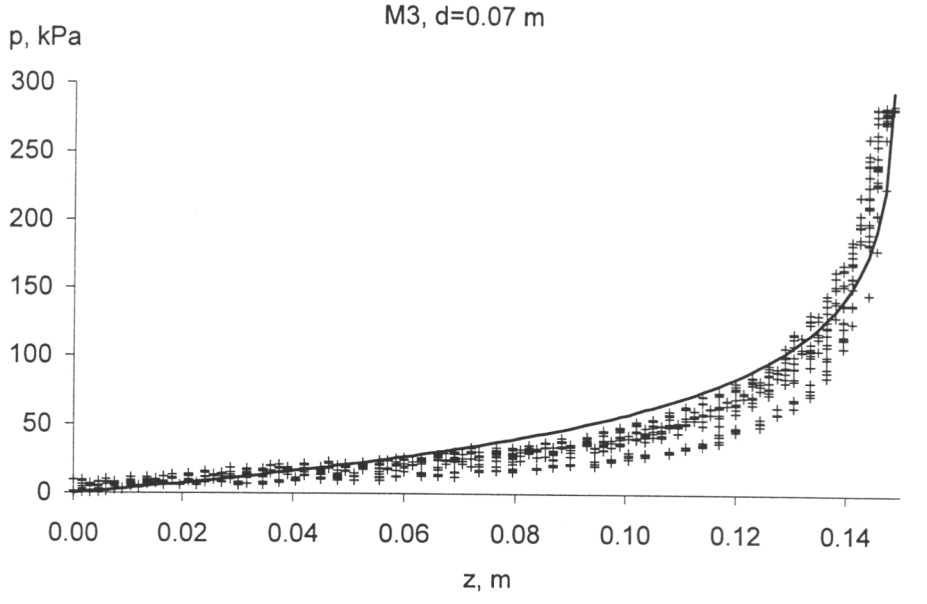
M3, d=0.07 m
p, kPa
300
250
200
150
100
50
0
0.00
0.02
0.04
0.06
0.08
0.10
0.12
0.14
z, m

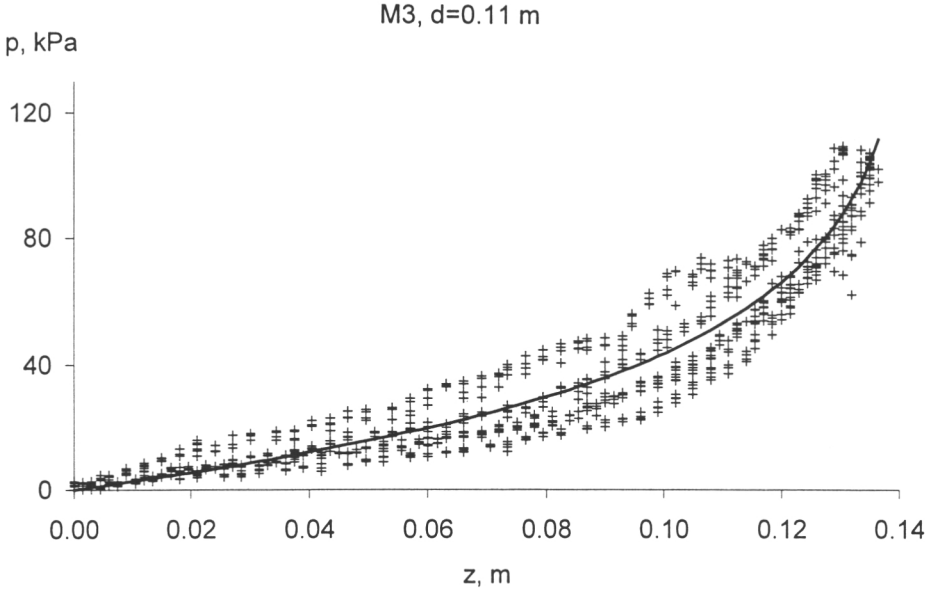
M3, d=0.11 m
p, kPa
120
80
40
0
0.00
0.02
0.04
0.06
0.08
0.10
0.12
0.14
z, m

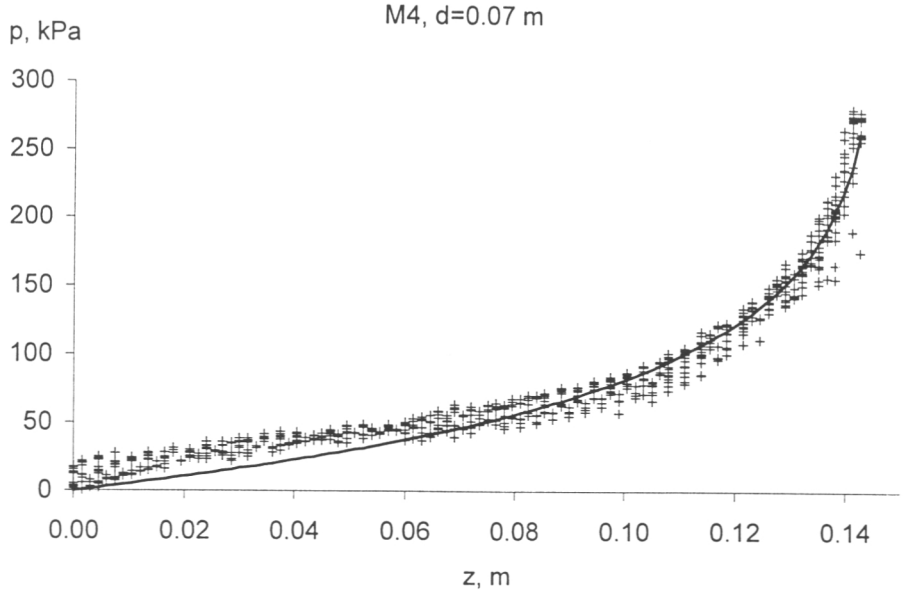
M4, d=0.07 m
p, kPa
300
250
200
150
100
50
0
0.00
0.02
0.04
0.06
0.08
0.10
0.12
0.14
z, m

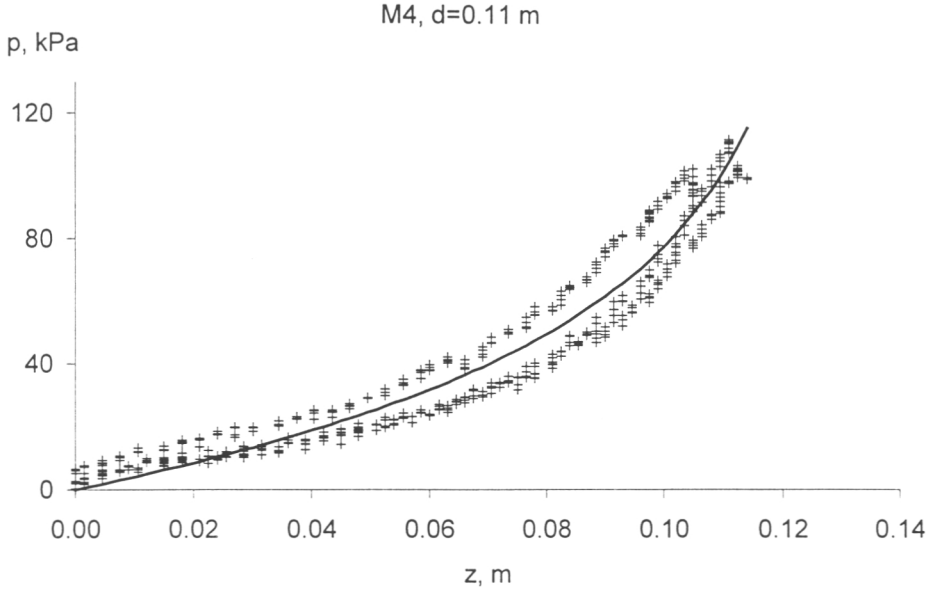
M4, d=0.11 m
p, kPa
120
80
40
0
0.00
0.02
0.04
0.06
0.08
0.10
0.12
0.14
z, m

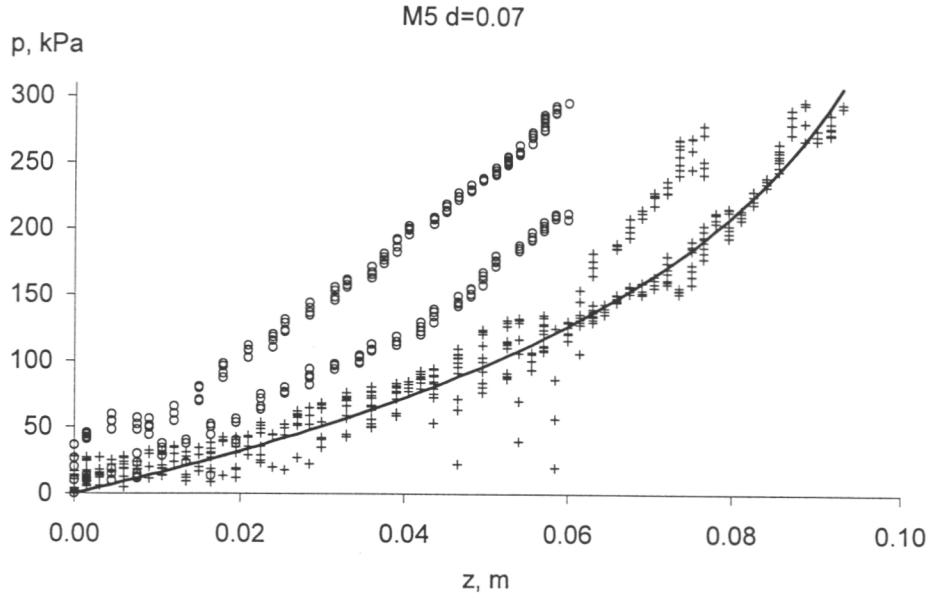
M5 d=0.07
p, kPa
300
250
200
150
100
50
0
0.00
0.02
0.04
0.06
0.08
0.10
z, m

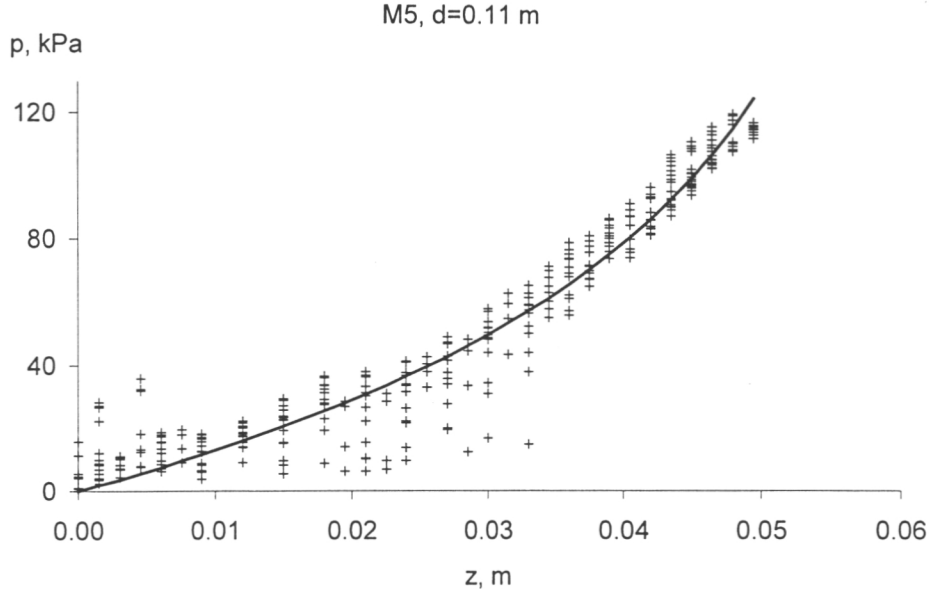
M5, d=0.11 m
p, kPa
120
80
40
0
0.00
0.01
0.02
0.03
0.04
0.05
0.06
z, m

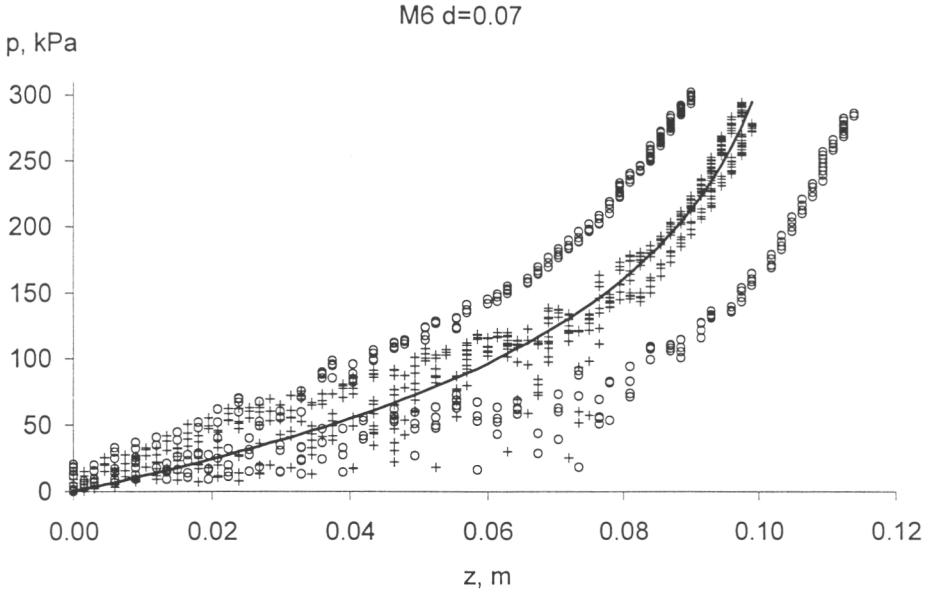
M6 d=0.07
p, kPa
300
250
200
150
100
50
0
0.00
0.02
0.04
0.06
0.08
0.10
0.12
z, m

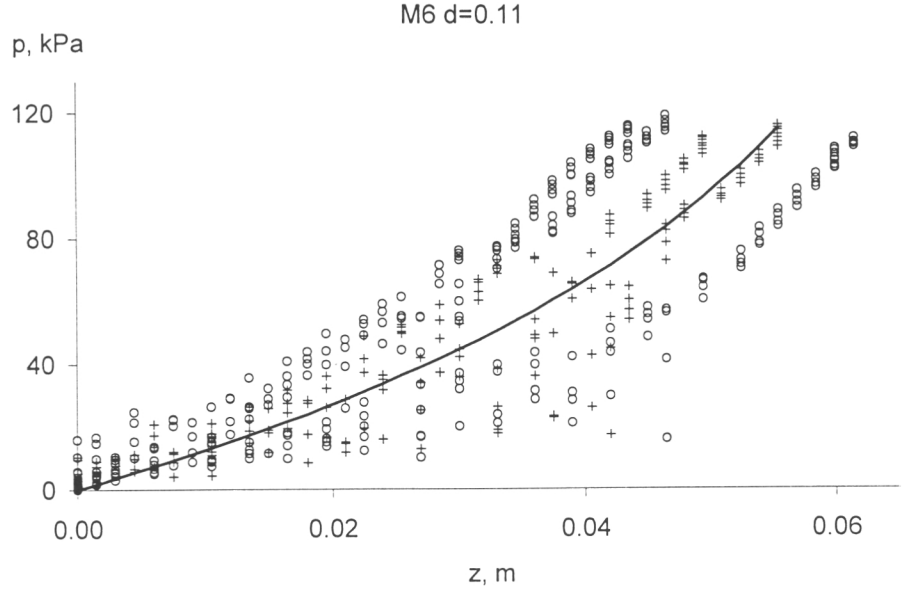
M6 d=0.11
p, kPa
120
80
40
0
0.00
0.02
0.04
0.06
z, m

Appendix 3. Shear strength (τ) vs. shear displacement (j) data and fitted models (Equation 73, p. 54 and Table 9, p. 55) for snow types M1 to M6.

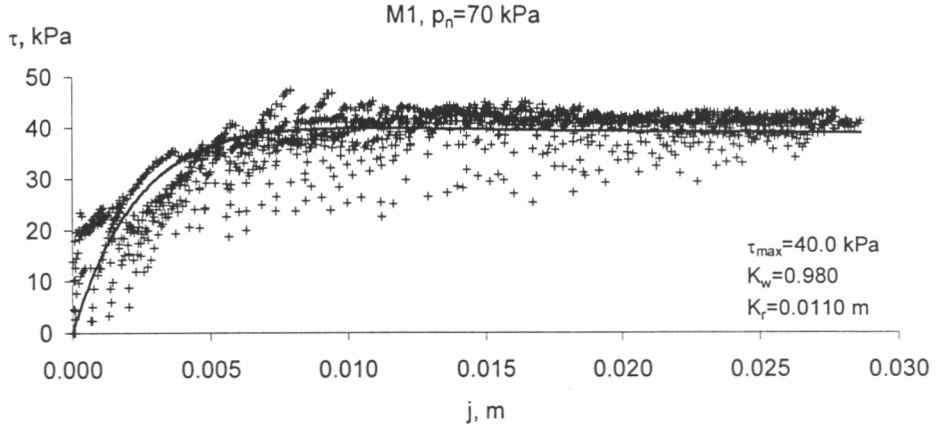

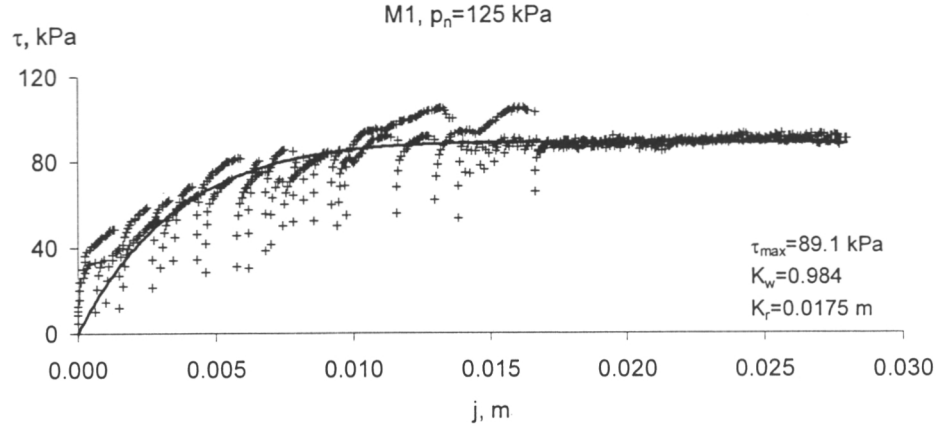

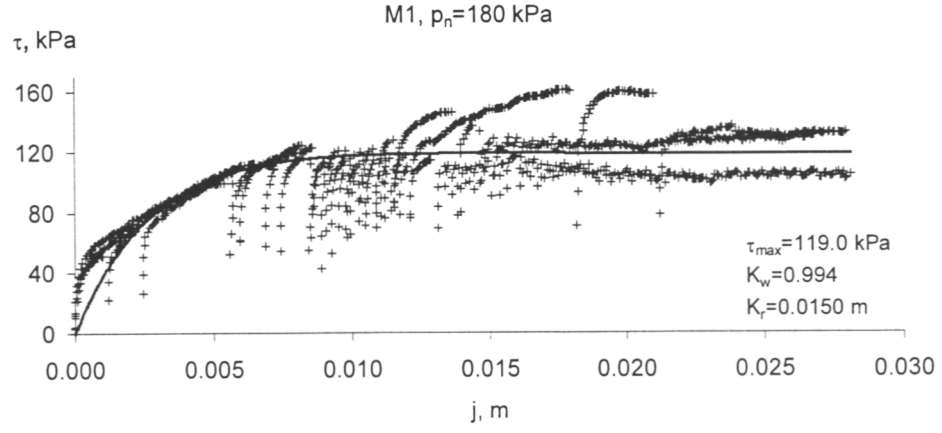

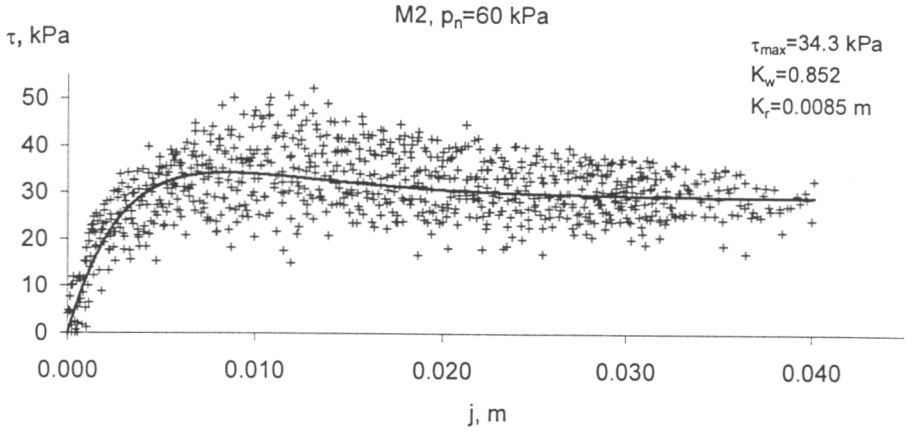
M2, p_n=60 kPa
τ, kPa
τ_{max}=34.3 kPa
K_w=0.852
K_r=0.0085 m
50
40
30
20
10
0
0.000
0.010
0.020
0.030
0.040
j, m

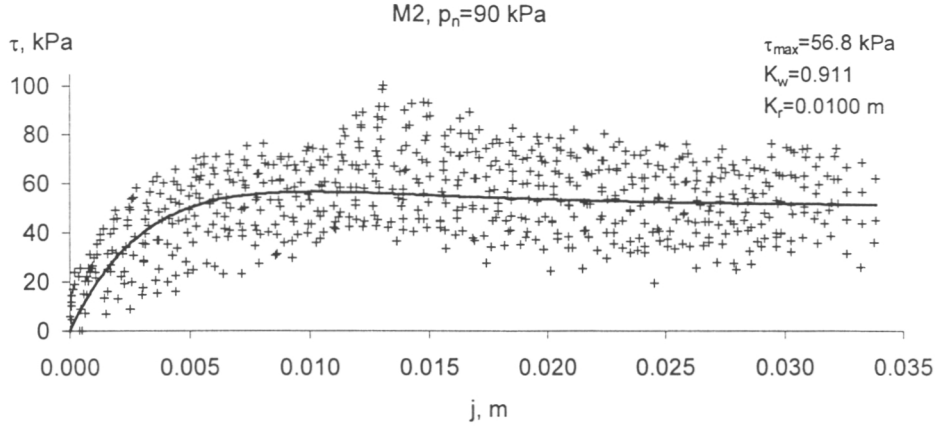
M2, p_n=90 kPa
τ, kPa
τ_{max}=56.8 kPa
K_w=0.911
K_r=0.0100 m
100
80
60
40
20
0
0.000
0.005
0.010
0.015
0.020
0.025
0.030
0.035
j, m

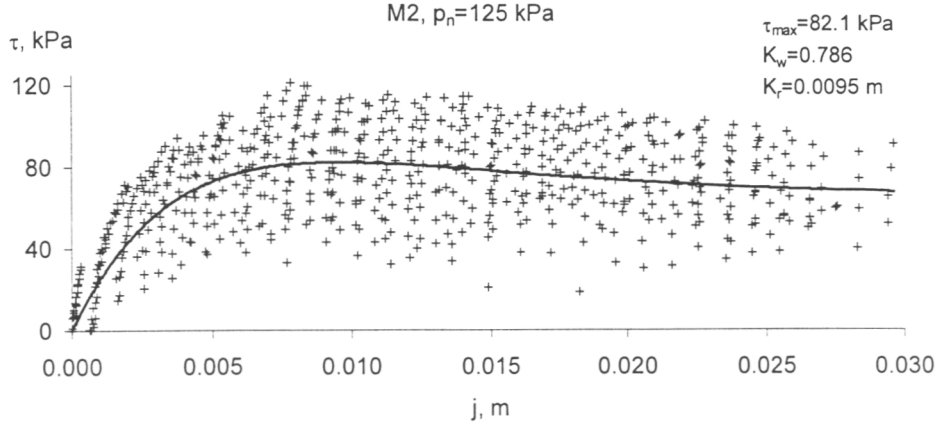
M2, p_n=125 kPa
τ, kPa
τ_{max}=82.1 kPa
K_w=0.786
K_r=0.0095 m
120
80
40
0
0.000
0.005
0.010
0.015
0.020
0.025
0.030
j, m

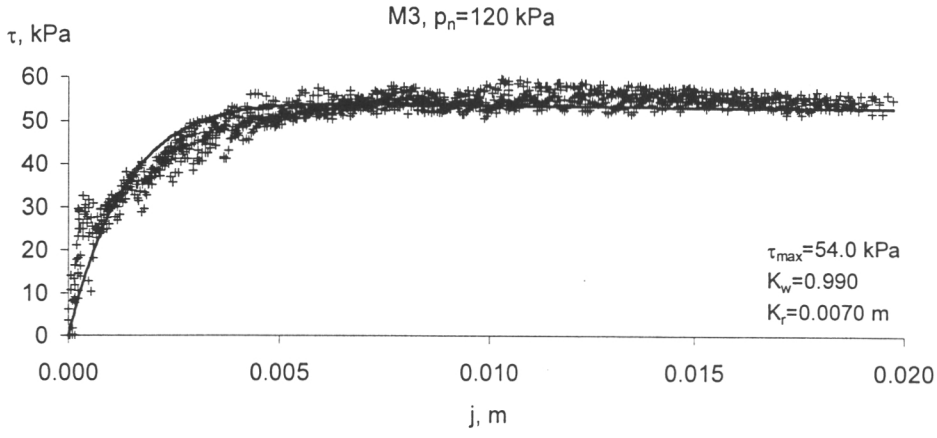
M3, p_n=120 kPa
τ, kPa
60
50
40
30
20
10
0
0.000
0.005
0.010
0.015
0.020
j, m
τ_{max}=54.0 kPa
K_w=0.990
K_r=0.0070 m

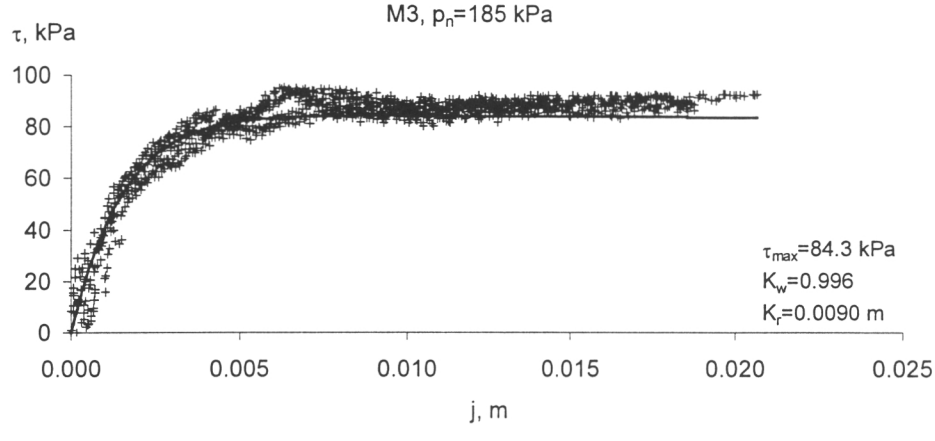
M3, p_n=185 kPa
τ, kPa
100
80
60
40
20
0
0.000
0.005
0.010
0.015
0.020
0.025
j, m
τ_{max}=84.3 kPa
K_w=0.996
K_r=0.0090 m

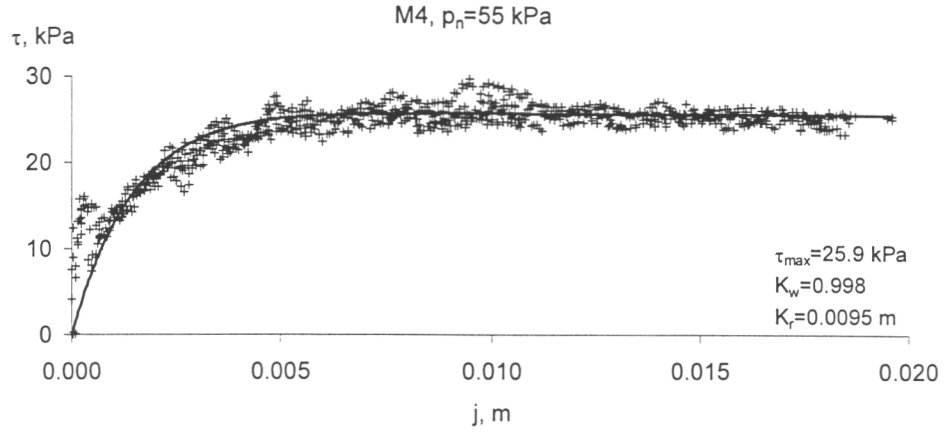
M4, p_n=55 kPa
τ, kPa
30
20
10
0
0.000
0.005
0.010
0.015
0.020
j, m
τ_{max}=25.9 kPa
K_w=0.998
K_r=0.0095 m

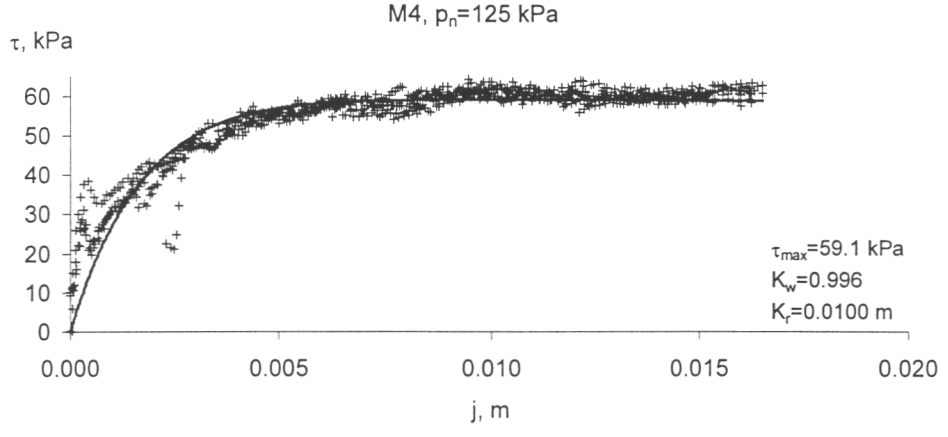
M4, p_n=125 kPa
τ, kPa
60
50
40
30
20
10
0
0.000
0.005
0.010
0.015
0.020
j, m
τ_{max}=59.1 kPa
K_w=0.996
K_r=0.0100 m

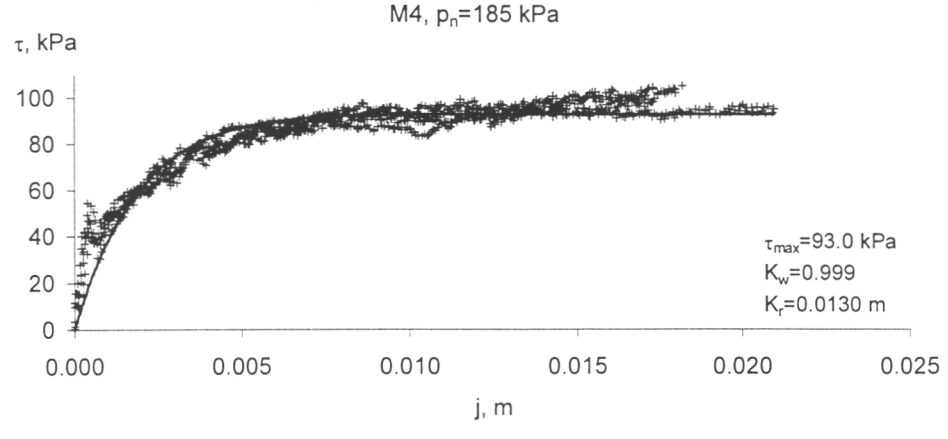
M4, p_n=185 kPa
τ, kPa
100
80
60
40
20
0
0.000
0.005
0.010
0.015
0.020
0.025
j, m
τ_{max}=93.0 kPa
K_w=0.999
K_r=0.0130 m

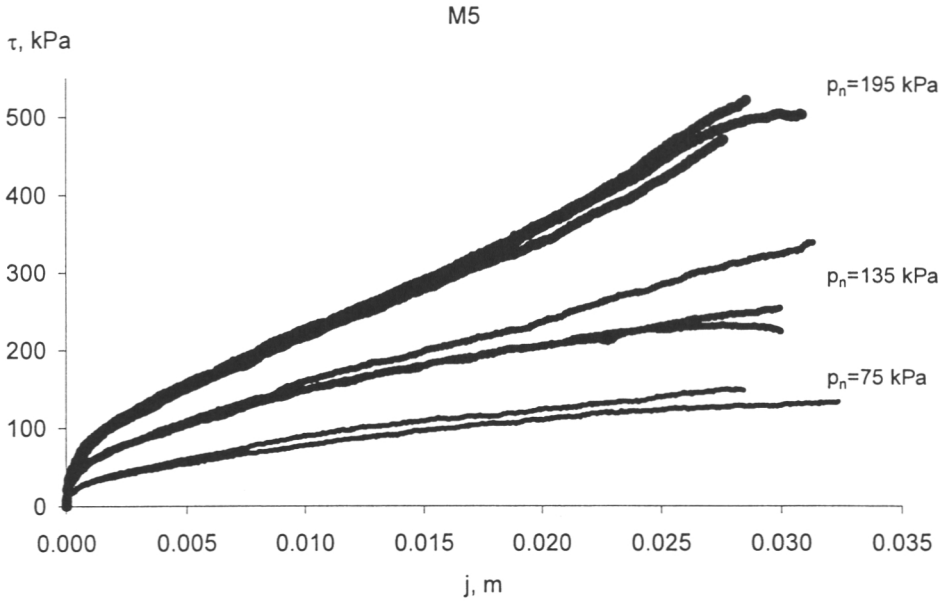
M5
τ, kPa
500
400
300
200
100
0
0.000
0.005
0.010
0.015
0.020
0.025
0.030
0.035
j, m
pn=195 kPa
pn=135 kPa
pn=75 kPa

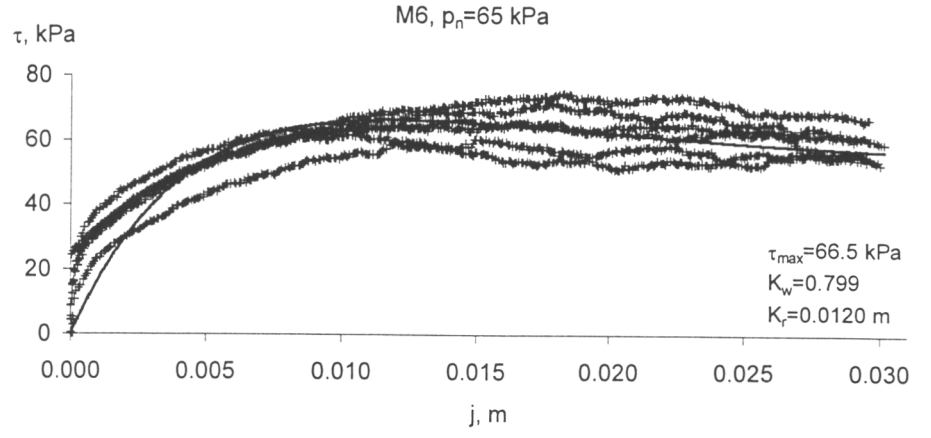
M6, p_n=65 kPa
τ, kPa
80
60
40
20
0
0.000
0.005
0.010
0.015
0.020
0.025
0.030
j, m
τ_{max}=66.5 kPa
K_w=0.799
K_r=0.0120 m

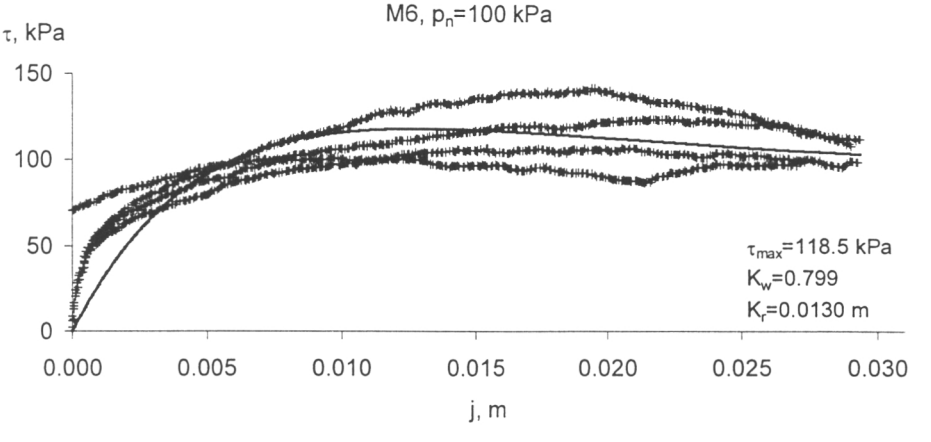
M6, p_n=100 kPa
τ, kPa
150
100
50
0
0.000
0.005
0.010
0.015
0.020
0.025
0.030
j, m
τ_{max}=118.5 kPa
K_w=0.799
K_r=0.0130 m

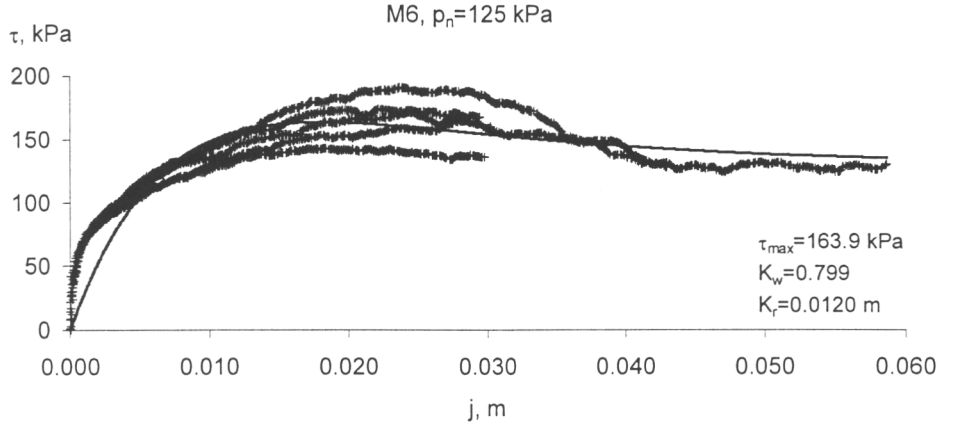
M6, p_n=125 kPa
τ, kPa
200
150
100
50
0
0.000
0.010
0.020
0.030
0.040
0.050
0.060
j, m
τ_{max}=163.9 kPa
K_w=0.799
K_r=0.0120 m

Appendix 4. Flow resistance pressure (p_f) vs. velocity (v) data and fitted models (Equation 79 and Table 12, p. 60) for snow types FI1 to FI5.

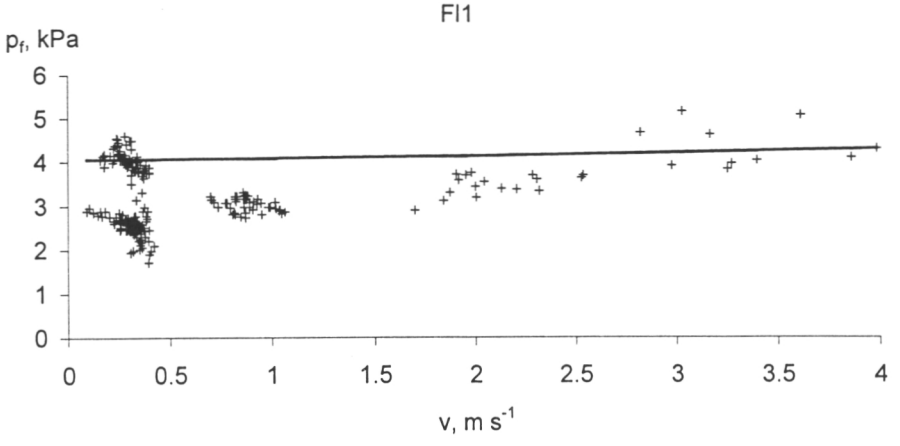

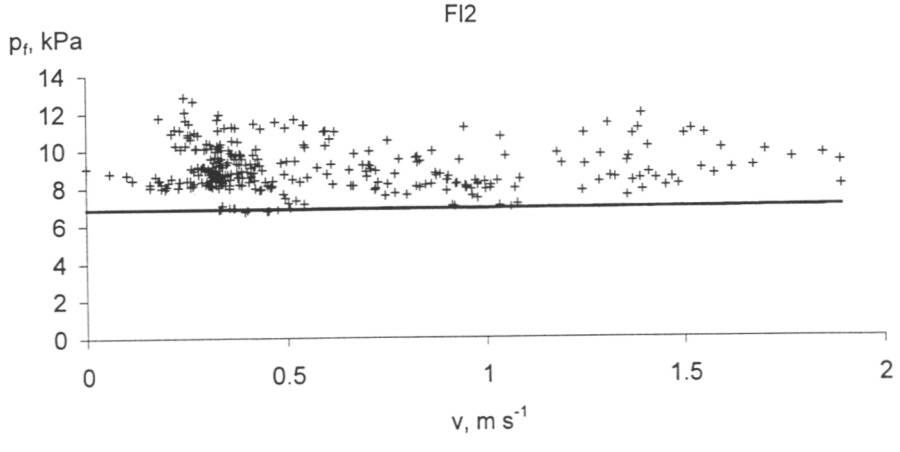

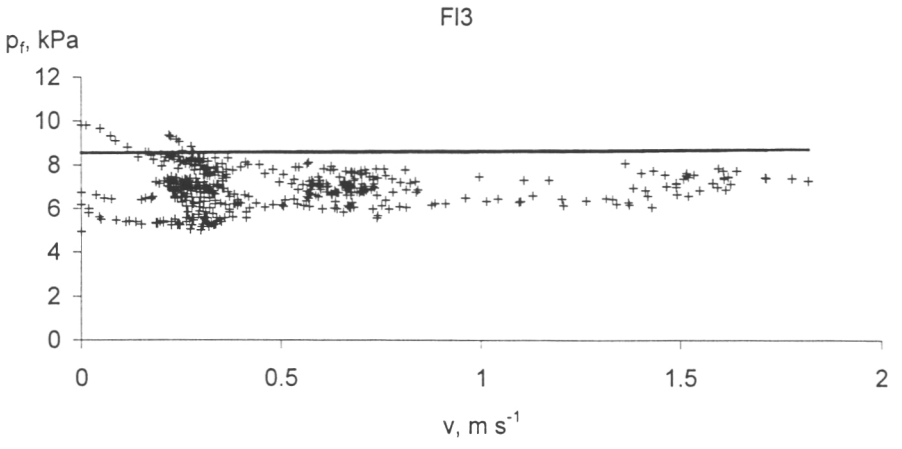
Fl3
p_f, kPa
12
10
8
6
4
2
0
0
0.5
1
1.5
2
v, m s^{-1}

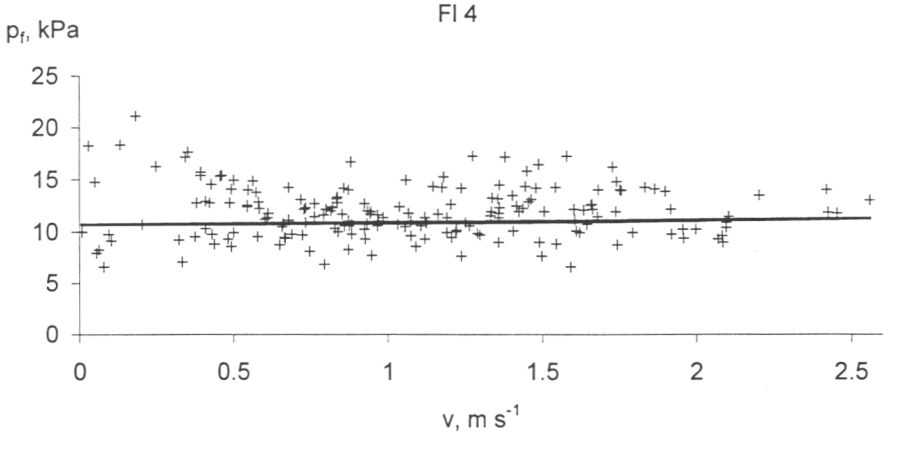
Fl 4
p_f, kPa
25
20
15
10
5
0
0
0.5
1
1.5
2
2.5
v, m s^{-1}

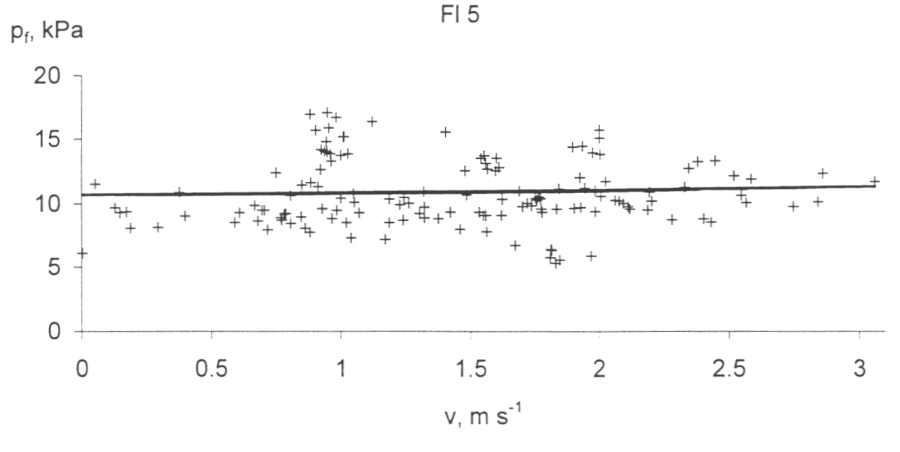
Fl 5
p_f, kPa
20
15
10
5
0
0
0.5
1
1.5
2
2.5
3
v, m s^{-1}

ISBN 951-40-1730-7
ISSN 0358-4283
Hakapaino Oy 2000